Magneto-Transport and Magnetization studies on the electron doped superconductor $Nd_{1.85}Ce_{0.15}CuO_{4\pm\delta}$

By

Nair Radhikesh Raveendran

PHYS 02 2013 04 005

Indira Gandhi Centre for Atomic Research

A thesis

Submitted to

The Board of Studies in Physical Sciences

In partial fulfillment of requirements for the Degree of

DOCTOR OF PHILOSOPHY

of

HOMI BHABHA NATIONAL INSTITUTE

August, 2018

Homi Bhabha National Institute

Recommendations of the Viva Voce Committee

As members of the Viva Voce Committee, we certify that we have read the dissertation prepared by Nair Radhikesh Raveendran entitled "Magneto-Transport and Magnetization Studies on the electron doped superconductor $Nd_{1.85}Ce_{0.15}CuO_{4\pm\delta}$" and recommend that it may be accepted as fulfilling the thesis requirement for the award of Degree of Doctor of Philosophy.

Chairman – Dr. N. V. Chandra Shekar	N.V. Chandra Shekar	**Date:** 21/12/18
Guide / Convener – Dr. Awadhesh Mani	Awadhesh Mani	**Date:** 21/12/18
Technical Advisor – Dr. Geetha Kumary	T.H.Kumary	**Date:** 21/12/18
Examiner – Prof. E. V. Sampathkumaran	E.V.Sampathkumaran	**Date:** 21/12/2018
Member 1 – Dr. R. Govindaraj	R. Govindaraj	**Date:** 21/12/2018
Member 2 – Dr. Tripura Sundari	S. Tripura Sundari	**Date:** 21/12/2018.
Member 3 – Dr. Santanu Bera	Santanu Bera	**Date:** 21/12/2018

Final approval and acceptance of this thesis is contingent upon the candidate's submission of the final copies of the thesis to HBNI.

I/We hereby certify that I/we have read this thesis prepared under my/our direction and recommend that it may be accepted as fulfilling the thesis requirement.

Date: 21/12/2018

Place: Kalpakkam

Awadhesh Mani 21/12/18

Dr. Awadhesh Mani

Guide

Statement by Author

This dissertation has been submitted in partial fulfillment of requirements for an advanced degree at Homi Bhabha National Institute (HBNI) and is deposited in the Library to be made available to borrowers under rules of the HBNI.

Brief quotations from this dissertation are allowable without special permission, provided that accurate acknowledgement of source is made. Requests for permission for extended quotation from or reproduction of this manuscript in whole or in part may be granted by the Competent Authority of HBNI when in his or her judgment the proposed use of the material is in the interests of scholarship. In all other instances, however, permission must be obtained from the author.

Nair Radhikesh Raveendran

Declaration

I, hereby declare that the investigation presented in the thesis has been carried out by me. The work is original and has not been submitted earlier as a whole or in part for a degree / diploma at this or any other Institution / University.

Nair Radhikesh Raveendran

List of Publications

Publications in Refereed Journal

a. Journal Publications

1. **"**Structural studies of the $Nd_{1.85}Ce_{0.15}CuO_4$ + Ag superconducting system", **N. Radhikesh Raveendran**, A.K.Sinha, R. Rajaraman, M. Premila, E. P. Amaladass, K. Vinod, J.Janaki, S.Kalavathi and Awadhesh Mani, *Bull. Mater. Sci***39**, 3, (2016)

2. "Investigation of the effect of Ag addition on the critical current density of the high temperature superconductor $Nd_{1.85}Ce_{0.15}CuO_4$"**N. Radhikesh Raveendran**, K. Vinod, E.P. Amaladass, J. Janaki and Awadhesh Mani *Supercond. Sci.Technol.***29,** 075012 (2016)

3. "Low temperature studies of granularity and upper critical field of superconducting $Nd_{1.85}Ce_{0.15}CuO_4$+Ag composite system" **N. Radhikesh Raveendran**, E. P. Amaladass, S. Sharma, A. T. Satya, J.Janaki and Awadhesh Mani, *J. Supercond. Nov. Magn.* **31**, 13 (2018)

b. In preparation:

1. "Study of anisotropy of $Nd_{1.85}Ce_{0.15}CuO_{4\pm\delta}$ films in its anti-ferromagnetic and superconducting regimes" **N. Radhikesh Raveendran**, A.K.Sinha, E. P. Amaladass, A. T. Satya, T. Geetha Kumary J. Janaki and Awadhesh Mani

Publications in conference proceedings

1. "Granularity and annealing effects in superconductivity of the electron doped cuprate system $Nd_{1.85}Ce_{0.15}CuO_4$" **N. Radhikesh Raveendran** , J.Janaki, E.P. Amaladass, S.Kalavathi, T.Geetha Kumary, Awadhesh Mani, T.R. Devidas, K.Vinod and A. Bharathi, *Indian Journal of Cryogenics **41 (1)**, 155-159*
   Oral presentation - National symposium on Cryogenics, (2014)

2. "Effect of granularity and annealing conditions on the magneto-resistance of the electron doped Superconductor $Nd_{1.85}Ce_{0.15}CuO_4$"**N. Radhikesh Raveendran**, E. P. Amaladass, J. Janaki, Awadhesh Mani, *AIP Conference Proceedings **1731 (1)**, 130028, 2015 (DAE SSPS-2015)*

Research papers presented in international / national conferences

1. "Magneto- Transport and Magnetization studies on the Superconducting system $Nd_{1.85}Ce_{0.15}CuO_4$ /Ag composites" **N. Radhikesh Raveendran**, E. P Amaladass, K. Vinod, J. Janaki and Awadhesh Mani *Poster Presentation, International Conference on Cryogenics, 2016*
2. "Annealing effects on the superconductivity and normal state properties of $Nd_{2-x}Ce_xCuO_4$ thin films" **N. Radhikesh Raveendran**, E. P Amaladass, T. Geetha Kumary, J. Janaki and Awadhesh Mani *Poster Presentation, International Conference on thin films, 2017*

Other Publications (Not part of the present thesis)

a. Refereed Journals

1."Characterization and Low Temperature Study of Iron Telluride Thin Films Upon Ageing and Oxygen Ion Irradiation" J. Janaki, T. Geetha Kumary, Awadhesh Mani, E. P. Amaladass, **N. Radhikesh Raveendran**, P. Magudapathy, S. Kalavathi, T. N. Sairam, T. R. Ravindran , *J. Supercond. Nov. Magn.* ***27,*** *11, (2014)*

b. Conference Proceedings / Symposium

1. "Synthesis and Study of FeSe thin films and $LiFeO_2$/FeSe bilayers" **N. Radhikesh Raveendran,** T. Geethakumary, S. Rajakumari, R. Pandian, J. Janaki and Awadhesh Mani, *AIP Conference Proceedings*, **1832(1),** 130034, (2017)

Nair Radhikesh Raveendran

“It moves,

It moves not.

It is far,

It is near

It is within all,

It is without all”

Isha Upanishad

Dedicated

To

My parents **Saraswathy Angathil**, **T. R. Raveendran** and

my brother **Shreekesh Raveendran**

To

My beloved teachers from Sree Kerala Varma College,

Thrissur

Prof. V. N. Purushothaman

Dr. M. Raveendranthan

Dr. A. P. Jayadevan

Prof. M. R. Jalaja

To

My ray of hope, philosopher and companion, **Ali**

Acknowledgements

"Walk on with hope in your heart, You will never walk alone"

In this journey of my Ph. D. life, I have not walked alone but it became possible by love, support and encouragement of numerous people, including my mentors, colleagues, friends and family.

First of all, I express my deep sense of gratitude to my research supervisors Dr. Awadhesh Mani and Dr. J. Janaki for their valuable guidance throughout my Ph. D. tenure. Their suggestions and above all their patience, are the major reasons, I could successfully complete my work. I specially thank Awadhesh Sir, for his care, support and affection during the turbulent times of Ph. D. days, especially during the struggle with thin films and the task of thesis writing. I am extremely grateful to my mentor Dr. J. Janaki for her whole hearted support, her ideas and suggestions.

I am extremely indebted to my Technical Advisor Dr. GeethaKumary. Her understanding, encouragement and personal attention professionally as well as personally, has helped me a lot during this part of my life. She will always be a source of joy as well as inspiration to me.

I would also like to thank my Doctoral committee members, Dr. N. V. Chandra Shekar, Dr. R. Govindaraj, Dr. S. Tripura Sundari and Dr. Santanu Bera. Their insightful comments regarding my work and constructive criticism has helped me to always question myself and look at my work from a different perspective. I specially thank Dr. N. V. Chandra Shekar for his constant support and his directions.

I gratefully acknowledge financial support given by Department of Atomic Energy, India. I sincerely thank the former directors of IGCAR Dr. P. R. Vasudeva Rao, Dr. S. A. V. Satyamurthy and the present director Dr. A. K. Bhaduri for allowing me to carry out my research work. I also express my thankfulness to the former directors of Materials Science Group Dr. C. S. Sundar and Shri. M. P. Janawadkar.

I would like to extend my deep gratitude to the Director, Materials Science Group, Dr. G. Amarendra for his unflinching support during this Ph. D. tenure.

I express my gratitude to Dr. Bharathi (Former Head LTSS) and Dr. B. V. R Tata (Former Dean of physical Sciences) for their support. I would like to thank my collaborators, Dr. A. K. Sinha for Synchrotron X-ray diffraction measurements and Dr. R. Rajaraman and Smt. Premila for Raman spectroscopy measurements. I sincerely thank Dr. N. Subramaniam, Dr. V. Sridaran, Dr. Sarguna and Shri. Magudapathy for allowing and carrying out X-ray diffraction measurements.

Apart from my mentor I had also enjoyed having scientific discussions with Dr. Kalavathi, Dr. Bhaskaran, Dr. Sharat Chandra and Dr. Dipak Kumar Baisnab related to various aspects like XRD, thin films and granular superconductivity. I gratefully remember the timely help extended by Dr. Krishnan whenever there was a requirement related to Pulsed Laser Depostion set up. I also thank Shri. S. Kanmani for his encouragement and for filling me with positivity during tough times.I must thank Dr. Gireeshan and all the members from the Helium plant namely, Mr. Parthiban, Mr. Kumar, Mr. Prashant, Mr. Arun, Mr. Selvam and Mr. Vasu for their kindly help on all the ocacasions. I thank Dr. M. Sai Baba and Dr. Lakshmi Narasimhan for the facilities provided and for ensuring our comfortable stay in the JRF Enclave.

Words are insufficient to thank my dear lab members. Dr. A. T. Satya, Dr. K Vinod, Dr. Shilpam Sharma and Dr. E. P. Amaladass. Without the scientific discussions, the criticisms and timely help that I was lucky to get, this would not have been possible. I thank my senior Dr. T. R. Devidas, his teaching ability is something I admire and look up to. I cherish all our memories and I miss our discussions on a variety of our favorite topics ranging from Science to Sports as well. I thank my fellow juniors, Abhirami and Gayathri for the wonderful time spent in lab. I must specially thank my fellow colleague Harimohan for his companionship and for always being there with your support.

I thank Dr. Anees from the bottom of my heart for his words of encouragement, moments of friendship and brotherly affection.

No words shall be enough to thank my seniors, Dr. Karthickeyan, Dr. Mahendran, Dr. Srinivasan, Dr. Raghavendra, Dr. Sanjay, Dr. Preethi, Dr. A. K. Sivadasan and Dr. Greeshma. I thank Dr. Jai Ganesh, Dr. Mohandoss and Dr. Vinod as well. I must specially mention

Srinivasan's mother also, for her love and affection towards us. I owe much gratitude to my fellow mates, Sivakumar, Dhilipan, Velraj, Ragavendran, Barath, Naveen, Thangam and Santosh. I also shared a lot of joyous moments with my fellow juniors, Manu, Paulson, Sachin, Prince, Sruthi, Reshma, Parvathy, Deepitha, Vaishnavi, Rajeswari, Rajitha K and Rajitha

Music was an integral part of my life in JRF Enclave and I owe it to a bunch of wonderful people. Sai, Balasubramanian, Reshmi, Abhirami, Sudheer, Darpan, Paravthy and Guna. The time I spent with you all is something that I will always cherish. Sports activities in enclave kept us ticking and helped us a lot in many ways. I thank all my fellow badminton players. It was a pleasure to spend time with you all in the Badminton Court. I thank all the cricketers and footballers as well.

I take this opportunity to thank my batchmates, Nilakantha, Vairavel, Padmalochan, Santosh, Shivang, Nidhin, Manoj, Vikas, Perumalsamy, Madhusmitha, Sumathi and Zaibudeen

I sincerely thank Uma Namangalam at this juncture for her support.

Gratitudes to my dear friend, Irshad K Abbas. Thank you for being the person you are and for being a great roommate. Thanks for accepting me as myself and honoring the differences.

My love and respect goes to my friend Lakshmanan Chelladurai, for being there for me, at any time, be it personal or professional. He was or He is, always the go to person for me. His work ethics is something that I admire and something I would want to emulate in my life.

Rasitha, thank you for having faith in me, when I was severely lacking faith on myself. If it weren't for your words of strength, I could not have completed this.

I take this moment to express my love to my parents and my brother

Lastly and most importantly I thank the Almighty….

As it is said "If you have GOD with you, you got a Friend and that Friend is YOU"

Table of Contents

List of Figures

List of tables

Synopsis

Hole-doped superconductors form a major part of the high T_C superconductors (HTSC). However, there is another interesting class of compounds namely electron doped cuprates which are relatively less investigated [1]. A study of various aspects of the electron doped cuprates indicates that they exhibit both similarities and differences with the hole-doped compounds. For instance copper-oxygen (CuO_2) plane is the crucial building block for both of them. There is a general consensus that the pairing necessary for High T_C superconductors involves interplay between doped charges and antiferromagnetic spin correlations [2]. In both the classes of cuprates, there exist charge reservoir layers which play the crucial role of the suppliers of charge carriers for the CuO_2 planes responsible for the superconductivity in these compounds. Nevertheless, the compounds belonging to the electron doped class exhibit conspicuous differences from that of the hole doped with respect to their normal (N) and superconducting (SC) states properties. For instance, the functional dependence of the resistivity of optimally electron doped $Nd_{1.85}Ce_{0.15}CuO_4$ (NCCO) with respect to temperature (T) is observed to be nearly quadratic(T^2), which is in contrast to the behaviour of the optimally hole doped $La_{1.85}Sr_{0.15}CuO_4$(LSCO) where the resistivity remains linear in T for a very large temperature range [2]. The resistivity behaviour in the latter (hole doped cuprates) has been attributed to be an outcome of non-Fermi-liquid behaviour. Another major difference between electron and hole-doped materials lie in their respective phase diagrams. In the electron-doped materials, the anti-ferromagnetic (AFM) phase spreads much larger in extent and persists up to higher doping levels than that of the hole doped systems. Superconductivity in the former occurs in a doping range that is almost five times narrower than their hole-doped counterparts. The two ground states (SC and AFM)

occur in much closer proximity to each other and may even coincide unlike in the hole-doped materials [1].

Among these interesting classes of superconductors, we have chosen $Nd_{1.85}Ce_{0.15}CuO_{4\pm\delta}$ (optimally electron doped) for our studies, which has a T_C= 24 K. In the synthesis of the compound $Nd_{1.85}Ce_{0.15}CuO_4$ various material issues remain unclear including the exact role of the dopant and reduction step absolutely necessary to induce superconductivity[3]. Furthermore, granularity is an essential feature of this superconductor as is the case with many of the novel unconventional superconductors and needs to be investigated in detail. In a granular superconductor microscopic superconducting grains are separated by non-superconducting regions; Josephson tunneling between the grains establishes the macroscopic superconducting state. In order to understand the intricate interplay of superconducting grains and no-superconducting regions, we have performed detailed investigation of granularity effects in the polycrystalline superconducting sample $Nd_{2-x}Ce_xCuO_4$ (x=0.15), synthesized under various annealing conditions, using magnetic field and current dependent electrical resistivity measurements.

The effect of silver addition on ceramic superconductors has always been a topic of interest as in many cases it has resulted in an improvement of superconducting properties [4]. Studies on the introduction of silver into high-T_C superconductors like Bi–(Pb)–Sr–Ca–Cu–O and $YBa_2Cu_3O_7$ have revealed that Ag addition improve their structural and superconducting properties. Ag addition also leads to the enhancement of critical current density (J_c) of almost all bulk high temperature superconductors including the rare earth cuprates, MgB_2 and rare earth iron pnictides, mainly due to an improvement in inter-granular coupling [5]. Furthermore, the electron doped cuprate $Nd_{1.85}Ce_{0.15}CuO_4$ (NCCO) is a unique example of a very highly granular ceramic superconductor system.

The effect of Ag addition in modifying the properties of this system and granular nature has not been performed earlier. This can be very important from the point of view of basic research as well as technological applications because Ag is used as cladding for HTSC wires. Interestingly, in addition to critical current density even the essentially intrinsic properties like upper critical field (H_{C2}) can improve upon addition of Ag, as seen in YBCO/Ag composites [6]. Hence, in the case of NCCO, the effect of Ag addition on superconducting properties may be considerably different and worth investigating. Therefore, in continuation of our studies on the polycrystalline sample of the electron doped superconductor $Nd_{1.85}Ce_{0.15}CuO_{4\pm\delta,}$ we have investigated the influence of materials modification by silver addition on the above properties such as critical current density (magnetization measurements) and upper critical field (magneto transport measurements).

The primary motivation of venturing into thin films $Nd_{1.85}Ce_{0.15}CuO_{4\pm\delta}$ was to tackle the problem of granularity. Single crystals and oriented thin films of $Nd_{1.85}Ce_{0.15}CuO_{4\pm\delta}$ do not show any double transitions in the resistivity behavior with respect to temperature [7, 8]. This is perhaps due to the fact that their increased crystal size, crystallographic order and better homogeneity may lead to a reduction in the overall granularity and weak link behaviour. However, we have to compromise on some other aspects like T_C (usually lower ≈ 14 K if synthesis is performed in O_2 atmosphere instead of N_2O) and the associated synthesis of high quality films or single crystals is not an easy task. An even more intriguing characteristic of these materials is that the long range anti-ferromagnetic order in electron doped $Nd_{2-x}Ce_xCuO_4$ can exist even for larger values of x ($x \geq 0.12$) and exhibit a co-existence with superconductivity [9]. Magneto-resistance of the under doped as well as the as grown electron doped cuprates (non-superconducting) has already provided new information regarding the coupling between the charges and background magnetism [10]. It is observed that the resistivity is sensitive to the interlayer

magnetic order. Hence, it would be interesting to study the magneto resistance of the $Nd_{1.85}Ce_{0.15}CuO_{4\pm\delta}$ both in its non-superconducting state (where we expect the magnetic properties to be prominent) and the superconducting state. Keeping the above intricacies in mind, we have synthesized $Nd_{1.85}Ce_{0.15}CuO_{4\pm\delta}$ thin films and have studied their magneto transport and magnetization behaviour.

The thesis is organized into six chapters and the contents of each chapter are summarized as follows

Chapter 1 presents a brief introduction about electron doped superconductors which involves a discussion on the electronic phase diagrams of the HTSCs. The comparison of superconductivity of the electron doped superconductors with their counter parts, i.e. the hole doped superconductors has also been discussed in detail as this forms an important part in understanding the mechanism of superconductivity of HTSC. This is followed by a discussion on the salient features of the electron doped superconductor $Nd_{1.85}Ce_{0.15}CuO_4$. The advent of granularity, challenges in synthesis and the crucial reduction process for the emergence of superconductivity in this system have been described. A section has been dedicated to provide a comprehensive review on the effect of Ag addition on various HTSC materials. A brief review on the thin films of electron doped superconductors has also been presented focusing on $Nd_{2-x}Ce_xCuO_4$ thin films.

Chapter 2 contains a brief description about Pulsed Laser Deposition which was the technique used for depositing superconducting films. The characterization tools such as X-ray diffraction and Scanning Electron Microscopy, which are important from the point of view of structural and morphological studies, have been briefly discussed. Dipstick resistivity method which is our preliminary characterization tool for measuring resistance with respect to temperature has been detailed. Other important experimental set ups such

as the Magneto - Resistance set up, the Vibration Sample magnetometer (VSM) and the SQUID VSM used to study magnetization have been described.

Chapter 3 brings out detailed studies on the polycrystalline $Nd_{1.85}Ce_{0.15}CuO4_{\pm\delta}$which has been synthesized via the solid state route and well characterized by X-ray diffraction. A brief description on granular superconductors has been included in order to understand the interesting features that granular nature brings in to superconductors. The superconducting transitions have shown characteristic double transitions which are common in weakly coupled granular superconducting systems. The bulk superconductivity was confirmed through magnetization measurements as well. From the resistivity measurements the samples which had undergone reduction in Ar atmosphere were found to be superconducting (T_C ~ 24 K). Since Ar annealing is a crucial factor in obtaining superconductivity, two different annealing schedules were performed on the sample. The effect of two different annealing conditions on the temperature dependent electrical resistivity behavior was also studied. The observed resistivity behavior has been qualitatively rationalized in terms of interplay of opposing effects of temperature and magnetic field on superconductor-insulator-superconductor junctions formed on account of coupling of superconducting grains dispersed in insulating matrix in this granular system.

Chapter 4 describes the detailed studies of $Nd_{1.85}Ce_{0.15}CuO_{4\pm\delta}$/Ag composites to bring out the effect of Ag addition on the electron doped cuprate superconductor $Nd_{1.85}Ce_{0.15}CuO4_{\pm\delta}$. The effect of Ag addition has not yet been studied on electron doped superconductors, to the best of our knowledge. Our SEM studies indicate an average grain size of 800nm and no significant changes in grain size occur upon Ag addition. This is in contrast to the YBCO/Ag system, wherein both grain size and texturing increases upon Ag addition. The low temperature electrical and magnetic property studies indicate

that the critical current densities (J_C) are significantly enhanced upon Ag addition. The resistive superconducting transitions of NCCO/Ag composites show large granular effects which exhibit anomalous features in magneto-resistance behaviour. These anomalies have been qualitatively understood based on the interplay of Josephson junction coupling and quasi-particle tunneling; the combined effects of which dictate the evolution of the observed temperature and field dependent resistivity behaviour. The overall effects of granularity persist even upon the addition of Ag.

Chapter 5 focuses on magneto transport and magnetization study of $Nd_{1.85}Ce_{0.15}CuO_{4\pm\delta}$ thin films. The films were grown by Pulsed Laser deposition technique. The films characterized by X – Ray diffraction showed preferred orientation in the (00L) direction. The as-grown unreduced films are non-superconducting and anti-ferromagnetic consistent with literature [11].The magneto-transport studies on these films have been performed by applying the magnetic field parallel (R_{in}) and perpendicular (R_{out}) to the plane. The in plane resistance R_{in} shows a step like transition in its magneto resistance behavior. Such kind of a transition (step like) is attributed to a transition from collinear to non-collinear spin alignment in adjacent CuO_2 planes which is induced by application of magnetic field. However, such a transition is not observed when magnetic field is applied out-of-plane. This behaviour is consistent with literature reports [12,13].

The films, subjected to ex-situ annealing in Ar atmosphere, were found to be superconducting at a moderate T_c ~14 K. The normal state resistivity versus temperature curves of the films have shown a T^2 dependence at low temperatures (T< 200K), attributable to electron-electron scattering, rather than the linear T dependence exhibited by hole-doped cuprates. The temperature dependent R_{in} and R_{out} measurements for various magnetic fields have revealed a sizeable anisotropy in this system. The anisotropy factor$\Gamma = H_{C2}^{\|ab} / H_{C2}^{\|c}$is defined as the ratio of upper critical field when the field is applied

parallel to the plane of the film ($H_{C2}^{\parallel ab}$) to the upper critical field when the field is applied perpendicular to the plane of the film ($H_{C2}^{\parallel c}$). The value of Γ was found to be ≈ 12 which is comparable with the values of $YBa_2Cu_3O_7$ (Γ ≈ 5-8) but lesser than that of $La_{2-x}Sr_xCuO_4$ (Γ ≈ 20) and $BiSr_2CaCu_2O_8$ (Γ ≈ 60). The intra granular J_C estimated from the magnetic hysteresis loops, using the Bean's model, was found to be 1.93×10^5 A/cm^2 in accordance with the reported values [14].

Chapter 6 summaries the major findings of the thesis and discusses on its relevance with respect to the existing literature. It also provides the directions for future work.

References

1) N. P. Armitage, P. Fournier and R. L Greene, Review of ModernPhysics**82**, 2422(2010).
2) "Current Research Issues for the Electron-Doped Cuprates"
   Fournier P., Maiser E., Greene R.L. (2002)
   The Gap Symmetry and Fluctuations in High-Tc Superconductors, NATO Science Series: B: vol 371. Springer, Boston, MA
   In: Bok J., Deutscher G., Pavuna D., Wolf S.A. (eds)
3) R. J. Cava, H. Takagi, R.M. Fleming, J.J. Krajewski, W.F.PeckJr, Border M. Marezio, B. Batlogg& L. W. Rupp Jr. Physica C**199** 65(1992).
4) Dhananjay Kumar, M. Sharon, P. R. Apte, R. Pinto, S. P. Pai, S. C. Purandare, C. P. D' Souza, L. C. Gupta &R. Vijayaraghavan, Journal of Applied Physics,**76** 1349 (1994).
5) Poonam Rani, Rajveer Jha &V.P.S. Awana, Journal of Superconductivity and Novel Magnetism, **26(7)** 2347 (2013).

6) Poonam Rani, Anand Pal., &Awana V. P.S. Physica C.**497**,19(2014).

7) Y. Wang & H. GaoPhysica C**470**, 689(2010).

8) M. Hoek, F. Coneri, D. P. Leusink, P. D. Eerkes, X. Renshaw Wang & H. Hilgenkamp Superconductor Science and Technology,**27**, 044017(2014).

9) T. Uefuji, T. Kubo, K. Yamada, M. Fujita, K. Kurahasi, I. Watanabe & K. Nagamine Physica C **357**, 208(2001).

10) T. Wu, C. H. Wang, G. Wu, D. F. Wang, J. L. Luo, G. T. Liu & X. H. Chen Journal of Physics: Condensed Matter**20**, 275226 (2008).

11) M. Horio, T. Adachi, Y. Mori, A. Takahashi, T. Yoshida, H. Suzuki, L.C.C Ambolode, K. Okazaki, K. Ono4, H. Kumigashira, H. Anzai,, M. Arita, H. Namatame, M. Taniguchi, D. Ootsuki, K. Sawada, M. Takahashi T. Mizokawa,Y.Koike and A. Fujimori, Nature communications**7,** 10567, (2016).

12) X. H. Chen, C. H. Wang, G. Y. Wang, X. G. Luo, J. L. Luo, G. T. Liu & N. L. Wang Physical ReviewB**72**, 064517(2005).

13) A. N. Lavrov, H. J. Kang, Y. Kurita, T. Suzuki, Seiki Komiya, J. W. Lynn, S. H. Lee, Penchneg Dai & Yoichi Ando *Physical Review Letter**92,** 22(2004).*

14) Carla Cirillo, Anita Guarino, Angela Nigro, and Carmine Attanasio Physical ReviewB **79,**144524(2009).

Chapter 1

Electron Doped Superconductors: An overview

Cuprate superconductors still remain as a topic of active interest in the research field because even after rigorously pursued experimental and theoretical research, the origin of superconductivity as well as the underlying physics of these systems is still debatable [1-3]. The parent compounds of High T_C cuprate superconductors (HTSCs) are antiferromagnetic Mott insulators [4]. As the CuO_2 layers (the building blocks of HTSCs) are doped with charge carriers either via holes or electrons, the antiferromagnetic phase is suppressed and superconductivity is emerged. If holes are the one to make the CuO_2 layers conducting, then these class of compounds are known as hole doped superconductors ($La_{2-x}Sr_xCuO_4$, $YBa_2Cu_3O_7$etc.,) and if electrons are doped into the CuO_2 layers to make them conducting, then they are known as electron doped superconductors ($R_{2-x}Ce_xCuO_4$, R= Nd, Pr, Sm and La, $Sr_{1-x}La_xCuO_2$). A useful way to understand more about the cuprate superconductors will be the comparison of the phase diagrams of hole doped and electron doped cuprates. A useful way to understand more about the cuprate superconductors will be the comparison of the phase diagrams of hole doped and electron doped cuprates. The comparison shall give us a picture on what aspects of the HTSCs are universal and what are not. It can throw light in to the various intriguing questions on mechanism of superconductivity, non-Fermi liquid behavior of hole doped cuprates and the exact effect of doping or annealing on the same.

1.1. Phase diagram

Figure 1.1 shows a comparison of phase diagrams of LSCO ($La_{2-x}Sr_xCuO_4$) and RCCO ($R_{2-x}Ce_xCuO_4$), where the former system represents the hole doped and the latter represents electron doped HTSCs. It can be seen from both sides of the phase diagram that only some approximate symmetry exists. The antiferromagnetic phase in the RCCO side is much more larger compared to that of the hole doped counterpart. It should be noted that the antiferromagnetic nature prevails upto larger values of doping level while the range of doping within which superconductivity occurs is quite narrow in the electron doped cuprates. The closeness of the antiferromagnetic and superconducting regimes in electron doped cuprates is an interesting aspect which provides an avenue for exploration of the co-existence of superconductivity and antiferromagnetism [5]. In contrast, for the hole doped cuprates, these two phases remain pretty distinct. In addition, the superconducting dome, i.e., the doping range within which superconductivity persists, is much wider.

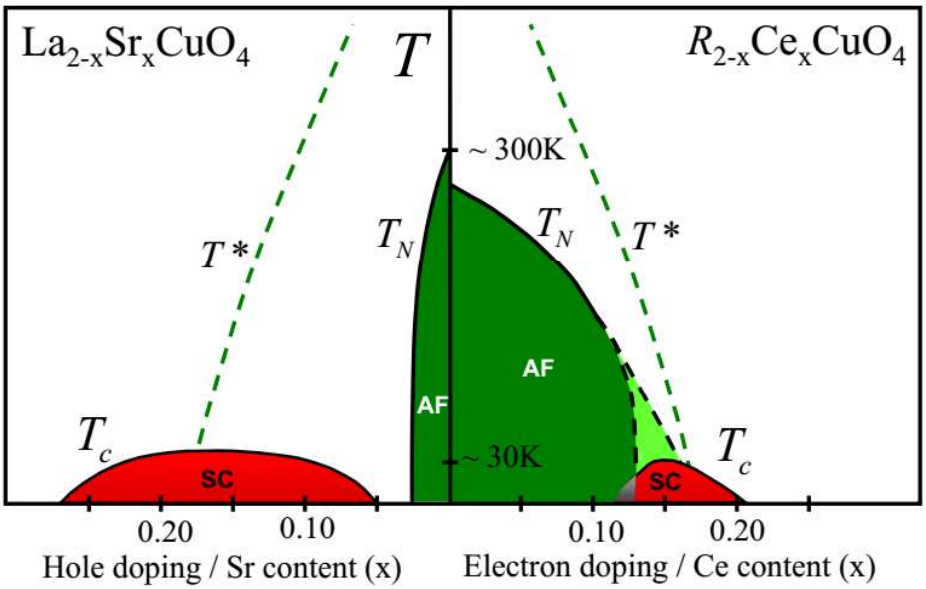

Fig. 1.1 Phase Diagram of the hole doped (LSCO) and electron doped (RCCO) cuprates; TN stands for Néel temperature, T* represents the approximate extent of pseudogap phase and T_C is the superconducting critical temperature (figure reproduced from a Ref. [4]).

In 1990, Luke et al.[6] has reported that the Néel temperature (T_N) of Nd_2CuO_4 , the parent compound of the electron doped superconductor $Nd_{2-x}Ce_xCuO_4$, to be at 250 K. Under systematic Ce substitution in$Nd_{2-x}Ce_xCuO_4$, the value of T_N gradually decreases and ultimately vanishes at optimal doping level (x ~ 0.15) and the compound becomes superconducting. On the other hand, for $La_{2-x}Sr_xCuO_4$, the antiferromagnetism subsides completely for the doping levels which are comparatively very low (x~0.02)[7]. Thus, antiferromagnetism persists for much larger values of doping level in NCCO. In nutshell, from comparison of phase diagrams, it is amply evident that hole doping and electron doping in the cuprates affect the electronic properties of the corresponding systems very differently.

1.2. Crystal structure of Electron doped Cuprate Superconductors

In Figure 1.2, the crystal structure of the hole doped and electron doped cuprates have been compared. R_2CuO_4 (where R= Nd, Sm, Eu, Gd) has a *T′* structure and the doping is performed by Ce at R sites. The compounds are tetragonal with the space group I4/mmm. They constitute a body centered unit cell where the copper ions of adjacent CuO_2 layers are displaced by (a/2, a/2) with respect to each other [4,8].

There are some important differences when we compare this crystal structure with the hole doped cuprates which has a *T* structure. It can be clearly observed that in the *T* structure, the in-plane Cu has six O atoms surrounding it whereas the *T′* structure is devoid of apical oxygen atoms and hence the coordination number of the in-plane Cu is 4. If we observe closely, in the *T′* structure the reservoir oxygen ion (O(2)) is positioned differently resulting in an expanded in-plane unit cell compared to the *T* structure (for instance, La_2CuO_4) and this leads to an overall decrease in unit cell volume. The lattice parameters of La_2CuO_4 are $a = b$ ~3.81 Å and c~ 13.2 Å which gives a unit cell volume of 191.6 $Å^3$. Among the *T′* cuprates the largest volume is found in Pr_2CuO4 (a=b ~3.96

Å, *c*~ 12.2 Å) with a value of 191.3 $Å^3$. Another factor that distinguishes these structures is the fact that in *T′* structure, the rare earth and oxygen ions do not share the same plane unlike the *T* structured cuprates.

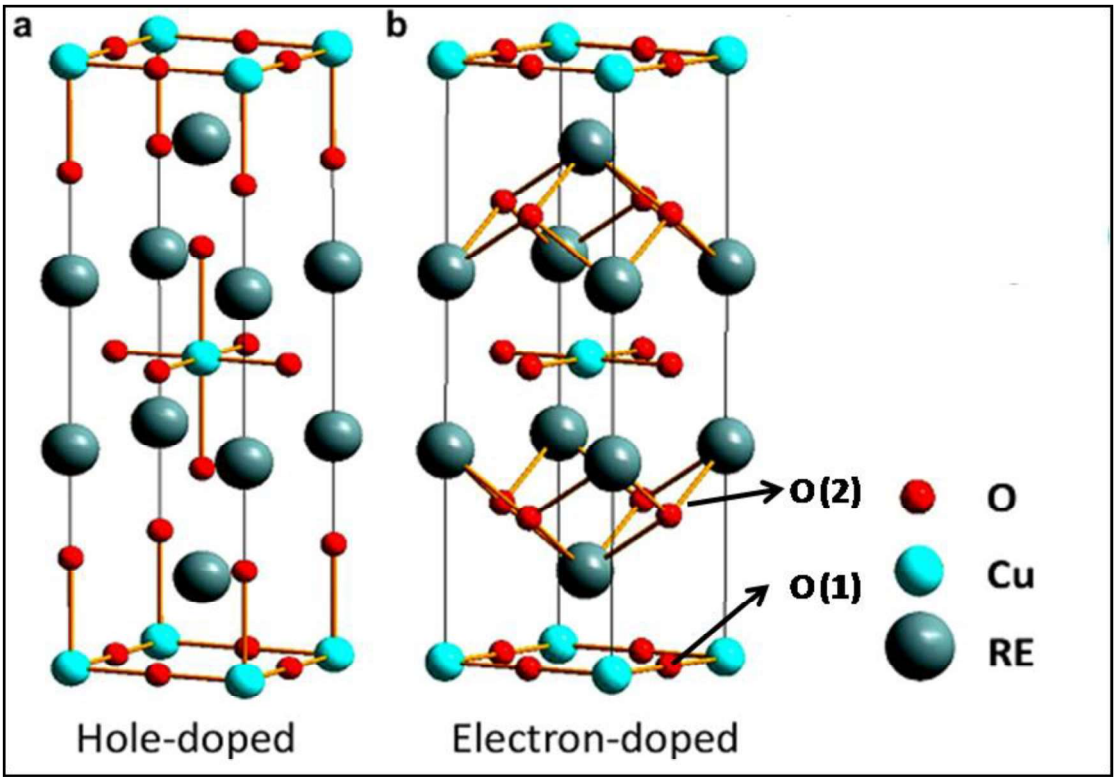

Fig. 1.2 Comparison of Structure (a) Hole doped cuprates (b) electron doped cuprates (Figure has been reproduced from Reference [8])

1.3. Electronic structure

The most important factor which decides the electronic and magnetic properties of the cuprates is their CuO_2 layers and the strong hybridization between Cu and O orbitals. It is believed that the superconductivity occurs primarily in the in-plane Cu $d_{x^2-y^2}$ and O $p_{x,y}$ orbitals [9].The band theory predicts that the undoped parent compounds (La_2CuO_4 and Nd_2CuO_4) to be metallic but in fact they are insulators. The presence of strong local coulomb interactions is believed to be responsible for this behavior. These materials are Mott insulators and the nature of strong on-site correlation energy is described by a single- band Hubbard model [10]. In the Zaanen- Sawatsky-Allen scheme these materials are aptly referred as charge transfer band insulators [11]. They suggested that the energy

to overcome charge motion is the energy associated with the potential difference of Cu $d_{x^2-y^2}$ and O $p_{x,y}$ orbitals. From the optical spectroscopy studies it was inferred that the holes reside on the charge transfer band comprised of O orbitals and the doped electrons reside on Cu sites [4,12]. The cuprates which are half filled with one electron in Cu $d_{x^2-y^2}$and have O $p_{x,y}$ orbitals are described by a three band Hubbard Model [13].

The observed asymmetry in the phase diagram points to the fact that although the superconductivity emerges in the CuO_2 planes with addition of charge carriers (electrons/holes), the way a hole or electron affects the electronic structure must be quite different. In an attempt to understand the phenomenon of antiferromagnetism persisting through a large range of doping in the electron doped cuprates, spin dilution models have been considered. Keimer et al.[14] have shown by neutron scattering measurements that Zn doping in La_2CuO_4 reduces the Néel temperature more or less in the similar rate as Ce doping does in $Pr_{2-x}Ce_xCuO_4$. Zn has a d^{10} filled shell and is considered as a spinless impurity. As per this picture, Zn substitution hence results in a dilution of the spin system. By adding Cerium, the added electrons neutralize the spin on d^9 Cu site. Similar studies were performed in $Nd_{1.85}Ce_{0.15}CuO_4$[15] and it was observed that the Néel temperature reduced drastically along with large reduction in spin stiffness, the results were explained using the same spin dilution model. On the other hand, very small value of hole doping is enough for the complete suppression of antiferromagnetism in the hole doped cuprates (x~ 0.02). In contrast, in the hole-doped case Aharony et al. 1988 proposed that only a small number of holes is required to suppress antiferromagnetism.[16]. The holes primarily reside on the in-plane oxygen atoms and cause spin frustration instead of spin dilution. An effective ferromagnetic Cu-Cu interaction is induced by the oxygen-hole/copper-hole interaction. This interaction competes with the antiferromagnetic super exchange which results in frustration of the

Néel order. Therefore a small density of doped holes destroys the long-range order. This phenomenon of spin frustration does not occur during electron doping with addition of Ce as electrons are introduced on to the Cu sites. Hence, the interaction of holes and electrons with the cuprates system and the associated physics related to them is very different.

1.4. Magnetic properties

There are two factors which decide the magnetic properties of electron doped cuprates, one is the antiferromagnetic ordering in the CuO_2 planes and the other is the magnetism of the rare earth ions. Antiferromagnetic order of Cu spins of the parent compounds of hole and electron doped cuprates are different. Even though the magnetic moments are confined to CuO_2 planes and they have strong antiferromagnetic interaction in plane, the spin alignment is different in each case. For electron doped superconductors the spins lie along the CuO bonds whereas they align at 45° angle with respect to the Cu-O bonds for La_2CuO_4 (parent compound of LSCO, a hole doped superconductor) [7]. The magnetic order is dictated by R-Cu coupling (where R is the rare earth ion) and the exchange interactions (super exchange, coulomb exchange etc.) [17,18]. Cu^{2+} spins have an antiferromagnetic collinear arrangement in the parent compounds of the hole doped [19] cuprates and a non-collinear arrangement in electron doped cuprates [20]. In underdoped electron doped cuprates (Ce doping, $x \sim 0.01$-0.03), the coupling between the charge carriers and the associated antiferromagnetism leads to an interesting result in the electrical transport measurement with applied magnetic fields. Large oscillations are observed in the angular magneto resistance measurements when the magnetic field is rotated in the CuO_2 plane. These are now believed to be spin flop transitions arising under the influence of a magnetic field. A transition from the non collinear to collinear moments is induced by the application of magnetic field [21-23]. A representation of non-collinear

and collinear Cu^{2+}spin arrangements is shown in Figure 1.3. The non-collinear arrangement of Cu^{2+} spins in Pr_2CuO_4 is shown in Figure 1.3(a). The collinear arrangement that takes place by application of magnetic fields in particular directions are shown in Figure 1.3 (b), (c) and (d).

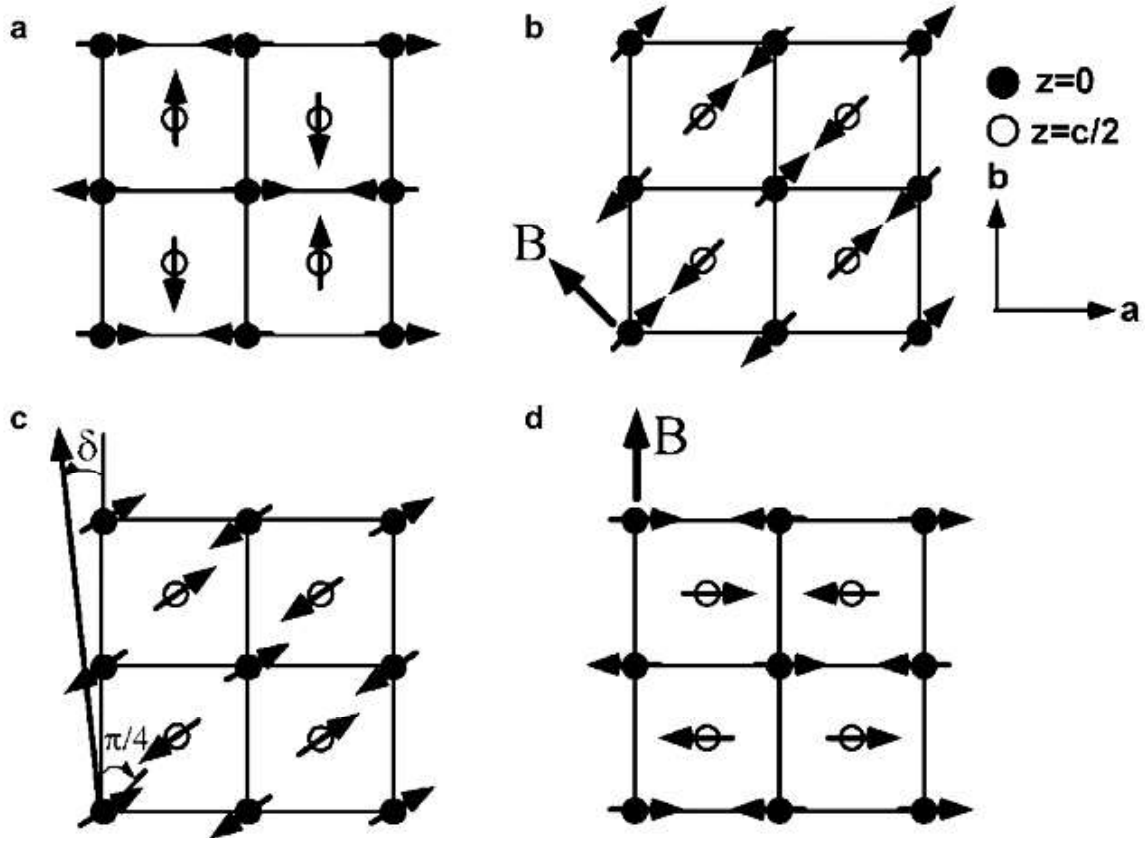

Fig. 1.3 Transition from non- collinear to collinear spin arrangement induced by a magnetic field in Pr_2CuO_4.(a) Non-collinear arrangement of Cu_{2+} spins, (b) Field (B) along the Cu-Cu direction, (c) B tilted from (010), (d) B along (010) (Figure reproduced Ref. [22])

The additional magnetism in the electron doped cuprates can also arise due to the effect of rare earth ions. Different spin structures arise with different rare earth ions as each have a different spin magnitude. In Nd_2CuO_4, Nd has a fairly large magnetic moment and it was observed that it couples with Cu sublattice [24]. Cu spin transitions in Nd_2CuO_4 have shown that the interaction between Nd and Cu spins increase with decrease of temperature [25]. In neutron scattering experiments Bragg reflections corresponding to antiferromagnetic ordering of the in plane oriented Nd moments were

observed below 1 K [26]. The magnetic ordering is caused due to Cu-Cu, Nd-Nd and Nd-Cu interactions. As the temperature is reduced Nd moments grow stronger and the interactions involving Nd becomes more prominent.

1.5. Superconductivity in $Nd_{2-x}Ce_xCuO_4$

The discovery of superconductivity in $Nd_{2-x-y}Sr_xCe_yCuO_4$ at 28 K [27] in 1988 triggered experimental research on $Nd_{2-x}Ce_xCuO_4$. The discovery of superconductivity in $Nd_{2-x}Ce_xCuO_4$ was reported in 1989 by Tokura et.al. [28]. The precursors CeO_2, $Nd_2O_3$and CuO were mixed and calcined at 950° C for 10 hours followed by sintering in air at 1150° C. Superconductivity was obtained only after a reduction annealing at 1000° C in Ar/O_2 ($P_{O2} \sim 8\times10^{-5}$atm) atmosphere for 10hours. The maximum value of superconducting transition temperature (T_C) attained was found to be at 24 K for the optimal doping value of x = 0.15. The lattice parameters were found to be *a* = 3.95 Å and *c* = 12.07 Å. The transport measurements were performed and the hall coefficient in the superconducting sample was found to be negative indicating that the charge carriers are electrons which are introduced by the substitution of tetravalent Ce ions on the trivalent Nd sites[29]. They also observed that superconductivity occurred in a very narrow range of Ce doping from x ~0.14 – 0.18. No superconductivity was observed below and beyond this range. Bulk superconductivity was confirmed via magnetic susceptibility measurement and the highest magnitude of diamagnetic signal observed for x ~ 0.15. Subsequent studies on the polycrystalline material of electron doped cuprates$R_{2-x}Ce_xCuO_4$ (R= Nd, Sm, Pr, Eu) revealed that granularity is an essential feature of these class of compounds and it heavily influences the transport and magnetic properties [30-33].

1.5.1. Transport properties of polycrystalline $Nd_{1.85}Ce_{0.15}CuO_4$ (NCCO)

Above T_C, for polycrystalline NCCO, the resistivity increases with decrease in temperature [34]. Below T_C, the resistance shows double resistive transitions which occurs due to the granular structure which is common in these class of compounds. The resistance drop involves two stages (a) the initial dip in resistance at T_{C1} ~ 24 K (b) and the second dip at T_{C2} ~20 K, these temperatures are more or less the same with a variation ± 2 K as per different reports [34-36]. This has been attributed to individual grains becoming superconducting at $T_{C1}$and inter-granular coupling with Josephson junction tunneling and quasi particle tunneling between the grains becoming prominent at T_{C2}.This behavior has been observed in hole doped superconductors also[37-39]which, however, is related to Aslamazov-Larkin [40] and Maki-Thompson [41] thermodynamic fluctuations and percolation ideas close to the zero resistance state. But, in electron doped superconductors the double transition feature is much more prominent. The double transitions persist and are independent of reducing atmosphere. The NCCO sample preparation has been tried out using simple oxides (CeO_2, $Nd_2O_3$and CuO) as well as using an intermediate oxide like $NdCeO_{3.5}$. The latter was done aiming for better Ce homogeneity. As a result, the normal state resistivity of the samples is found to be lower than that of the samples synthesized with simple oxides. Nonetheless, the double transitions were still found to be present in all the samples [35]. Therefore, the double transition feature in the electron doped cuprates is an intrinsic property of the polycrystalline samples and it is very different from what is seen in the hole doped cuprates. For instance, the zero resistance state of hole doped compounds is not that sensitive to sample preparation technique or oxygen deficiency [42]. But, in electron doped superconductors, the zero resistance and superconducting transitions are sensitive to reduction annealing conditions, the cooling rates, temperature, time etc.,[34,35].

1.5.2. Magnetization of $Nd_{1.85}Ce_{0.15}CuO_4$ (NCCO)

Above T_C, magnetization of bulk NCCO shows paramagnetic behavior. It is also important to note that the effective diamagnetic behavior occurs only below T_{C2} and not at T_{C1}. This leads to the picture that the sample constitutes of small superconducting islands embedded in the insulating matrix because the diamagnetic response is high only when there is significant coupling between the grains as long range superconductivity grows more significantly [43]. Klamutet al.[36] reported the AC Susceptibility studies on NCCO in 1993 (see Figure 1.4) . The imaginary part of AC susceptibility (χ') showed a drop at T_{C1} ~ 23.2 K which was attributed to the superconductivity within the grain, i.e. the intra-granular transition.

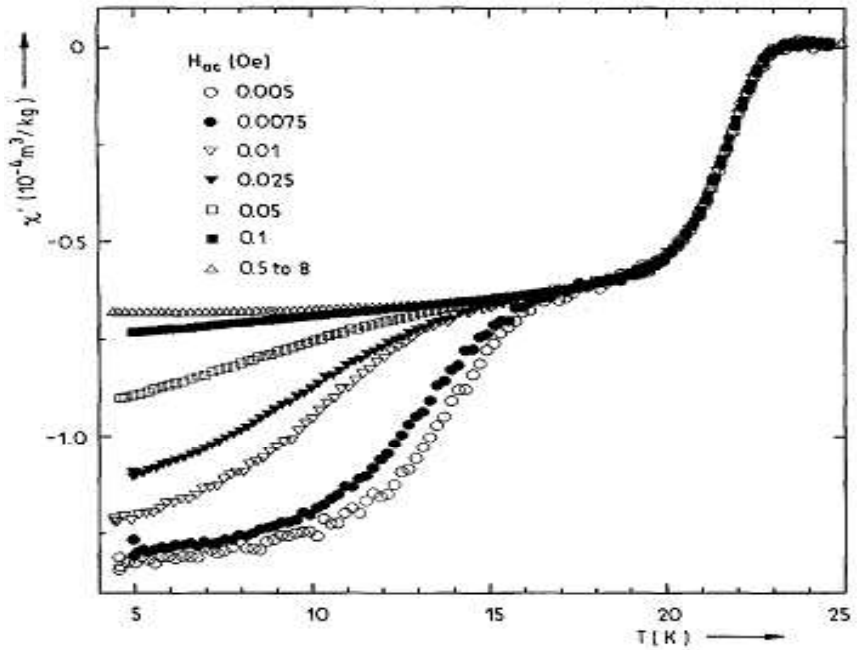

Fig. 1.4 Temperature dependent AC susceptibility of NCCO (reproduced from Reference [35])

They observed the inter-granular transitions at comparatively lower temperatures of 17 K. No temperature dependence of the intra-granular transition was observed in the applied AC magnetic field range of 0.005 to 0.5 Oe. It was also observed that the inter-granular transitions broadened for fields ranging from 0.005 Oe to 0.1 Oe. Above 0.1 Oe the inter-granular transition disappears and only the intra-granular transition was

observed. They also discovered that the coupling between the grains in this material was very weak from the temperature dependence of imaginary AC susceptibility (χ''). From these observations it was seen that the inter-granular critical field of bulk NCCO is very low (~10^{-1}Oe).

1.5.3. Ce and O: the two crucial factors

From the studies conducted on NCCO, it was confirmed that there are two important factors which dictate its electrical and magnetic properties namely Ce and O. Samples prepared with better homogeneity of Ce have lower resistivity values [44]. In addition to that, the samples which were fast cooled during the reduction annealing had better T_{C1} and T_{C2} values than the slow cooled ones and smoother decrease in resistivity when it approaches zero resistance. The Ce diffusion rate at the reduction temperatures of 950°C-1000°C is low [35]. Hence, the change in behavior observed with respect to cooling rate must be dependent on oxygen removal. The oxygen gradient along the grains was found to be higher in the fast cooled samples. This oxygen gradient seems to be crucial as it produces better T_{C1} values. The oxygen gradient should be influencing the coupling of Josephson junctions in the inter-granular regime as well because the T_{C2} values are also found to be increased [44,45]. There are two gradients in consideration here, one is the cationic distribution which decreases from the grain shell to centre as a result of the slow diffusion of Ce and the other is of the anionic distribution which increases (increasing concentration of O) from the grain shell to the centre due to the kinetics involved in the process of oxygen removal. Only an optimization of both these factors gives us better T_C, better superconducting fraction and better inter-granular coupling. This is why preparing NCCO in its most optimized form has always been a challenging process [46].

1.6. Reduction annealing

As it has been discussed in the preceding sections, the electron doped cuprates, in general (and hence NCCO) are very much sensitive to the process of reduction annealing which induces superconductivity in these compounds[47]. The as-grown crystals are never superconducting. Only a small quantity of oxygen is removed via reduction annealing as per literature reports but the impact the process has on the superconducting and magnetic properties is huge [48,49]. The reduction annealing in effect results in contribution of electrons but this process is not equivalent to the addition of tetravalent Ce because one cannot replace the process of annealing with addition of Ce. Annealing process is indispensable for superconductivity. The amount of Oxygen removed ranges from 0.1 % to 2% and when the Ce content increases, the amount of oxygen removed generally is observed to decrease [50,51]

The transition of Cu^{2+}/Cu^{+} with (CuO/Cu_2O) with the emergence of superconductivity was reported by Kim et al.in 1993 [50]. The removal of oxygen from the CuO_2 planes results in localized electrons on the Cu sites near by the oxygen vacancies. It was also reported that annealing NCCO at higher temperatures result in decomposition of sample into Nd_2O_3, $NdCeO_{3.5}$ and Cu_2O [46]. The challenging thing is the fact that the highest T_C was attained only when the reduction conditions take the sample to the verge of decomposition. Therefore, optimizing the reduction conditions for the samples of highest quality involves submitting the sample to the annealing conditions close to decomposition. This is why synthesizing high quality samples NCCO still remains a big challenge. The as-grown samples are antiferromagnetic with T_N~ 100 K for NCCO [5]. The reduction annealing suppresses antiferromagnetism and gives way to superconductivity. The exact mechanism regarding the effect of oxygen and the high sensitivity of the properties of NCCO to the oxygen stoichiometry is still not clear.

One of the mechanisms proposed is that the apical atom in the interstitial site of the *T′* structure acts a strong scattering centre (in Nd_2CuO_4)[49] and is responsible for pair breaking [52]. Radaelliet al.(1994) [49] showed that apical occupancy decreases as a result of reduction. The oxygen loss is lower in the doped compounds in comparison to the undoped compounds. The loss of oxygen in apical positions have been reported for NCCO also [51].

There is a second interpretation which suggests that the in plane 'O(1)' oxygen and out of plane oxygen 'O(2)' ions are removed in the reduction process. Raman studies [53] performed on $Nd_{2-x}Ce_xCuO_4$suggest that the local Raman mode associated with the apical site is not affected by the reduction processes indicating that it is not the apical site oxygen that gets removed contrary to popular consensus. This conclusion was initially put forward by Brinkmannet al.in 1996 from the transport measurements studies carried out on $Pr_{2-x}Ce_xCuO_4$ single crystals. They suggested O(2) ions as the likely site for the vacancies to occur.

A different interpretation was proposed by Kurahashiet al.in 2002 [54]. They reported an impurity phase which appears after reduction and disappears after a re-oxygenation. This phase was later shown to be $(Nd,Ce)_2O_3$ which has undergone epitaxial growth during the reduction process [46]. High resolution transmission electron microscopy studies showed that this parasitic phase was about 60 Å thick and extended for about 1 μm in the CuO_2 plane. It was suggested that the Cu atoms move from these layers to the NCCO structure to repair the defects in the as-grown materials resulting in Cu deficiency in the intercalated parasitic phase. The decrease in concentration of Cu vacancies in the CuO_2 layers, results in removal of pair breaking sites, thus supporting the occurrence of superconductivity[54,55].

1.7. Thin films of NCCO

As discussed earlier, Ce and O are the two crucial factors which influence the properties of NCCO. Thin film growth is very important in this regard because we have better control on the stoichiometry of both the constituents. Thin films have been synthesized by Pulsed Laser Deposition (PLD)[56,57], sputtering [58] and molecular beam epitaxy [59]. The films grown from these techniques are found to result in form of thin films with preferred orientation in some cases [58]and single crystalline thin films in the other cases[59]. The Cerium content in the films are found to be more homogenous compared to single crystals [4]. They can be reduced much more efficiently by annealing methods after deposition, for 10 to 15 minutes and in some cases ex-situ annealing is employed [58]. The transition width observed in most of the films is very small compared to the polycrystalline materials and this is also a consequence of better stoichiometry control. For instance transition width ~ 0.2 K has been observed in $Pr_{2-x}Ce_xCuO_4$ thin films [60]. Films are grown in N_2O and O_2 atmosphere as well. It is seen that films grown in N_2O atmosphere requires lesser reduction annealing time. The highest quality films reported are grown in N_2O atmosphere [57,60]. Recent reports of films in NCCO have shown lower T_C~ 16 K [61]. Films are grown on substrates such as $LaAlO_3$, $SrTiO_3$ and MgO whose lattice parameters are closely matched. The grown films are highly oriented in (001) direction with c axis directed normal to the substrate. There are reports of films grown in [(110) and (103) orientations also [62].

The main drawback associated with thin films prepared by PLD is the growth of parasitic phases [56,57]. On the other hand these phases are absent in films grown by Molecular Beam Epitaxy [59]. Efforts like, using Cu rich targets, have been made to improve the quality of thin films made from pulsed laser deposition [61,63]. This has

resulted in suppression of the parasitic phase and the resistivity value has decreased and the quality is comparable to the best films made by Molecular Beam Epitaxy.

1.8. Effect of Ag addition in Superconductors

The effect of Ag addition has not been studied in electron doped superconductors to the best of our knowledge. A brief review of the effect of Ag addition in some superconductors is presented here.

The effect of Ag addition in modifying the properties of superconductors still remains as a topic of interest and research is still being pursued on that direction in order to improve the superconducting properties [64,65] This can be very important from the point of view of basic research as well as technological applications because Ag is used as cladding for HTSC wires. It has been reported that Ag addition has resulted in improvement of mechanical properties of HTSCs [66,67]. In Sm-Ba-Cu-O systems the tensile strengths of the sample was twice large as that of the sample without Ag. The improvement is caused due to the enhancement in densification and resistance to crack propagation. The Ag addition in YBCO resulted in improved fracture toughness and a higher resistance to thermal shock. It has also been reported that Ag when appropriately added can aid closing the macro-cracks by filling them up [68].

It has been reported that Ag addition increases the intergranular coupling through minimization the area of boundary and grain alignment [69]. Enhancement of critical current density and critical field also has been reported with Ag addition [70,71]. Poonam Rani et al.[71] reported that the surface texture and the grain size increases upon Ag addition. They observed significant amount of Ag residing at the grain boundaries as well. This leads to the conclusion that in the Ag added samples the inter-granular coupling has improved. Even though, as per most of the literature reports, Ag does not get substituted and exists as a different phase, there are some reports suggesting that some

part of Ag gets substituted at Cu sites as well and consequently influences the superconducting properties [72,73].

The effect of Ag addition on the structure and the superconducting properties has been investigated on Iron based superconductors as well like $Sr_{0.6}K_{0.4}Fe_2As_2$[74]and $FeSe_{0.5}Te_{0.5}$[75]. It was seen that Ag improves the inter-grain connections and critical current density. A nominal amount of Ag has entered the crystal structure of $FeSe_{0.5}Te_{0.5}$. In the case of FeSe superconductors, Ag gets added into the grain and there by improves the intra and intergranular superconducting properties. In addition to this, it was also observed that Ag addition suppresses the unwanted hexagonal phase (non-superconducting phase) formation of FeSe and improves critical current density and upper critical field [76,77].

In MgB_2 superconductor, Ag addition has been tried out and this was reported by D Kumar et al.[78]. SEM and TEM studies performed on the samples indicated that Ag resides in the grain boundaries and no Ag content was found within the grains. X-ray diffraction studies showed that apart from MgB_2 peaks they had additional peaks of $AgMg_3$. These small precipitates of $AgMg_3$(~ 20 – 30 nm) were found to be crucial as they could be potential flux pinning centers. They also observed high critical current in their samples.

1.9. Direction of the Thesis

This thesis is divided into six chapters and the content of each chapters are briefly summarized below.

- In the first chapter, a brief overview on electron doped cuprates is presented initially with discussions on the electronic phase diagram, electronic structure and magnetic properties. This is followed by a detailed description of the

electron doped superconductor NCCO, its transport properties and magnetization behavior. The importance of reduction annealing to induce superconductivity in these compounds and the possible mechanisms of the process has also been explained. In addition to this, a brief review on thin films of NCCO and the effects Ag addition on superconductors has also been discussed.

- In the second chapter, the important experimental techniques involved during the course of this thesis work have been discussed. In short, the chapter includes description on the synthesis methods, transport measurement and magnetization measurement set ups.
- As mentioned earlier granularity and annealing conditions are crucial factor which dictates the transport properties of NCCO. In the third chapter effect of granularity and annealing effects on the transport properties of superconducting properties of NCCO has been studied.
- Noting the fact that Ag addition has improved superconducting properties of various superconductors, the effect of Ag addition on the superconducting properties of NCCO has been explored in the fourth chapter of the thesis.
- It has already been discussed that the thin films of electron doped superconductors offer better stoichiometric control and higher quality compared to their bulk counter parts. Hence, in the fifth chapter, aiming towards improving the quality of the sample by minimizing the granular effects, we have ventured into thin films of NCCO. Detailed Magneto transport and magnetization studies have been performed on the same.

1.10. References

[1] H. Alloul, T. Ohno, and P. Mendels, Physical Review Letters **63**, 1700 (1989).

[2] D. S. Fisher, G. Kotliar, and G. Moeller, Physical Review B **52**, 17112 (1995).

[3] J. Orenstein and A. J. Millis, Science **288**, 468 (2000).

[4] N. P. Armitage, P. Fournier, and R. L. Greene, Reviews of Modern Physics **82**, 2421 (2010).

[5] T. Uefuji, T. Kubo, K. Yamada, M. Fujita, K. Kurahashi, I. Watanabe, and K. Nagamine, Physica C: Superconductivity **357-360**, 208 (2001).

[6] G. M. Luke *et al.*, Physical Review B **42**, 7981 (1990).

[7] M. A. Kastner, R. J. Birgeneau, G. Shirane, and Y. Endoh, Reviews of Modern Physics **70**, 897 (1998).

[8] X. Zhang, H. Yu, G. He, W. Hu, J. Yuan, B. Zhu, and K. Jin, Physica C: Superconductivity and its Applications **525-526**, 18 (2016).

[9] P. W. Anderson, Science **235**, 1196 (1987).

[10] B. Dalla Piazza, M. Mourigal, M. Guarise, H. Berger, T. Schmitt, K. J. Zhou, M. Grioni, and H. M. Rønnow, Physical Review B **85**, 100508 (2012).

[11] J. Zaanen, G. A. Sawatzky, and J. W. Allen, Physical Review Letters **55**, 418 (1985).

[12] D. N. Basov and T. Timusk, Reviews of Modern Physics **77**, 721 (2005).

[13] C. M. Varma, S. Schmitt-Rink, and E. Abrahams, Solid State Communications **62**, 681 (1987).

[14] B. Keimer, A. Aharony, A. Auerbach, R. J. Birgeneau, A. Cassanho, Y. Endoh, R. W. Erwin, M. A. Kastner, and G. Shirane, Physical Review B **45**, 7430 (1992).

[15] M. Matsuda, Y. Endoh, K. Yamada, H. Kojima, I. Tanaka, R. J. Birgeneau, M. A.

Kastner, and G. Shirane, Physical Review B **45**, 12548 (1992).

[16] A. Aharony, R. J. Birgeneau, A. Coniglio, M. A. Kastner, and H. E. Stanley, Physical Review Letters **60**, 1330 (1988).

[17] J. W. Lynn and S. Skanthakumar, in *Handbook on the Physics and Chemistry of Rare Earths* (Elsevier, 2001), pp. 315.

[18] D. Petitgrand, S. V. Maleyev, P. Bourges, and A. S. Ivanov, Physical Review B **59**, 1079 (1999).

[19]D. Vaknin, S. K. Sinha, D. E. Moncton, D. C. Johnston, J. M. Newsam, C. R. Safinya, and H. E. King, Physical Review Letters **58**, 2802 (1987).

[20] I. W. Sumarlin, J. W. Lynn, T. Chattopadhyay, S. N. Barilo, D. I. Zhigunov, and J. L. Peng, Physical Review B **51**, 5824 (1995).

[21] X. H. Chen, C. H. Wang, G. Y. Wang, X. G. Luo, J. L. Luo, G. T. Liu, and N. L. Wang, Physical Review B **72**, 064517 (2005).

[22] A. N. Lavrov, H. J. Kang, Y. Kurita, T. Suzuki, S. Komiya, J. W. Lynn, S. H. Lee, P. Dai, and Y. Ando, Phys. Rev. Lett. **92**, 227003 (2004).

[23] T. Wu, C. H. Wang, G. Wu, D. F. Fang, J. L. Luo, G. T. Liu, and X. H. Chen, Journal of Physics: Condensed Matter **20**, 275226 (2008).

[24] A. S. Cherny, E. N. Khats'ko, G. Chouteau, J. M. Louis, A. A. Stepanov, P. Wyder, S. N. Barilo, and D. I. Zhigunov, Physical Review B **45**, 12600 (1992).

[25] M. Matsuura, P. Dai, H. J. Kang, J. W. Lynn, D. N. Argyriou, K. Prokes, Y. Onose, and Y. Tokura, Physical Review B **68**, 144503 (2003).

[26] S. Skanthakumar, J. W. Lynn, J. L. Peng, and Z. Y. Li, Physical Review B **47**, 6173 (1993).

[27] A. Jun, S. Seiichiro, W. Masaru, and S. Hiroshi, Japanese Journal of Applied Physics **27**, L1859 (1988).

[28] Y. Tokura, H. Takagi, and S. Uchida, Nature **337**, 345 (1989).

[29] H. Takagi, S. Uchida, and Y. Tokura, Physical Review Letters **62**, 1197 (1989).

[30] A. Gerber, J. Beille, T. Grenet, and M. Cyrot, EPL (Europhysics Letters) **12**, 441 (1990).

[31]A. Gerber, T. Grenet, M. Cyrot, and J. Beille, Physical Review B **43**, 12935 (1991).

[32] T. Grenet and M. Cyrot, Applied Superconductivity **1**, 925 (1993).

[33] C. L. Seaman *et al.*, Physica C: Superconductivity **159**, 391 (1989).

[34] R. F. Jardim, L. Ben-Dor, and M. B. Maple, Journal of Alloys and Compounds **199**, 105 (1993).

[35] R. F. Jardim, E. A. Early, and M. B. Maple, Journal of Alloys and Compounds **221**, 1 (1995).

[36] P. W. Klamut, physica status solidi (a) **136**, 181 (1993).

[37] M. Ausloos and C. Laurent, Physical Review B **37**, 611 (1988).

[38] P. P. Freitas, C. C. Tsuei, and T. S. Plaskett, Physical Review B **36**, 833 (1987).

[39] S. E. Inderhees, M. B. Salamon, N. Goldenfeld, J. P. Rice, B. G. Pazol, D. M. Ginsberg, J. Z. Liu, and G. W. Crabtree, Physical Review Letters **60**, 1178 (1988).

[40] A. I. Larkin, Soviet Physics Uspekhi **13**, 407 (1970).

[41] R. S. Thompson, Physical Review B **1**, 327 (1970).

[42] M. Hervieu, B. Domengès, B. Raveau, M. Post, W. R. McKinnon, and J. M. Tarascon, Materials Letters **8**, 73 (1989).

[43] E. A. Early, C. C. Almasan, R. F. Jardim, and M. B. Maple, Physical Review B **47**, 433 (1993).

[44] T. Williams, Y. Maeno, I. Mangelschots, A. Reller, and G. Bednorz, Physica C: Superconductivity **161**, 331 (1989).

[45] F. Izumi, Y. Matsui, H. Takagi, S. Uchida, Y. Tokura, and H. Asano, Physica C:

Superconductivity **158**, 433 (1989).

[46] P. K. Mang *et al.*, Physical Review B **70**, 094507 (2004).

[47] P. W. Klamut, A. Sikora, Z. Bukowski, B. Dabrowski, and J. Klamut, Physica C: Superconductivity **282-287**, 541 (1997).

[48] E. Navarro, D. Jaque, J. E. Villegas, J. I. Martín, A. Serquis, F. Prado, A. Caneiro, and J. L. Vicent, Journal of Alloys and Compounds **323-324**, 580 (2001).

[49] P. G. Radaelli, J. D. Jorgensen, A. J. Schultz, J. L. Peng, and R. L. Greene, Physical Review B **49**, 15322 (1994).

[50] J. S. Kim and D. R. Gaskell, Physica C: Superconductivity **209**, 381 (1993).

[51] A. J. Schultz, J. D. Jorgensen, J. L. Peng, and R. L. Greene, Physical Review B **53**, 5157 (1996).

[52] X. Q. Xu, S. N. Mao, W. Jiang, J. L. Peng, and R. L. Greene, Physical Review B **53**, 871 (1996).

[53] P. Richard, G. Riou, I. Hetel, S. Jandl, M. Poirier, and P. Fournier, Physical Review B **70**, 064513 (2004).

[54] K. Kurahashi, H. Matsushita, M. Fujita, and K. Yamada, Journal of the Physical Society of Japan **71**, 910 (2002).

[55] H. J. Kang *et al.*, Nature Materials **6**, 224 (2007).

[56] A. Gupta, G. Koren, C. C. Tsuei, A. Segmüller, and T. R. McGuire, Applied Physics Letters **55**, 1795 (1989).

[57] S. N. Mao *et al.*, Applied Physics Letters **61**, 2356 (1992).

[58] A. Guarino, G. Patimo, A. Vecchione, T. Di Luccio, and A. Nigro, Physica C: Superconductivity **495**, 146 (2013).

[59] M. Naito, H. Sato, and H. Yamamoto, Physica C: Superconductivity **293**, 36 (1997).

[60] E. Maiser, P. Fournier, J. L. Peng, F. M. Araujo-Moreira, T. Venkatesan, R. L. Greene, and G. Czjzek, Physica C: Superconductivity **297**, 15 (1998).

[61] M. Hoek, F. Coneri, D. P. Leusink, P. D. Eerkes, X. R. Wang, and H. Hilgenkamp, Supercon. Sci. Technol. **27**, 044017 (2014).

[62] A. I. Ponomarev, T. B. Charikova, G. I. Kharus, N. G. Shelushinina, A. O. Tashlykov, A. V. Tkach, and A. A. Ivanov, The Physics of Metals and Metallography **104**, 67 (2007).

[63] G. Roberge, S. Charpentier, S. Godin-Proulx, P. Rauwel, K. D. Truong, and P. Fournier, Journal of Crystal Growth **311**, 1340 (2009).

[64] A. Galluzzi, M. Polichetti, K. Buchkov, E. Nazarova, D. Mancusi, and S. Pace, Superconductor Science and Technology **30**, 025013 (2017).

[65] B. A. Malik, M. A. Malik, and K. Asokan, Current Applied Physics **16**, 1270 (2016).

[66] C. Leblond-Harnois, R. Caillard, I. Monot-Laffez, G. Desgardin, and B. Raveau, Physica C: Superconductivity **341-348**, 2439 (2000).

[67] N. Sakai, A. Mase, H. Ikuta, S. J. Seo, U. Mizutani, and M. Murakami, Superconductor Science and Technology **13**, 770 (2000).

[68] N. D. Kumar, T. Rajasekharan, and V. Seshubai, Superconductor Science and Technology **24**, 085005 (2011).

[69] P. Rani, R. Jha, and V. P. S. Awana, Journal of Superconductivity and Novel Magnetism **26**, 2347 (2013).

[70] S. Hadi, A. B.-B. Ali, and S. Medhi, Superconductor Science and Technology **14**, 816 (2001).

[71] P. Rani, A. Pal, and V. P. S. Awana, Physica C: Superconductivity and its Applications **497**, 19 (2014).

[72] C. Zhang, A. Kulpa, and A. C. D. Chaklader, Physica C: Superconductivity **252**, 67 (1995).

[73] P. d. Azambuja, P. Rodrigues JÃºnior, A. R. Jurelo, F. C. Serbena, C. E. n. Foerster, R. n. M. Costa, G. B. d. Souza, C. M. c. Lepienski, and A. L. Chinelatto, Brazilian Journal of Physics **39**, 638 (2009).

[74] W. Lei, Q. Yanpeng, G. Zhaoshun, W. Dongliang, Z. Xianping, and M. Yanwei, Superconductor Science and Technology **23**, 025027 (2010).

[75] M. Migita, Y. Takikawa, K. Sugai, M. Takeda, M. Uehara, T. Kuramoto, Y. Takano, Y. Mizuguchi, and Y. Kimishima, Physica C: Superconductivity **484**, 66 (2013).

[76] E. Nazarova, N. Balchev, K. Nenkov, K. Buchkov, D. Kovacheva, A. Zahariev, and G. Fuchs, Superconductor Science and Technology **28**, 025013 (2015).

[77] E. Nazarova, K. Buchkov, S. Terzieva, K. Nenkov, A. Zahariev, D. Kovacheva, N. Balchev, and G. Fuchs, Journal of Superconductivity and Novel Magnetism **28**, 1135 (2015).

[78] D. Kumar, S. J. Pennycook, J. Narayan, H. Wang, and A. Tiwari, Superconductor Science and Technology **16**, 455 (2003).

Chapter 2

Experimental methods

This chapter deals with sample synthesis methods and experimental techniques utilized for the thesis work. Polycrystalline samples of $Nd_{1.85}Ce_{0.15}CuO_4$ in bulk and thin film forms were used in this thesis work. Superconductivity has been achieved and the observed critical temperatures are 24 K and 14 K for bulk and thin film samples respectively. The bulk samples were synthesized using the solid state reaction route and for thin films Pulsed Laser deposition was employed. The samples were characterized by powder X-ray diffraction measurements in laboratory and also by using Synchrotron sources at INDUS II. Scanning Electron Microscopy was used to study the surface morphology and calculation of grain size. Preliminary resistivity characterizations were done by a Dipper Cryostat (by the dipstick method). Magneto transport measurements were performed in commercial cryogen free 15 T Magneto Resistance Set up. Magnetization measurements were performed using a commercial Vibration Sample Magnetometer (VSM) and SQUID VSM.

2.1. Bulk sample preparation

Solid state reaction route was used for the preparation of polycrystalline samples of $Nd_{1.85}Ce_{0.15}CuO_4$ which was followed by repeated air annealings and a final reduction stage in Ar atmosphere. The details regarding this process are explained in Chapter 3.

2.2. Preparation of thin films – Pulsed Laser Deposition

Pulsed Laser deposition has gained a lot of attention because it is quite suitable for the growth of high quality superconducting thin film oxides [1]. Stoichiometric transfer which happens between target and substrate is one of its important advantages. A variety of materials can be deposited like High T_C superconductors, oxides, nitrides, carbides,

semiconductors metals and polymers also [2]. It is possible to tune different kind of thin film properties like stress, textures, reflectivity and magnetic properties by changing the kinetic energy of deposited particles.

The schematic diagram of a Pulsed Laser deposition system is shown in Figure. 2.1. In a high vacuum chamber, a highly focused and pulsed laser beam is made incident on a target at an angle of 45 °. The atoms and ions ablated from the targets are deposited on substrates. These substrates are attached with its surface parallel to the target surface. The target to substrate distance is typically around 2 – 5 cm.

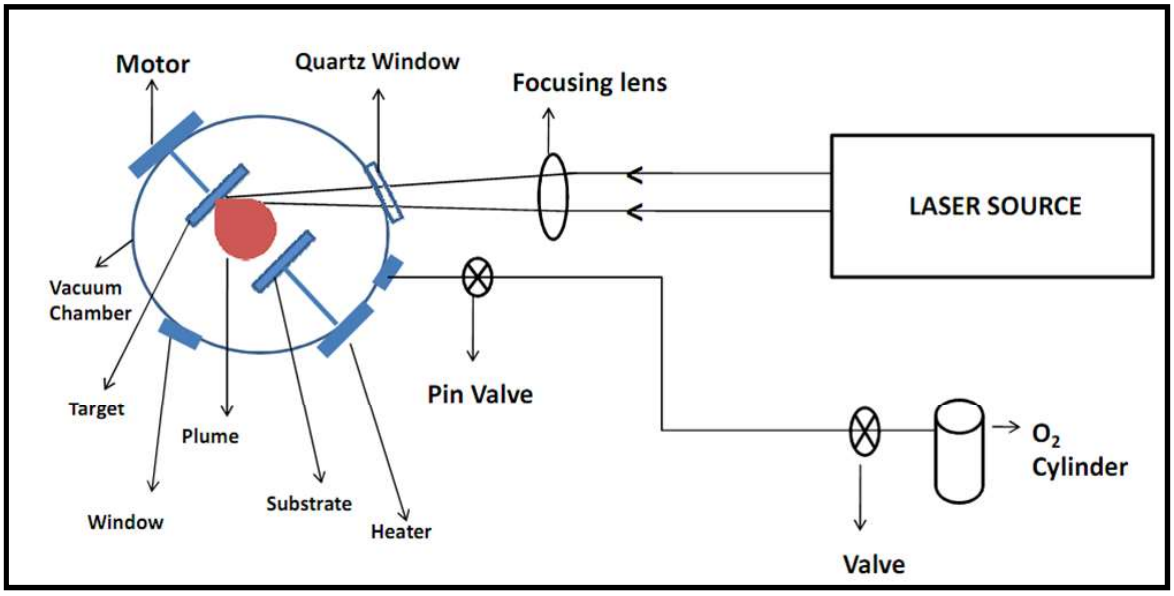

Fig. 2.1 Schematic diagram of our Pulsed Laser Deposition Set up

2.3. Growth of thin films

The deposition of thin films is performed in a suitable environment (in our case, O_2 atmosphere) containing gas or gas mixtures. The laser source used for the depositions was a KrF Excimer Laser. The important constituents of the set up are briefly explained below:

2.3.1. The Laser source – Excimer Laser

The term Excimer means a molecular complex of two excited atoms which is stable only in an electronically excited state. These lasers are pulsed lasers and they have

an output which belongs to the ultraviolet region. XeFl (351 nm), XeCl (308 nm), KrF (248 nm) and KrCl (222 nm) are some of the lasers which fall into this family. The formation of Excimer molecules happen in the mixture of component gases. Energy is pumped in to the gas through electrical stimulation (electric discharge excitation). As a result, the ions and electronically excited species react, leading to the formation of Excimer molecules. These molecules which can exist only in the excited state are the source of laser. The important gas collision and photon processes involved in producing Excimer molecules for suitable laser action are as follows:

Pumping:

$e^- + Kr \rightarrow Kr^+, Kr^*, Kr^{2+}$	[Positive rare gas ion production (Kr^+) and Rare gas metastable production (Kr^*)]
$F_2 + e^- \rightarrow F^- + F$	[Negative halogen ion production]
$Kr^+ + F + M \rightarrow KrF^* + M$	[KrF production, M represents a third body (He, Ne)]
$Kr^* + F_2 \rightarrow KrF^* + F$	[KrF production]

Stimulated emission:

$KrF^* + h\nu \rightarrow Kr + F + 2h\nu$	[Laser emission]

The excited KrF* molecules will decay via spontaneous emission of a photon into Kr and F. These from the ground state which is bonded covalently and contains Kr and F atoms separately. The components Kr and F are available for another excitation cycle [3].

2.3.2. The Laser Beam

The beam should be homogeneous. It should have sufficiently high energy density and short pulse duration so that all the elements in the target are heated up to their

evaporation temperature. Materials in the target are dissociated and ablated out with nearly the same stoichiometry as that of the target material.

2.3.3. Target material

The target material is prepared from sintered pellets, pressed powders, single crystals etc. The target quality is important for synthesizing high quality thin films. It is preferable to have targets with high density and smooth surface. During the deposition the target is rotated by the help of a motor in order to minimize the consumption/erosion of the target.

2.3.4. The Plume

The laser ablation constitutes of three stages[1]:

First stage →Photon absorption at the target surface where the incident laser energy is converted into thermal, chemical and mechanical energy. The temperature of the irradiated area rises up to several thousands of Kelvin, at the rate of 10^{11} K/s, due to the ultraviolet irradiation of the Excimer Laser.

Second stage →It consists of target material vaporization and plasma formation. Species in the heated area are ejected from the target during the multi photon ionization of the gaseous phase leading to the creation of a characteristic plume. These ejected species continually absorb the incident laser light, resulting in a strong interaction between the plume and the incident laser beam.

Third stage →The third stage involves the expansion of the plume after the laser pulse. Ejected atoms, molecules, electrons, ions and particulates flow away from the target surface at high mass transport velocity and collide with the ambient gas molecules or atoms. These processes depend on laser energy, power density, pulse duration, repetition rate and on the properties of target as well.

2.3.5. Background gas

The use of a background gas is classified into active and passive background gas. The passive type is used to compensate the loss of a constituent element during deposition. For instance, oxides are usually deposited in O_2 atmosphere.

2.3.6. Substrate

The ablated target via the action of the plume is coated on to a substrate. The substrate is kept parallel and opposite to the target. The substrate is maintained at a necessary temperature with a heater attached to the substrate holder. Optimum substrate temperature for deposition is dependent on the nature of the target material. Heating of the substrate is essential for adhesion, preservation of stoichiometry of the films and rate of crystallization. The substrate to target distance also is an important factor as the best sample quality is obtained when this distance is neither very small nor very large compared to the plume length.

2.3.7. Pulse frequency

The pulse frequency is important when the deposition is carried out at higher temperatures. If the period of pulsing is larger than the time constant related to diffusion, dissociation etc., the pulse frequency will not have much effect on the sample.

2.3.8. Surface profile measurement – Dektak 3030

The Dektak 3030 Surface Profilometer is an instrument to measure the vertical profile of samples, thin film thickness, roughness etc. A diamond stylus is moved vertically into in contact with the sample and then moved laterally across the sample for a specified distance and specified contact force. The instrument can measure small surface variations in vertical stylus displacement as a function of position. The height position of the diamond stylus generates an analog signal which is converted into a digital signal stored, analyzed and displayed. The radius of diamond stylus is 12.5 microns, and the horizontal resolution is controlled by the scan speed and scan length. The vertical

resolution is 0.1 nm. A particular region of the substrate is masked during deposition. Hence after deposition, this region is devoid of coating. Hence, the surface profilometer, while laterally scanning the sample picks up this surface variation (variation between the coated region and the region devoid of coating) and gives us the thickness value.

2.4. Characterization: X–Ray Diffraction (XRD) and Scanning Electron Microscopy (SEM)

2.4.1. X – Ray Diffraction

All the samples used for the present thesis work were characterized for the phase purity using XRD measurements. A STOE diffractometer (X–ray used is Cu − K_α) operated with a power of 40kV and 30 mA, in the Bragg Brentano Geometry was used for initial characterization of the samples. For extracting the lattice parameters, we have used the *PowderCell software*[4]. Advancing in this direction, to get high quality XRD data, to perform Rietveld Structural Refinement, XRD measurements were performed using BL-12 beam-line of Indus II Synchrotron source, RRCAT – Indore. The experiment was carried out in transmission Debye-Scherrer geometry wherein x-rays of a defined energy were incident on the sample enclosed in a circular depression in kapton tape and the data was collected using a MAR 3450 image plate detector positioned beyond the sample. The energy of the incident x-ray and the sample to detector distance are 12.6 keV and 120 mm respectively. The 2D image plate data was converted into a 1D 2θ vs. intensity format using FIT2D software[5].

BL-12 beam-line was also employed for carrying out XRD measurements on thin films which form a part of this thesis. These measurements were performed in θ − 2θ mode using a six circle diffractometer (Huber – 5020) with NaI scintillation detector. Typical powder XRD patterns of bulk $Nd_{1.85}Ce_{0.15}CuO_4$ and thin films of $Nd_{1.85}Ce_{0.15}CuO_4$ recorded from BL-12 are shown in Figure 2.2.

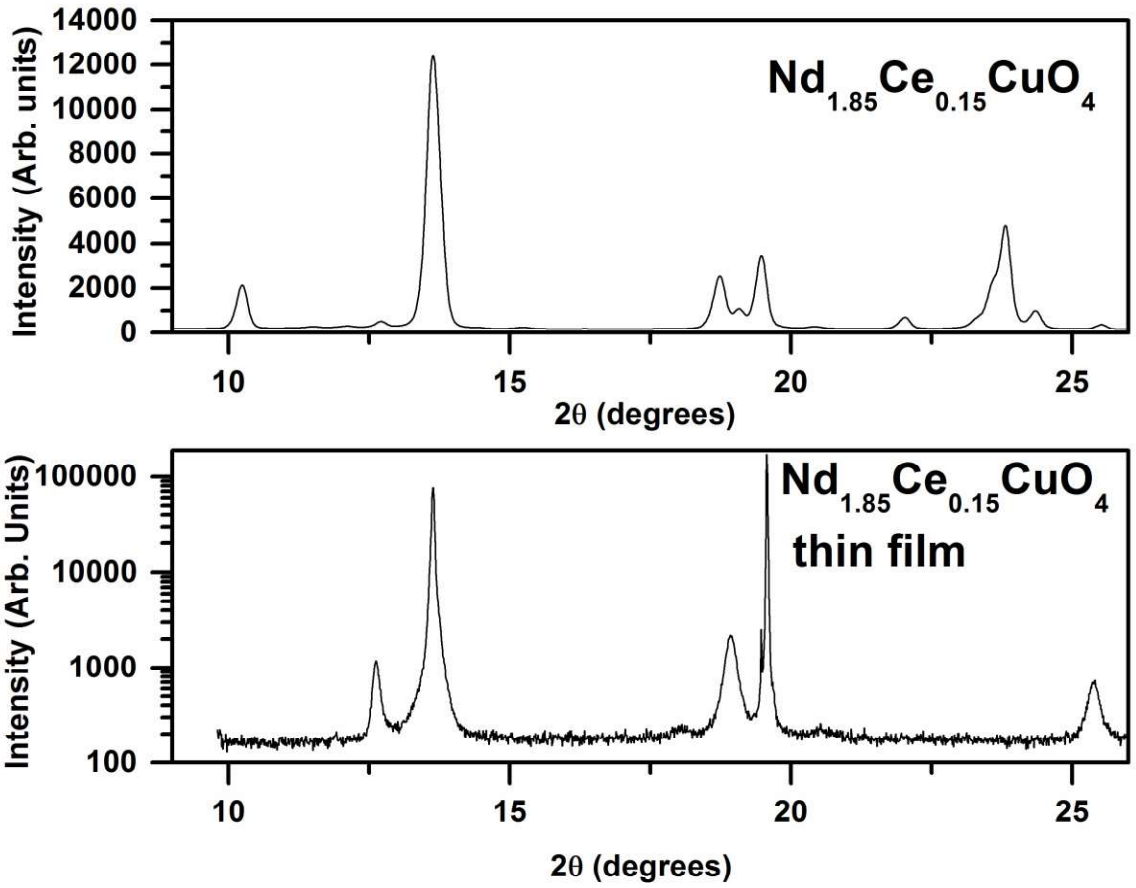

Fig. 2.2 Typical XRD patterns of NCCO (bulk and thin film) recorded in BL-12 at Indus II synchrotron source, RRCAT, Indore.

2.4.2. Scanning Electron Microscopy

A scanning electron microscope (SEM) uses a focused electron beam which scans over a surface and creates an image. It offers high resolution to the range of less than 1 nm [6]. The electrons in the beam interact with the sample, producing various signals which give us information about surface morphology and composition. A schematic diagram of SEM is shown in Figure 2.3. The major components of SEM are the following:

Electron Source

Electrons are produced at the source by thermionic heating. These electrons are accelerated to very high voltages (kV range) and then condensed into a narrow beam which is used for imaging. The sources used usually are, tungsten filament, solid state crystal (like LaB_6) and field emission gun

Lenses

A series of lenses condenses the beam which moves from the source down the column. The more narrow the beam is, small will be the associated spot when it contacts the surface

Scanning coils

They deflect the beam in X and Y direction thereby enabling scans in a raster fashion on the samples

Sample chamber

Sample is mounted in a chamber which is evacuated. It can include, translation stage, tilt and rotation devices, temperature stages, optical cameras and other devices to help the imaging process

Detectors

When the electron beam interacts with the sample, multiple events occur. Detectors of different type are required to detect secondary electrons, backscattered electrons and characteristic X-rays. The signals come from different penetration depths depending upon accelerating voltage and sample density.

Secondary electron detector (SED) is used to create topographical SEM image. The SEM images are of high resolution and are created from inelastically scattered electrons close to the surface of the sample. No material composition information is available.

A back scattered electron detector (BSD) detects electrons which are elastically scattered. These electrons are higher in energy from the atoms below the surface of the sample. Back scattered electrons vary in their quantity and direction depending upon the composition and topography of the specimen. The contrast of the back scattered image

depends on atomic number (Z) of the sample, accelerating voltage of the primary beam and sample angle with respect to the primary beam.

Energy dispersive Spectroscopy (EDS)

In SEM, X – rays are emitted when electrons are displaced from an inner shell and that is replaced by electrons in the outer shell. For each element, this energy difference is unique [7]. Hence this technique is used for element identification. The EDS spectrum gives us the plot of intensity of X-rays for each of the energy emitted. From this spectrum we can calculate the atomic weight percentage and hence the stoichiometry of the various elements present in the sample.

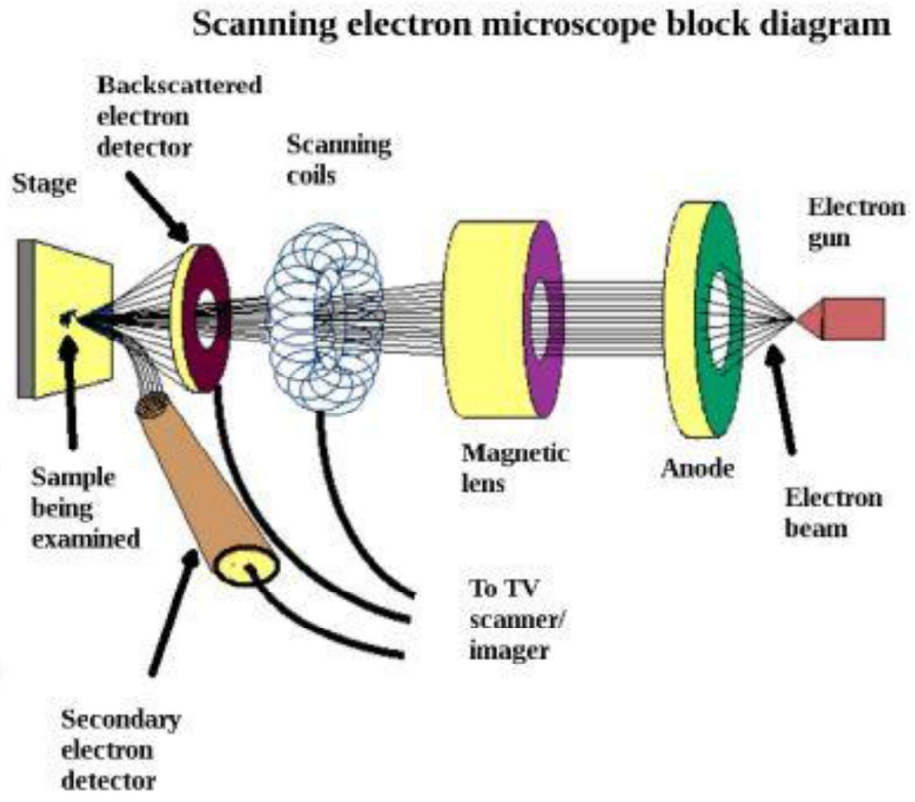

Fig. 2.3 Schematic diagram of SEM. (The figure has been reproduced from Reference [6])

2.5. Electrical Resistivity

The resistivity of the synthesized samples was measured by the Van der Pauw method [8]. The four Van der Pauw configurations used for resistivity measurement is represented schematically in Figure 2.4.

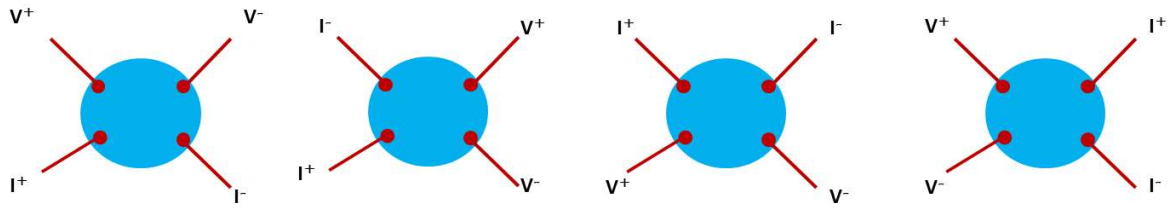

Fig. 2.4 The four Van der Pauw configurations used for resistivity measurements. I+, I- stand for current and V+, V- stand for voltage

The resistivity ρ at a particular temperature is determined by solving the following equation iteratively

$$e^{\frac{-\pi r_1}{\rho t}} + e^{\frac{-\pi r_2}{\rho t}} = 1 \qquad (2.1)$$

Where r_1 and r_2 are the resistance values from different van der Pauw configurations and t is the thickness of the sample. The set up consists of a dipstick, the Helium Dewar ((see Figure 2.5 (a)), the current sources and nano voltmeters. The sample is mounted in an OFHC (Oxygen free high conductivity) copper block with the help of a double sided sticky tape ((see Figure 2.5 (b)). 44 SWG copper wires, de-enameled at the ends are used as leads and the contacts are made on the sample using silver paste. The other end of the leads are connected to the current source and nano-voltmeter through a connector mounted on the dipstick. A calibrated Si diode thermometer which is also fixed in the copper block is used to record temperature. The sample is mounted in close vicinity to the thermometer in order to avoid any thermal gradients. Dewar contains liquid Helium where the liquid bath is at 4.2 K (boiling point of liquid Helium) and the neck of the Dewar is at 300 K. The dipstick with the sample mounted is then attached to the neck of the Dewar using clamps and then slowly dipped inside while resistance is measured

throughout the process. Hence resistance can be measured throughout the temperature range from 300 K to 4.2 K. The resistance of the sample is measured by passing a steady DC of few mA through it, measuring the voltage drop across the sample and converting it into resistance using the formula R = V/I. A DC of 10μA is passed through the Si diode sensor and the resulting voltage drop across it is used for calculating temperature using pre-calibrated Chebyshev polynomial coefficients. The sample voltage and the Si diode voltage are measured simultaneously by using the respective nano-voltmeters at the same instant using a *LabView* program through GPIB interface with the computer. The measured voltage across the sample will include an additional thermo-emf component (as contacts are involved). For a current I^+, the measured voltage V^+ is given by

$$V^+ = V^+_{sample} + V_{thermo} \tag{2.2}$$

To eliminate this thermo emf, the current is reversed and we calculate V^-, noting that the thermo emf is independent of voltage.

$$V^- = V^- + V_{thermo} \tag{2.3}$$

The two voltages are subtracted and the modulus of the average is taken as the final voltage and the resistance is given by

$$R = V/I \tag{2.3}$$

where $V = (|V^+ - V^-|)/2$

The data is collected throughout the dipping process until the sample reaches the liquid Helium bath where the minimum temperature of 4.2 K is reached.

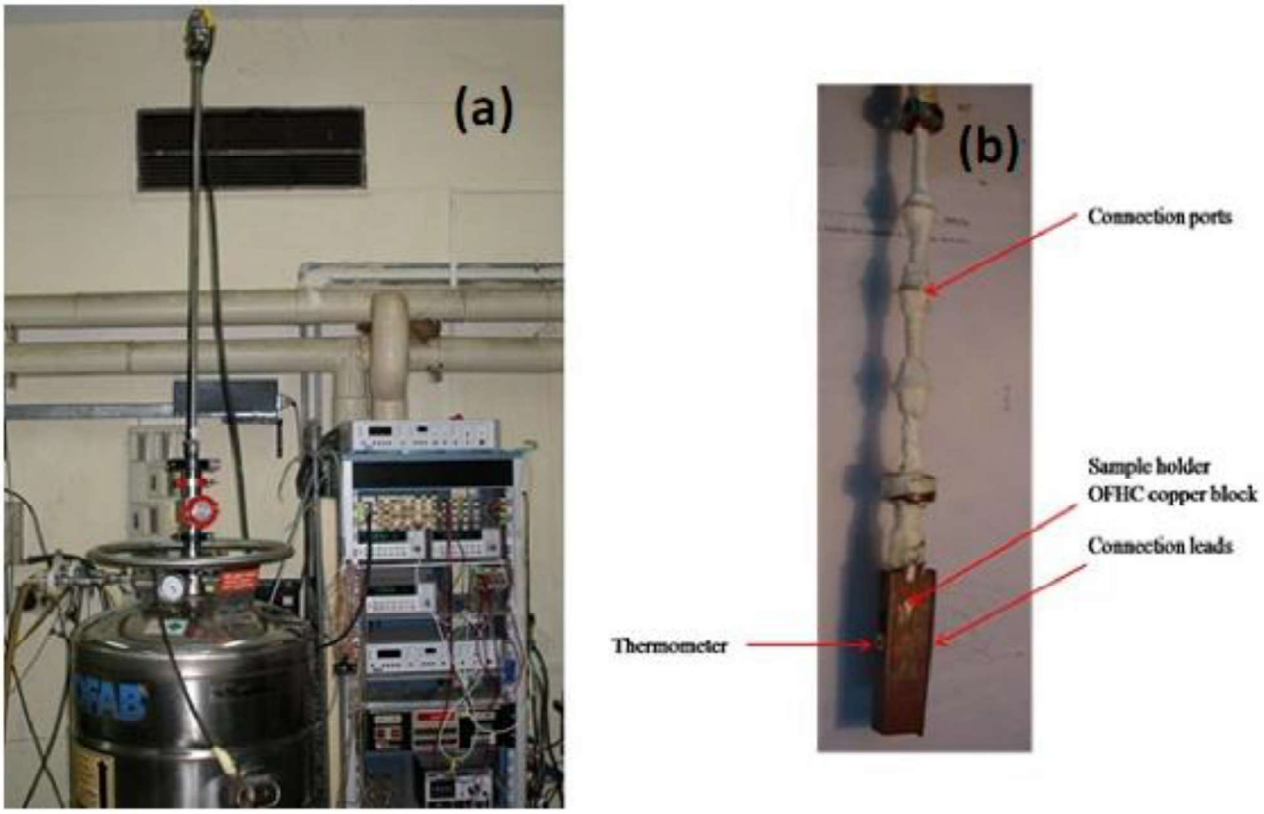

Fig. 2.5 (a) The Dip stick Resistivity Measurement Set up (b) The Sample holder portion

In Figure 2.6, the resistance of a typical $YBa_2Cu_3O_7$ (YBCO) film with respect to temperature, measured in this dipstick system has been shown.

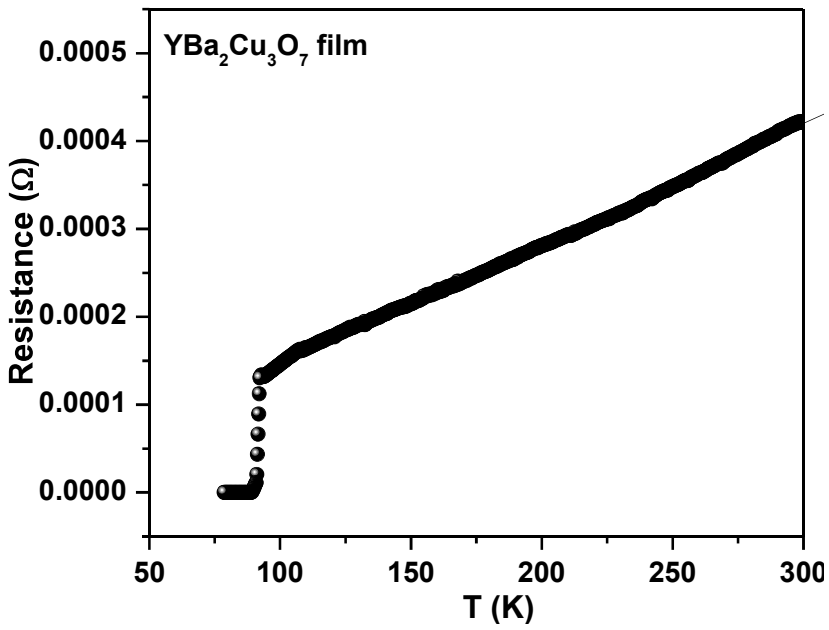

Fig. 2.6 Resistance vs. Temperature plot of a YBCO film

2.6. Magneto Transport

Magneto-transport measurements were carried out in a commercial cryogen free 15 T MR system from Cryogenics Ltd., UK. The setup is shown in Figure 2.7. Cryogen-free magnet system includes a Cryostat and a Superconducting magnet. The magnet is a vertically oriented solenoid wound from copper stabilized filamentary superconducting wire either NbTi only (low field) or NbTi with Nb_3Sn (high field). The magnet is energized via high temperature superconducting current leads. The temperature of the magnet is monitored with the help of temperature sensors mounted at various positions. As mentioned earlier the system is cryogen free. A Pulse tube refrigerator (two stage cryo cooler) is used for cooling the whole system from the 300 K to base temperature. The first stage cools the radiation shield which surrounds the low temperature parts in the system and the second stage is used to cool the magnet and the variable temperature insert (VTI).

Fig. 2.7 The commercial 15T Cryogen free Magneto-resistance set-up from Cryogenic Ltd., UK for carrying out magneto-resistance measurements

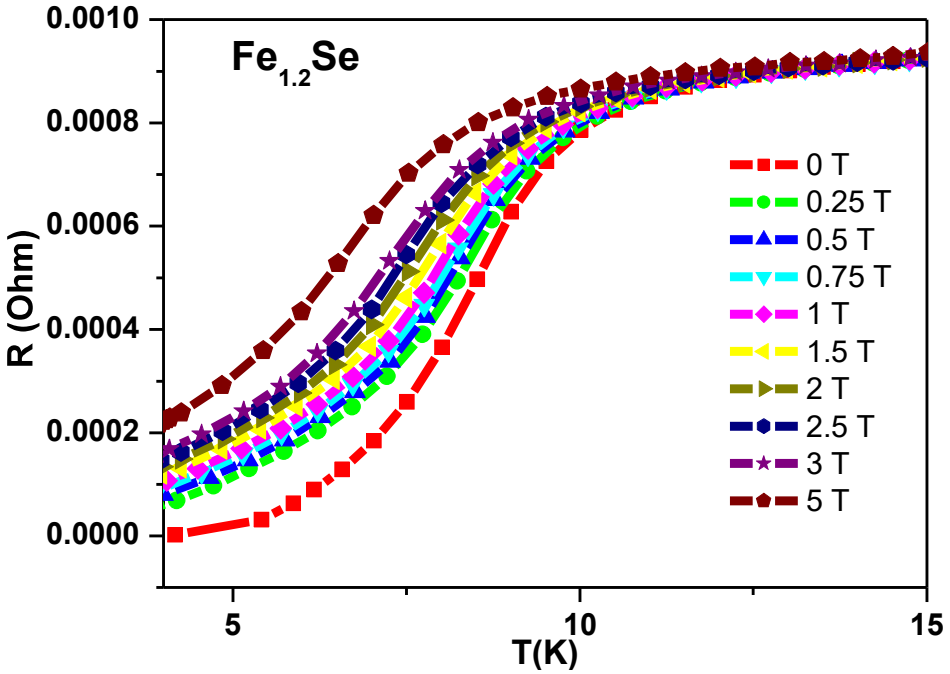

Fig. 2.8 Resistance vs Temperature plot of Fe1.2Se at various fields

The VTI helps in regulating the temperature of the sample from the 1.6 K to 325 K. The major electronic units involved in functioning of this system are the temperature controller, Keithley 2700 multimeter and Magnet controls (Cryogenics Ltd.) The measurement probe platform has two sample sockets, a calibrated CERNOX sensor and a separate 100 Ω heater. Figure 2.7 represents the temperature dependent resistance measurements as a function of different magnetic fields of polycrystalline $Fe_{1.2}Se$ superconductor, measured in this set up.

2.7. Magnetization Measurements

2.7.1. Vibration Sample Magnetometer

The magnetization measurements were performed using a 16 T liquid helium based Vibrating Sample Magnetometer (VSM), which is shown in Figure 2.9. The schematic diagram of VSM is shown in Figure 2.10. The cryostat constitutes a single vacuum insulated chamber with one inner helium reservoir (100 liters capacity) and an outer liquid nitrogen jacket (90 liters capacity) in it. For minimizing the radiation loss, high purity aluminum radiation shields are surrounded by a super-insulation blanket of

alternative layers of reflective aluminized-mylar and nylon netting .The superconducting magnet is a vertically oriented solenoid wound from copper stabilized filamentary superconducting wire of NbTi with Nb_3Sn. The magnet is cooled by liquid helium through tubes wound along with the magnet from the bottom of the liquid helium reservoir (figure 2.10 (a)).

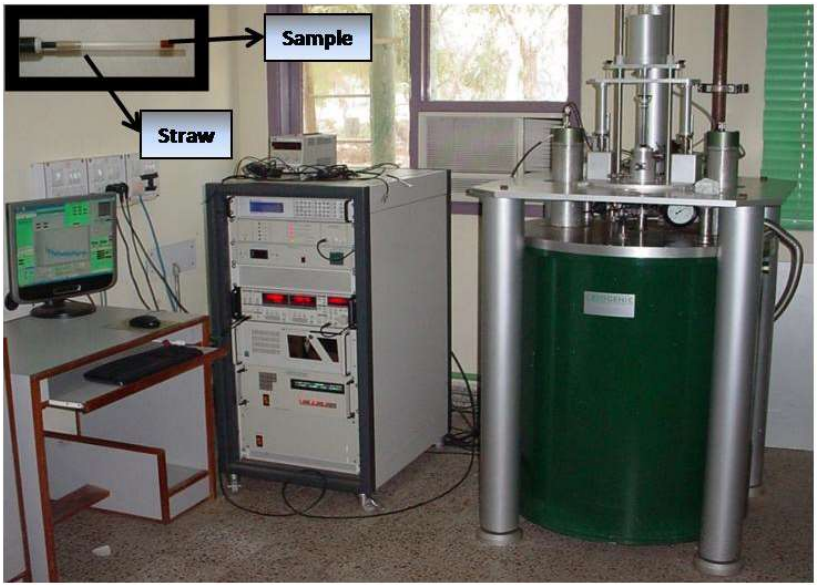

Fig. 2.9 The VSM set up. Cryogenic Ltd. In the inset the non magnetic straw is shown where the sample is mounted

The cryostat has a variable temperature insert (VTI) to operate in the temperature range of 1.6-325 K. The VTI is fitted inside the central bore of the magnet A Cernox thermometer and a heater are fitted at the bottom of VTI. The VTI is connected to a helium reservoir via a small capillary tube and the helium pot is connected to the helium reservoir through a needle valve (see figure 2.10 (a)). The needle valve is adjusted manually to control the flow of liquid He to the pot. The temperature of the VTI is controlled by controlling the heater power at the VTI bottom by a *LakeShore (Model 340)* temperature controller. An oil-free rotary vacuum pump, connected to the VTI outlet is used to drive back the He gas to the recovery line. The sample loaded inside the sample chamber, is in thermal contact with the VTI via static helium exchange gas. The sample

chamber has an internal diameter of 14 mm, and the temperature of the sample is monitored by a Cernox thermometer. A small vibrator provides the sinusoidal vertical motion of the sample within the pickup coils. The frequency of vibration is around 20 Hz and the amplitude around 1 mm. A small permanent magnet is mounted inside the vibrator on the driving rod which vibrates near a reference coil.

2.7.2. Measurement using VSM

Firstly, the vacuum space of the VSM is pumped down to 10^{-3} mbar before the cooling process. The cryostat is first pre-cooled with liquid nitrogen, before cooling with liquid helium. For pre-cooling the cryostat is filled with liquid nitrogen and is kept as such for roughly a day so that the sufficient cooling of the radiation shields and super insulations are insured. The liquid nitrogen is then removed by pressurizing the cryostat with nitrogen gas. The heater mounted at the base of the reservoir will boil any left of liquid nitrogen. As the liquid nitrogen is completely removed, the cryostat is purged twice or thrice with helium. After the purging, liquid helium is transferred. With the transfer of liquid helium, the temperature of the He reservoir decreases and once it reaches 4.2 K, the liquid He gets collected and there is an increase in He transfer rate. The capillary tubes from the helium reservoir are used to cool the magnet and VTI with liquid He (see figure 2.10 (a)).

The sample is loaded for measurement after cooling. The sample is mounted on a non-magnetic plastic straw and attached to the lower end of a rod (shown inset of the figure-2.9). This is made to oscillate vertically. If the sample has some magnetic moment and responses to the external applied field, it induces an AC signal in the pickup coils. The amplitude of the signal is directly proportional to the magnetic moment of the sample. The pick-up signal is fed to the lock-in amplifier (LIA) which is tuned to lock the signal precisely at the sample's vibration frequency using a reference signal from the

vibrator control. The pick-up coil is wound in such that, an external field would induce equal and opposite voltages producing no overall signal. When we move a magnetic sample vertically through the center of the pickup coils, in upward direction, the flux will increase for one set of coils and decrease for the other. Once the sample is centered, we use the LabView software, where we can run the already written sequence of programs for the required measurements.

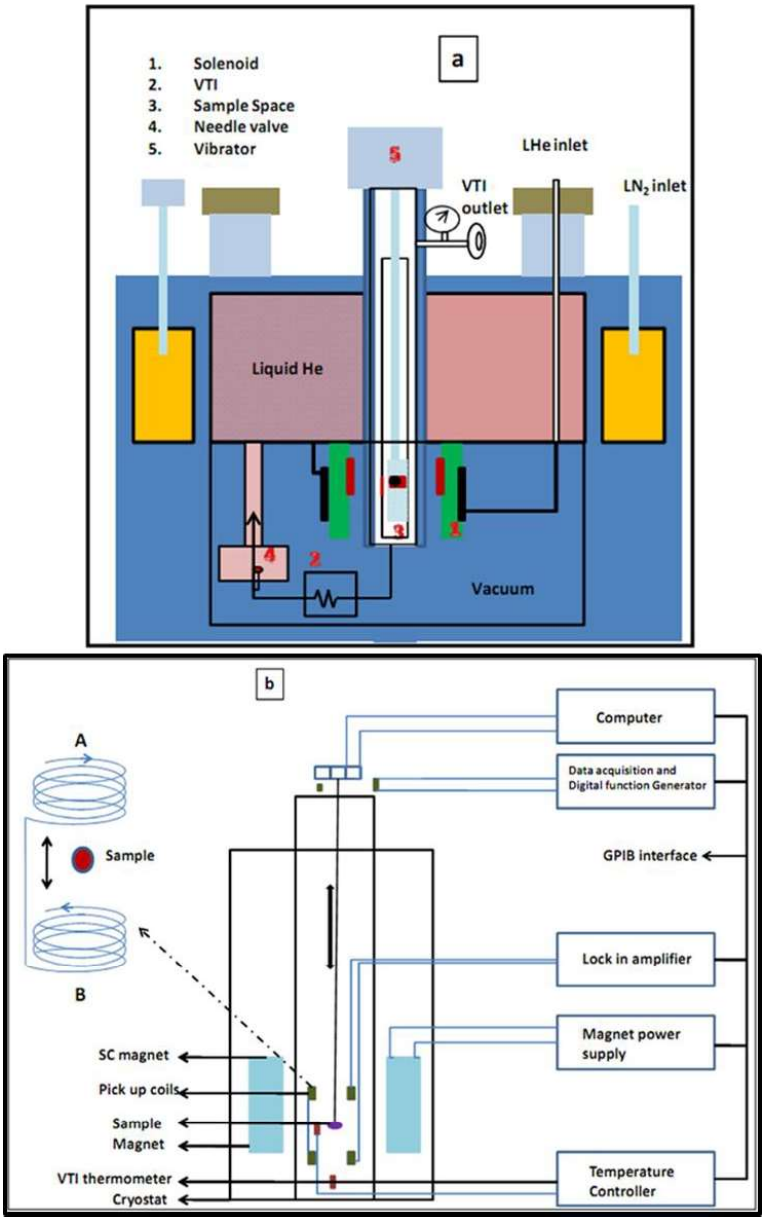

Fig. 2.10 (a) Schematic Diagram of VSM (b) Block diagram of VSM, pick up coil and sample shown separately

The temperature dependent magnetziation of polycrystalline NCCO is shown in Figure 2.11. The diamagnetic signal confirming bulk superconductivity is noted.

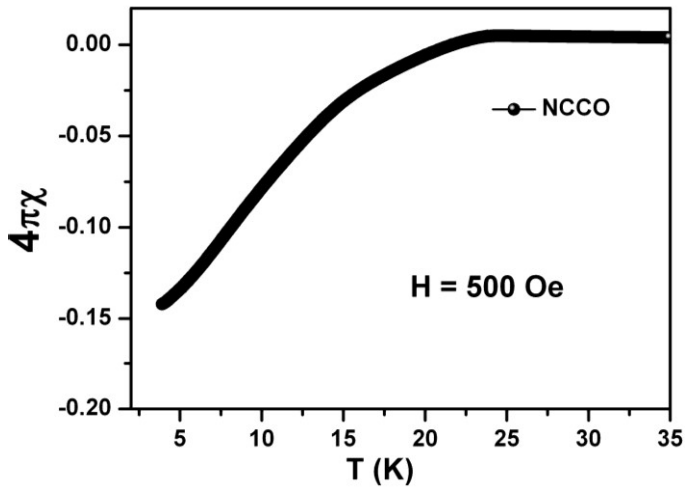

Fig. 2.11 Temperature dependent magnetization of polycrystalline NCCO

2.7.3. SQUID VSM

SQUID stands for superconducting quantum interference device. These are highly sensitive magnetometers which can measure extremely low magnetic fields of the order of ~ 10^{-18} T [9]. As discussed earlier, VSM measures the voltage induced in a pickup coil, when the sample vibrates nearby it. The measurement is comparatively faster than a SQUID magnetometer but the associated sensitivity is comparatively poor. In a SQUID VSM both these qualities, i.e., it is both fast and highly sensitive when we perform magnetization measurements.

In a SQUID two parallel Josephson junctions are connected to form a loop. We know that in a superconducting loop the magnetic flux remains quantized. The current applied is divided equally in the two Josephson junctions. The application of external magnetic field to the superconducting loop will trigger screening currents in the loop which will oppose the magnetic field. If the magnetic field applied externally reaches half a flux quantum (say 0.5 ϕ), it is easier for the SQUID to keep the 0.5 ϕ inside rather than taking 0.5 ϕ out, because the flux remains quantized in a superconducting loop. The way to make this possible is reversal of screening currents in the loop. Hence it can be

understood that the screening current changes its direction whenever the applied magnetic field is increased by half integral multiples of the flux quantum. Hence for a constant bias current, the voltage oscillates with a period of a flux quantum. The change in flux associated with the loop is calculated by counting the number of oscillations.

The magnetization measurements have been performed in a Magnetic Properties Measurement System (MPMS) SQUID Magnetometer, Quantum Design. A schematic diagram of the MPMS SQUID VSM detection is shown in Figure 2.12. [10]

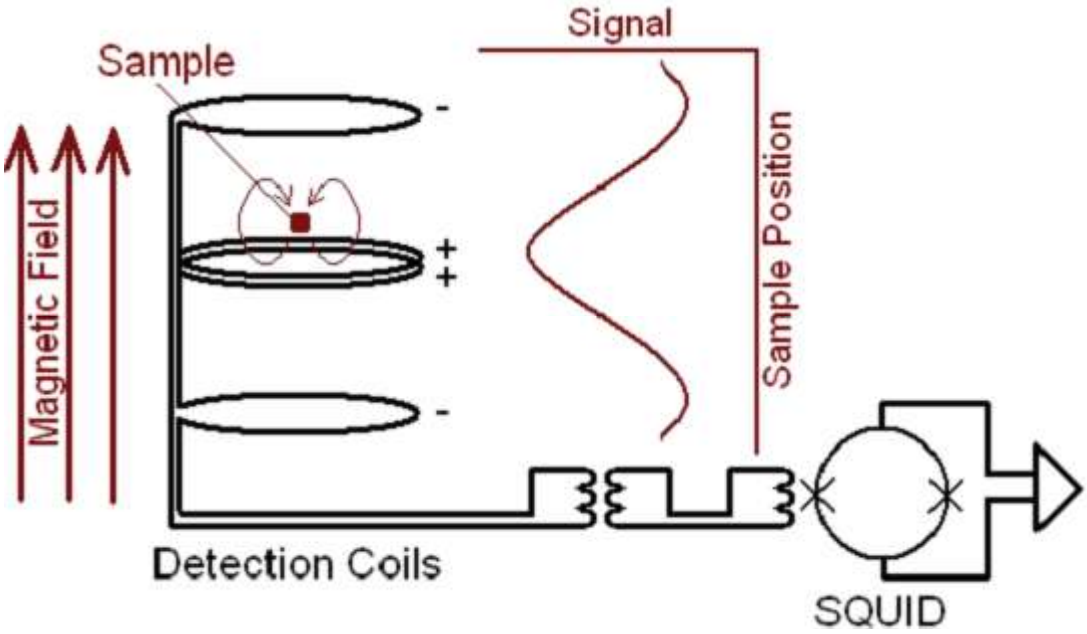

Fig. 2.12 SQUID VSM detection schematic (taken from Reference [9], QUANTUM DESIGN Manual)

The system measures the change in magnetic flux density produced by the sample as it moves through the superconducting pick up coils which are located at the centre of the superconducting magnets. The sample which is mounted in a material (plastic) with negligible magnetic moment is situated at the end of the sample rod. This rod is inserted in the sample space which is at low temperatures as it is surrounded by liquid Helium. The positioning of the sample at the centre of the pick-up coils is ensured by a stepper motor arrangement. The sample dimensions should be smaller than the dimensions of the

detector coils (~3 mm). The current in the detection coil is a function of sample position. When the sample moves through the coils, current is induced in the pick-up coils. The pick-up coils are coupled with a SQUID loop. The SQUID serves as an extremely sensitive current to voltage converter. The change of current in the detection coils result in change of the voltages in the SQUID as well. The voltage in SQUID is proportional to the magnetic moment of the sample. Magnetization measurements can be performed for the temperature range of 1.8 K – 300 K and fields up to 7 T in this system. In Figure 2.13, the temperature dependence of imaginary part of AC susceptibility (AC χ") of polycrystalline NCCO has been plotted. The measurement has been done at a temperature of 4 K and the drive field used is 1 Oe.

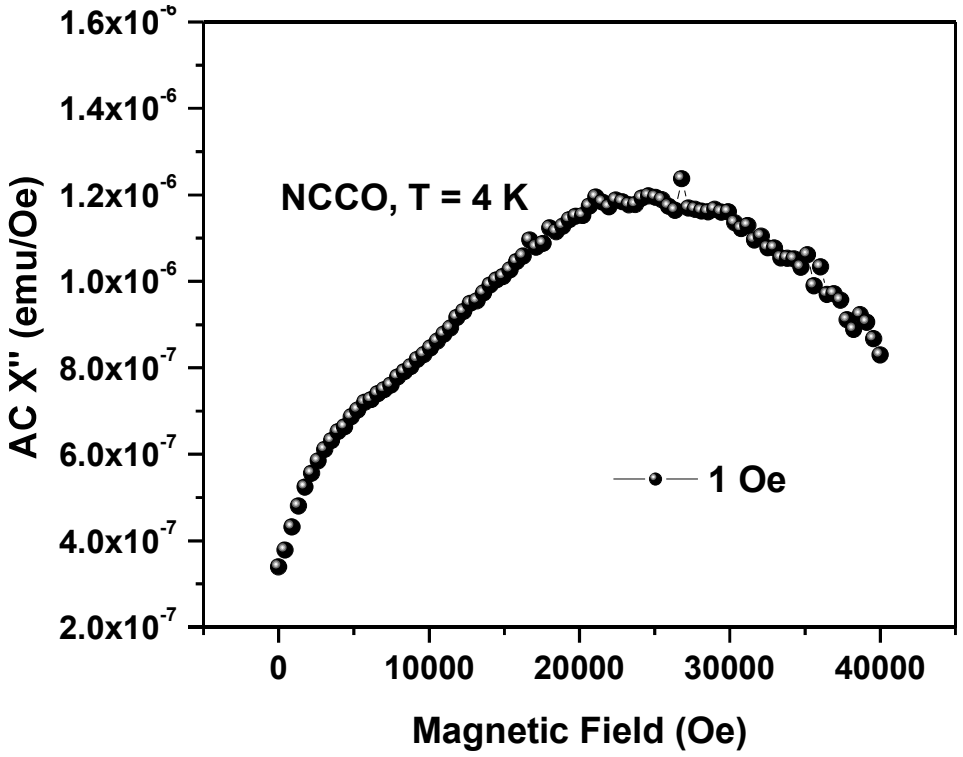

Fig. 2.13 AC χ" vs Magnetic field of polycrystalline NCCO

2.8. References

[1] H. Fujioka, in *Handbook of Crystal Growth (Second Edition)*, edited by T. F. Kuech (North-Holland, Boston, 2015), pp. 365.

[2] H.-U. Krebs *et al.*, in *Advances in Solid State Physics*, edited by B. Kramer (Springer Berlin Heidelberg, Berlin, Heidelberg, 2003), pp. 505.

[3] D. Basting, K. D. Pippert, and U. Stamm, *History and future prospects of excimer lasers* 2002), Vol. 4426.

[4] W. Kraus and G. Nolze, *POWDER CELL-A Program for the Representation and Manipulation of Crystal Structure and Calculation of the Resulting X-Ray Powder Pattern* 1996), Vol. 29.

[5] A. Hammersley, Journal of Applied Crystallography **49**, 646 (2016).

[6] https://www.testandmeasurementtips.com/basics-of-the-scanning-electron-microscope/.

[7] https://www.nanoscience.com/techniques/scanning-electron-microscopy/components/.

[8] L. J. van der Pauw, in *Semiconductor Devices: Pioneering Papers* (WORLD SCIENTIFIC, 1991), pp. 174.

[9] http://einstein.stanford.edu/content/education/GP-B_T-Guide4-2008.pdf.

[10] https://manualzz.com/doc/6686090/magnetic-property-measurement-system-squid-vsm-user-s-manual.

Chapter 3

Magneto-Transport and Magnetization studies on the electron doped superconductor $Nd_{1.85}Ce_{0.15}CuO_{4\pm\delta}$

.

3.1. Introduction

This chapter deals with the synthesis of electron doped superconductor $Nd_{1.85}Ce_{0.15}CuO_{4\pm\delta}$ and provides detailed magneto-transport studies on this system. True to the metastable nature of electron doped superconductors which crystallizes in *T′*- type K_2NiF_4 structure, the $Nd_{1.85}Ce_{0.15}CuO_{4\pm\delta}$ (NCCO) system is difficult to prepare in pure form. In the synthesis of the compound $Nd_{1.85}Ce_{0.15}CuO_4$, various material issues remain unclear including the exact role of the dopant and reduction steps which are absolutely necessary to induce superconductivity. It is proven in literature [1], that the compound synthesized in air is Cu deficient and non-superconducting. This problem seems to be circumvented by annealing the samples in Ar, which results in segregation of $Nd_2O_3/(NdCe)_2O_3$ impurities at the grain boundaries. As a consequence grains become stoichiometric with respect to copper and hence superconducting. Granularity is an essential feature of this superconductor like many unconventional oxide superconductors and needs to be investigated in detail. Here we provide the outcomes of our investigation on granularity effects in the polycrystalline $Nd_{2-x}Ce_xCuO_4$ (x=0.15) superconducting sample performed using temperature and magnetic field dependent electrical resistivity measurements as well as current dependence of resistivity. Effect of annealing conditions on the magneto resistance of the same has also been described in detail.

3.2. Synthesis of electron doped super conductor $Nd_{1.85}Ce_{0.15}CuO_{4\pm\delta}$(NCCO)

3.2.1. Synthesis and X-Ray diffraction

Single phase polycrystalline samples have been synthesized starting from high pure (> 99.9%) oxides Nd_2O_3, CeO_2, and CuO by solid state reaction at 1000°C for 24 hours, followed by repeated regrinding and annealing. Argon annealing has been subsequently carried out between 875°C and 900°C with progressive increase in annealing temperature and time. As discussed earlier, the Argon annealing step is found to be absolutely indispensable to induce superconductivity in the sample.

The compounds $Nd_{2-x}Ce_xCuO_4$ (x=0, 0.15) synthesized in the present work have been characterized for phase purity and structure by powder X-ray diffraction using . The XRD analysis studies indicate that both the compounds are essentially single phase and fit well to the I4/mmm structure. The XRD patterns are shown in Fig 3.1.

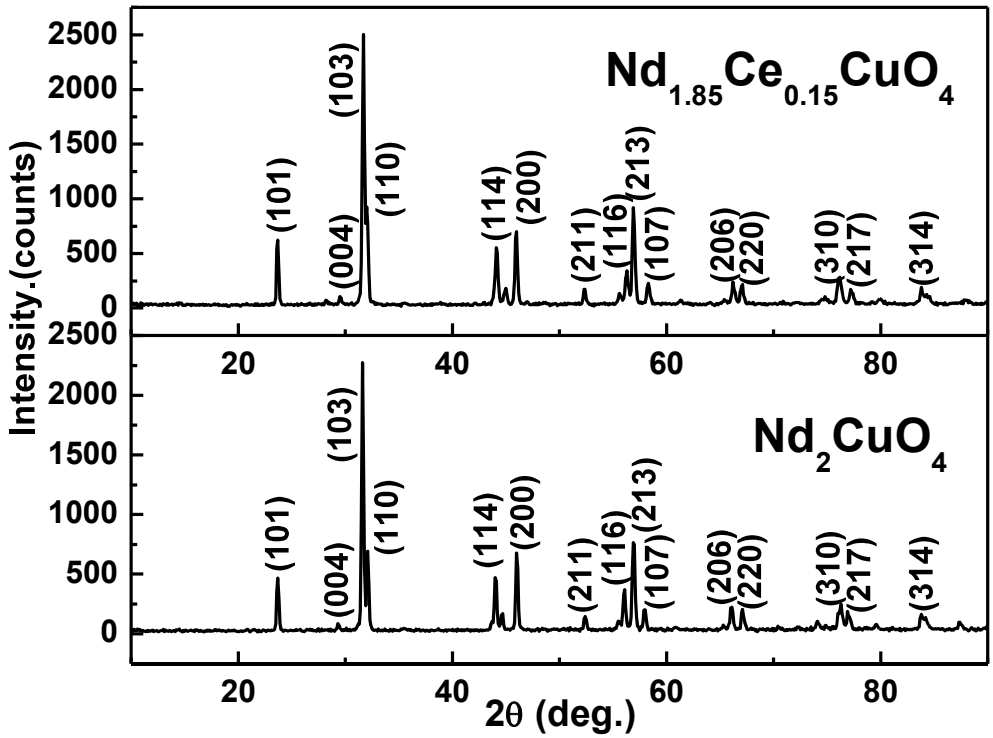

Fig. 3.1 XRD patterns of the system $Nd_{2-x}Ce_xCuO_4$ (x=0, 0.15)

The lattice parameters deduced from the fit are found to be *a*=*b*=3.941Å and *c*=12.162Å for the pristine compound and *a* =*b*=3.946 Å and *c*=12.082 Å for the Ce doped compound

as shown in Table 3.1. The observed changes in lattice parameters indicate the successful substitution of Ce at Nd sites which is expected due to the smaller ionic radius of Ce^{4+} compared to $Nd^{3+}$and are in accordance with literature [2].

Table 3.1 Lattice parameters of the parent compound Nd_2CuO_4 and $Nd_{1.85}Ce_{0.15}CuO_4$

Compound	*a* (Å)	*c* (Å)
Nd_2CuO_4	3.941	12.162
$Nd_{1.85}Ce_{0.15}CuO_4$	3.946	12.082

3.3. Brief account of granularity issues in high temperature superconductors

The intrinsic granular structure of the high temperature superconductors have profound effect on their physical properties which manifest in their resistivity and magnetization behaviour. In the granular structure the material is composed of small grains separated by dielectric barriers [3]. The two crucial factors that control the superconducting and normal state properties are the grain size and inter grain electrical resistance. The main practical sources of granularity envisaged in polycrystalline superconducting materials include impurities and defects at the grain boundaries and mis-orientation between the grains. One of the striking features of granular superconductors is the occurrence of a double resistive superconducting transition [4,5]. The first dip in resistance occurs at a comparatively higher temperature, at which superconductivity is developed in isolated superconducting islands. This is known as the intra-grain transition. As it is mentioned earlier, the sample has now reached a state where it exists as an ensemble of superconducting grains embedded in an insulating matrix [6]and therefore behaving as Josephson Junctions. The overall system now can be visualized as collection of Superconductor-Insulator-Superconductor Junctions (SIS junctions). The second

transition leads the system into the zero resistance state. This is known as the inter-grain transition. After the advent of intra-granular transition, when the temperature is further lowered, more and more superconducting grains get coupled. Eventually it results in the establishment of a conducting path that leads to the achievement of zero resistivity [7].

3.4. Resistivity

The temperature dependent resistance R(T) of the Ce doped compound $Nd_{1.85}Ce_{0.15}CuO_4$ in the temperature range 4.2 to 300K is presented in Figure. 3.2 as a function of annealing schedule. R(T) reveals double superconducting transitions which can be observed clearly in Figure. 3.3. The double superconducting transition is known to arise due to the unavoidable granularity problem and has been reported in literature for several systems [8,9]. These transitions, as mentioned earlier, can be attributed to intra-grain and inter-grain contributions to superconductivity.

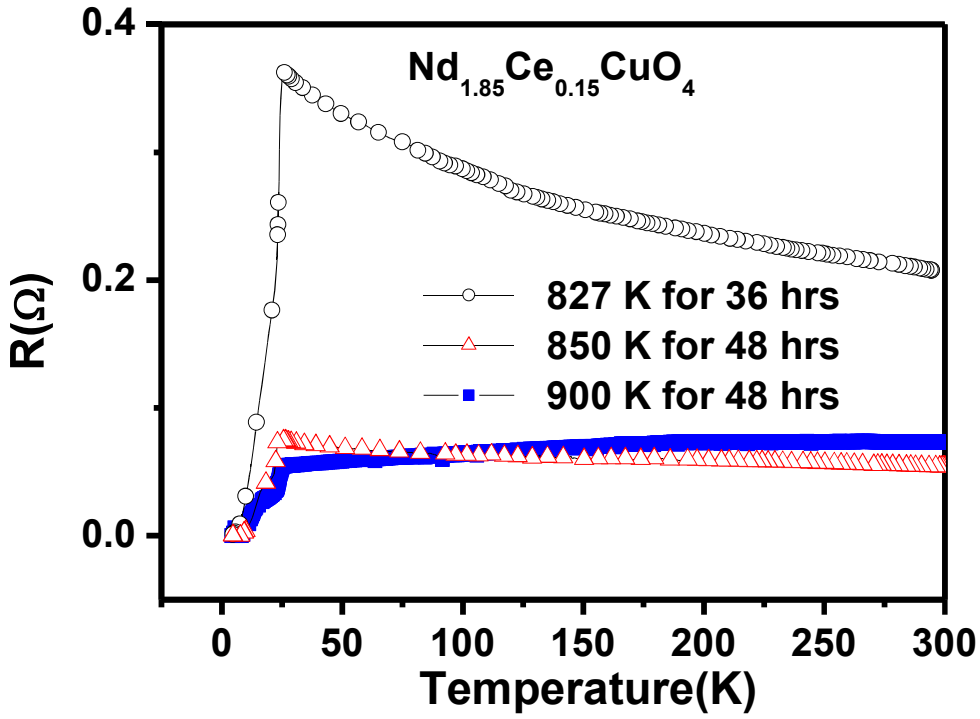

Fig. 3.2 Resistance versus Temperature from 4.2 K to 300K

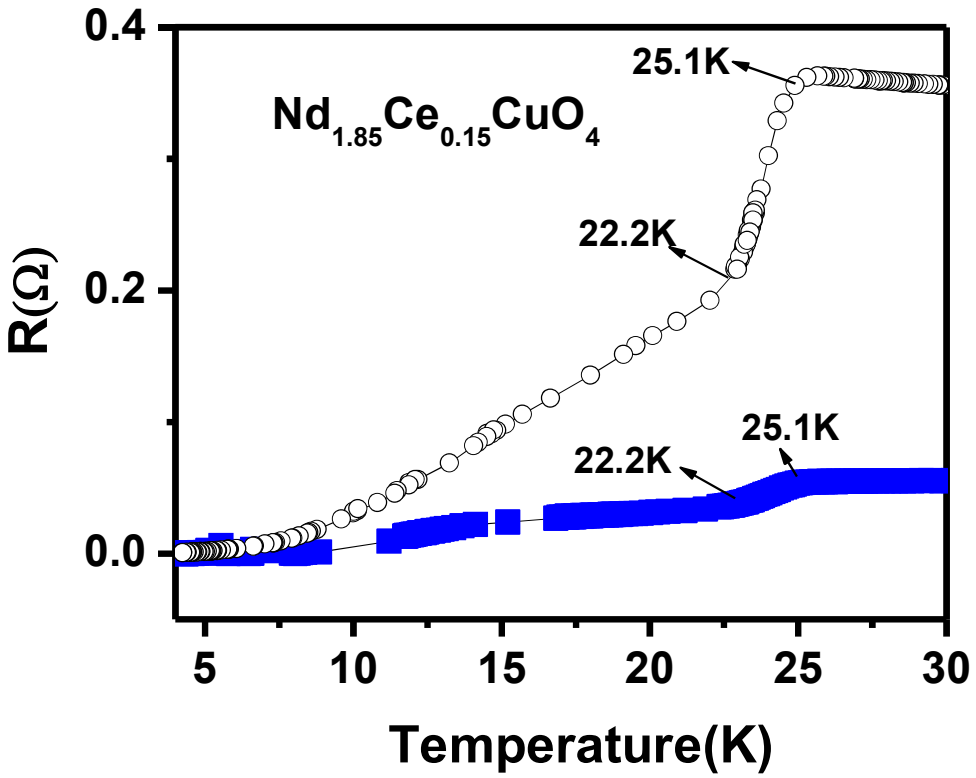

Fig. 3.3 Resistance versus Temperature from 4.2 K to 30 K (showing double transitions)

The intra and inter-grain transition temperatures (TC1 and TC2 respectively) are found to remain unchanged at around 25 K and 22K respectively with increasing annealing temperature and time. Samples showed semiconducting nature when Ar annealing was performed for 36 hours, 48 hours at 827 K and 850 K respectively (Figure 3.2) . However, R (T) shows slight metallic nature when submitted to Ar annealing at 900 K for 48 hours (Figure 3.2). Hence R(T) exhibits a gradual change from semiconducting-like behaviour to metallic behaviour with increase in Argon annealing temperature and time.

3.5. Magnetization

The results of magnetization (M) versus temperature (T) studies in the range 4 K - 28 K with excitation field of 100 Oe have been presented for the compound $Nd_{1.85}Ce_{0.15}CuO_4$ in Figure 3.4. The ZFC & FC curves reveal a clear superconducting transition at 23 K with diamagnetic signal attributed to arise from the intra-grains. It should be mentioned that the superconducting transition due to inter-grains could not be captured in this measurements as the excitation field (100 Oe) used was larger than the critical field pertaining to superconductivity of the inter-grains (Hc2 ~1 Oe) [7].

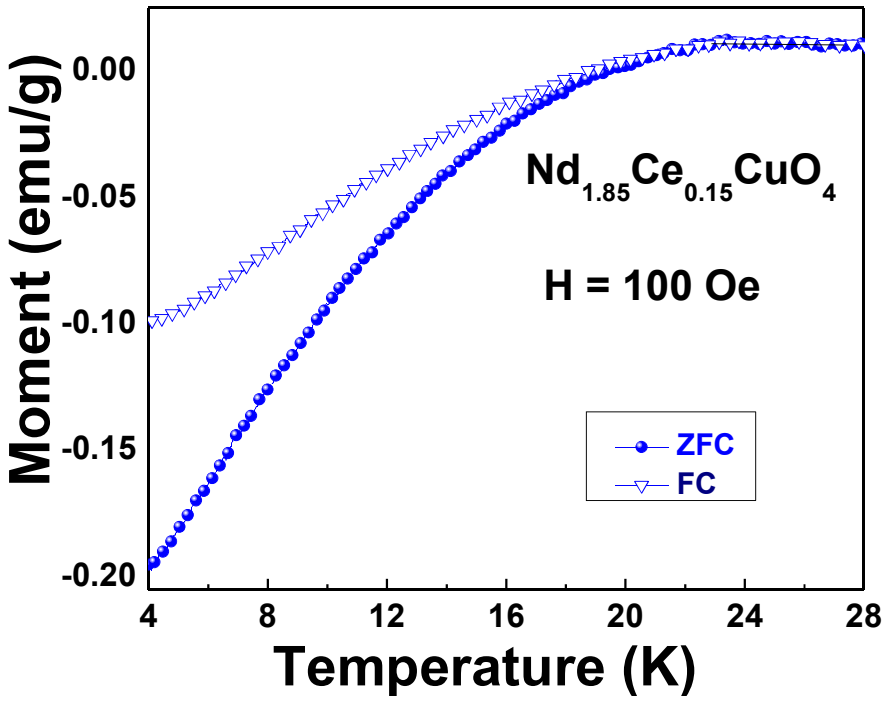

Fig. 3.4 Magnetization versus temperature curves in the range 4-28 K for the sample

3.6. Effect of granularity and annealing conditions on magneto-resistance

There are two factors which influence the superconducting properties in these class of compounds in a very significant way. One is the granular structure and the other being the sensitivity to Ar annealing. In order to study the effect of granularity and annealing conditions on magneto resistance we chose an NCCO sample which was Ar annealed at 800°C for 24 hours (referred as S1) and one of the pellets of the same batch has been

subjected to prolonged Argon annealing for a period of 92 hrs (referred as S2). The resistivity of S1 and S2 with respect to temperature as a function of field was measured. Magneto resistance measurements have been carried out on the samples by a 15 Tesla cryogen free system, Cryogenics Ltd.

The Temperature (T) and magnetic field (B) dependent electrical resistivity ρ (T, B) of S1 is shown in Figure 3.5. It is evident from this figure that ρ(T) shows a double superconducting transition at zero field. The intra-grain transition (T_{C1}) occurs at 22K. The inter-granular transition (at T_{C2}), appears at 19.5 K. The ρ(T) in normal state of S1 exhibits negative temperature coefficient like an insulator and exhibits negligible change under application of magnetic field. However, in the superconducting regime of S1, the transition temperatures T_{C1} (intra-grain) and T_{C2} (inter-grain) progressively shift to lower temperatures as the magnetic field is increased from 0 to 4 Tesla. The ρ (T) values in $T_{C2} < T < T_{C1}$ range consistently increase with increasing B. An intriguing dramatic change in the ρ (T) behaviour is observed below T_{C2}. Here even a small field of B~0.03Tesla has inflicted change in slope of ρ (T) leading to a drastic increase in its value which peaks around $T_{J,E}$~ 6.5K (defined as Josephson junction coupling temperature) and decreases with further lowering of temperature. $T_{J,E}$ appears to shift to lower temperatures while increasing B up to 1Tesla. However, at higher magnetic fields, the resistivity dip at T_{C1} is not observed. Such non-monotonic ρ (T) behaviour below T_{C2} has been reported in literature for electron doped superconductors and has been explained to arise either due to a quantum phase transition or inter-granular coupling. For the present system, we find the latter mechanism consistent with our observations as seen in the case of the Sm-Ce-Cu-O system [10].

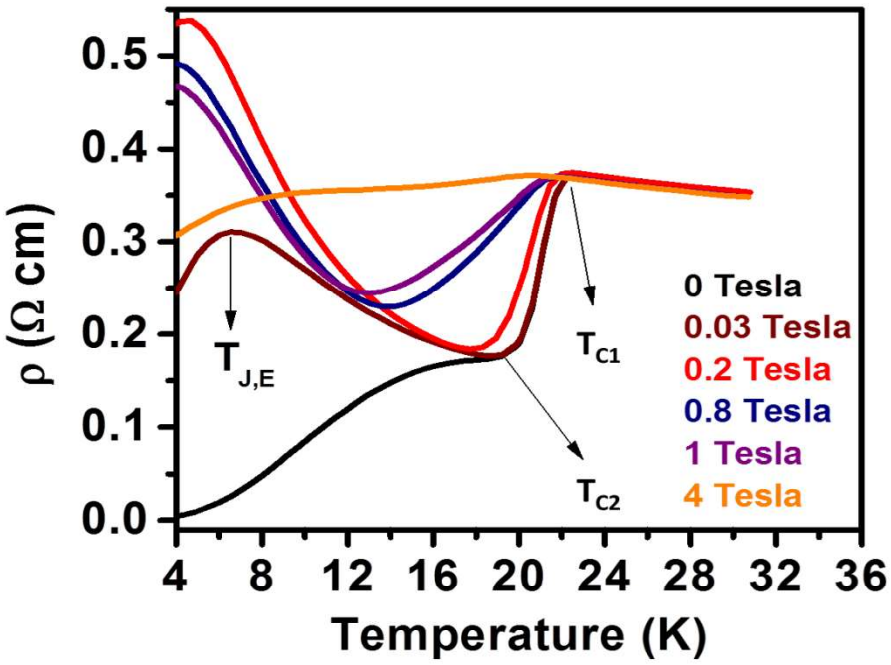

Fig. 3.5 Resistivity vs. Temperature for different fields for S1

The temperature (T) and magnetic field (B) dependent electrical resistivity ρ(T, B) of S2 is shown in Figure 3.6. It can be seen that the ρ(T, B) behaviour of S2 is quite different from that of S1 (see Figures 3.5& 3.6). Firstly, ρ(T) in normal state of S2 exhibits positive temperature coefficient akin to metallic behaviour. In this case, T_{C1}~24 K and T_{C2}~16 K, which means that the inter-granular transition temperature has decreased compared to the value of S1.Second, the width of double transition ($T_{C1}$to T_{C2}) is around 6 K for S2, whereas it is around 2.5 K for S1 at zero field. In contrast to S1, the slope of ρ(T) of S2 below T_{C2} remains unchanged, though its value is found to increase gradually with increasing field B = 0 to 4 Tesla. This change in ρ(T, B) behaviour of S2 may be arising as a consequence of prolonged annealing causing enhancement in grain-size as well as a slightly better inter-granular coupling.

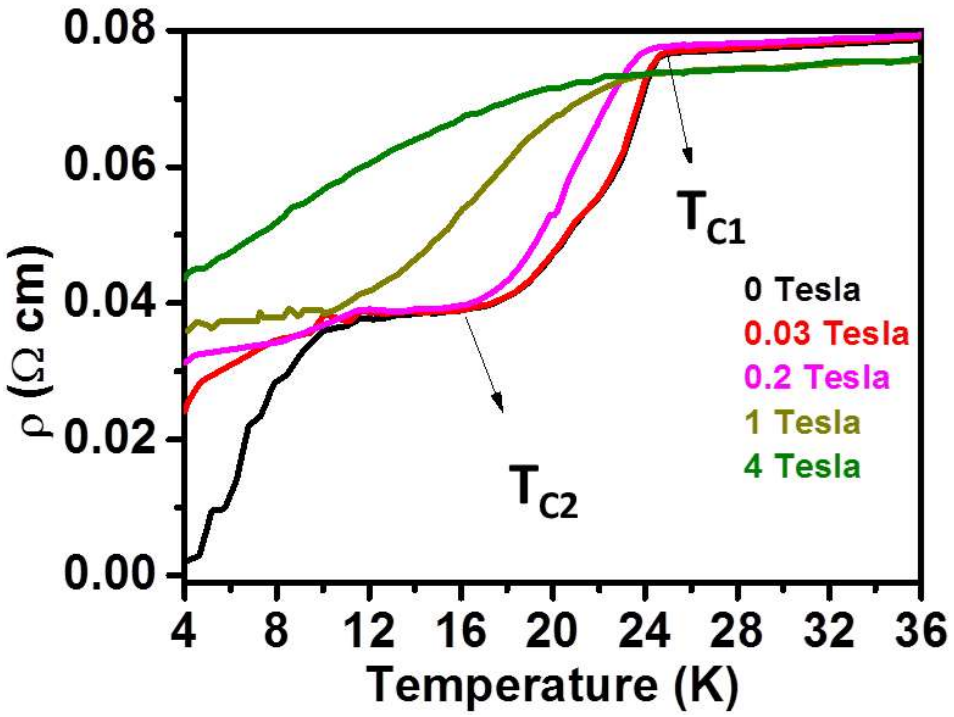

Fig. 3.6 Resistivity vs Temperature for different fields for S2

In what follows, we try to explain the observed ρ(T, B) behaviour of sample S_1 qualitatively consistent with the model provided in reference [2]. The system is considered to be comprised of collection of S-I-S (superconductor – insulator – superconductor) and S-N-S (superconductor-normal-superconductor) networks. While the tunneling characteristics remains temperature independent for the S-N-S type networks, the evolution of temperature dependence of the ρ(T, B) behaviour is solely dictated by the temperature dependence of the S-I-S junctions. S-I-S networks contain two types of Josephson junctions. In type-1, the normal state resistance R_N is below the critical state value $R_Q \sim h/4e^2$, while in type-2 the normal state resistance $R_N > R_Q$. In the latter the charge transfer is governed by quasi particle tunneling. In type-1 junctions, Josephson tunneling current starts flowing when thermal energy becomes lower than the Josephson junction coupling energy (E_J). For an applied magnetic field, the junction's coupling temperature (T_{JE}) is shifted down as application of field suppresses the Josephson junction coupling energy. For the temperature range $T_{J,E}<T<T_{C2}$, the transport is

governed by quasi-particle tunneling and total resistance increases with temperature reduction due to the decrease in quasi-particle tunneling. At temperature T_{JE}, sufficient number of superconducting grains is coupled which leads to decrease in resistance. It is to be noted that reduction of temperature results in an increase of the superconducting energy gap which in turn reduces the quasi particle tunneling and hence results in huge increase in resistance as observed in Fig 3.5. The value of resistivity, due to this increase, is even larger than the normal resistance. Meanwhile, the lowering of temperature strengthens E_J which competes over the depressing effect of B on E_J. These two inter competing effects result in non-monotonic variation of ρ(T), which peaks at $T_{J,E}$ where two effects balance each other. Below $T_{J,E}$, the effect of T on E_J supersedes over the effect of B on E_J which results in observed decrease in ρ(T). For a similar system $Sm_{1.85}Ce_{0.15}CuO_4$, ρ(T) behaviour has been simulated by Grenet et al. [11] wherein they have generated similar plots and have attributed the differences in behaviour to difference in tunnel junction characteristics. Magneto-resistance plot of S1 and S2 are shown in Figures 3.7 and 3.8 respectively.

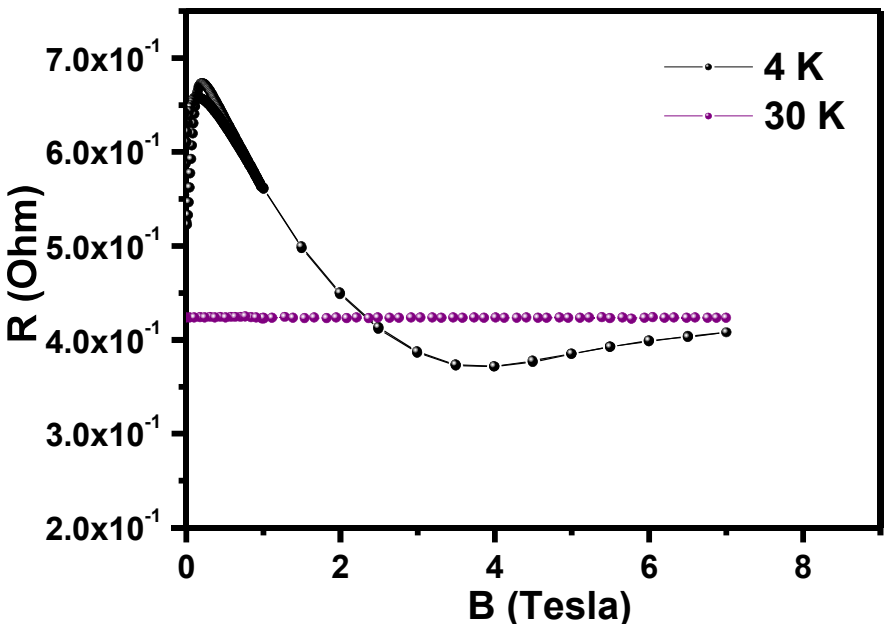

Fig. 3.7 Magneto resistance of the sample S1

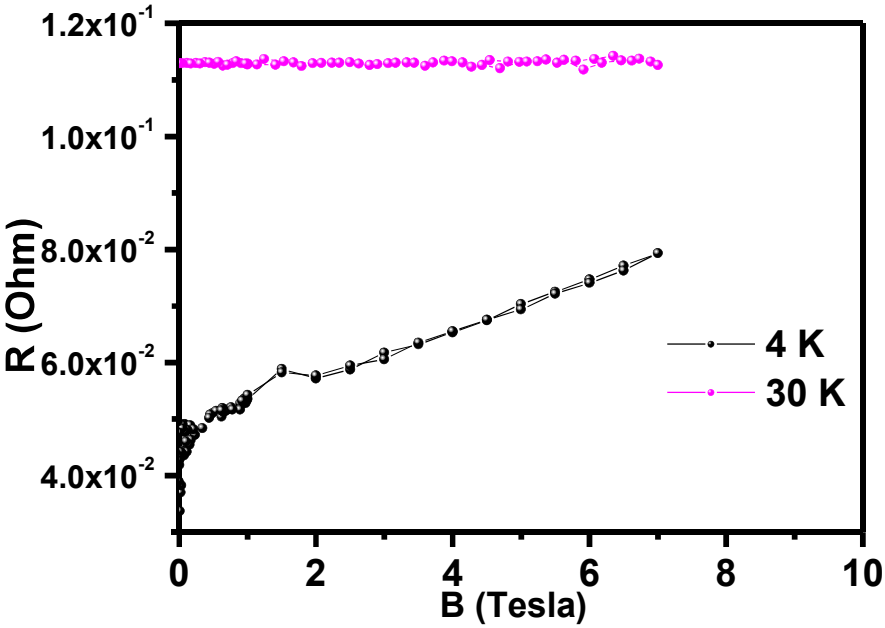

Fig. 3.8 Magneto resistance of the sample S2

For the samples S1, at 4 K, the resistivity shows an initial steep increase due to the destruction of Josephson junction coupling for small fields B≤0.2Tesla. Increase in B from 0.2 Tesla to 3 Tesla results in decrease of resistance probably due to the fact that magnetic field suppresses the superconducting energy gap which in turn enhances quasi particle tunneling. For B > 4 Tesla, increase in ρ(T) can be attributed to the suppression of intra-grain superconductivity. Magneto-resistance plots of S2 (Figure 3.8) give us a very different picture. For temperatures below transition temperature such as 4 K, resistance increases in the low field regime followed by a gradual increase at the high field regime. Meanwhile, the resistance above the transition temperature remains independent of field for both samples. The SEM images of S_1 and S_2 are shown in Figure 3.9. The grain sizes of S_1 and S_2 have been deduced using ImageJ software and they are found to be approximately 0.8 μm and 3 μm respectively. The larger grain size observed in S_2 is consistent with the above mention arguments.

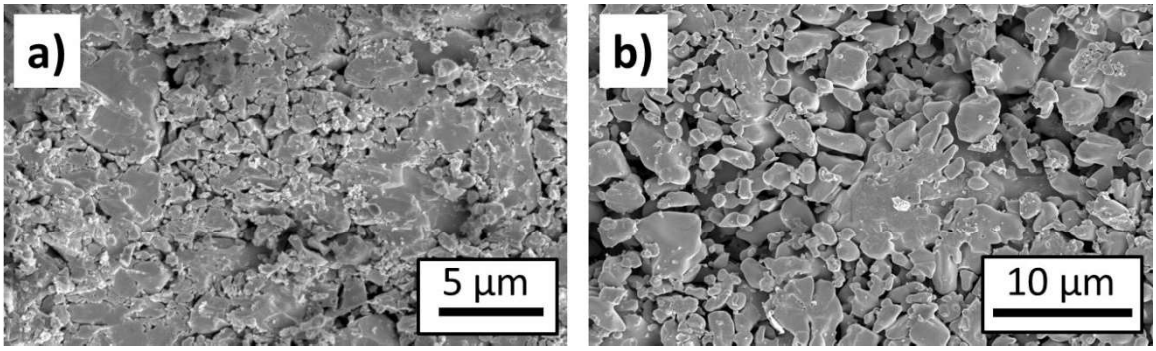

Fig. 3.9 SEM images of S_1 and S_2 shown in a) and b), respectively.

Figure 3.10 depicts Current dependent ρ(T) of S_1. The branching of ρ(T) with respect to different currents below T_{C2} is observed, which is a signature of granularity. The dissipation in granular samples is perhaps a consequence of the normal current flowing in parallel with the super-current.At the current of 25mA, the resistivity starts showing an increase when temperature is reduced below T_{C2}. The distribution of E_J (Josephson Junction Coupling energy) dictates the rate of fall of ρ(T) to zero. When we increase current, the self-field generated by current results in a suppression of coupling between superconducting clusters and ρ(T) is governed by thermally activated hopping between neighbouring grains, leading the system in to a non-zero resistance state at low temperatures.

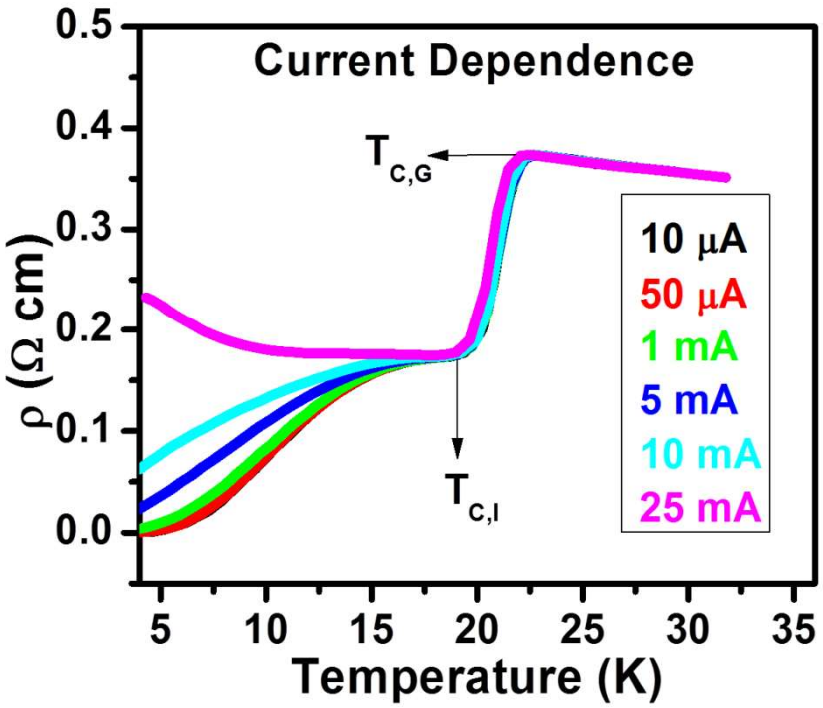

Fig. 3.10 Current dependence of ρ (T) in S1

3.7. Conclusions

Superconducting samples of polycrystalline $Nd_{1.85}Ce_{0.15}CuO_{4\pm\delta}$ have been synthesized. The phase purity of samples has been established by X-ray diffraction. The resistivity measurements have revealed double superconducting transitions arising from intra & inter grain contributions akin to weakly coupled granular superconducting systems. It is found that reduction annealing in Ar is crucial to induce superconductivity in this system. The durations and temperatures, at which the annealing has been performed, profoundly dictate the resistance behaviour. The effect of two different annealing conditions on the temperature dependent electrical resistivity behaviour has also been studied. The observed resistivity behaviours have been qualitatively rationalized in terms of interplay of opposing effects of temperature and magnetic field on SIS junctions formed on account of coupling of superconducting grains dispersed in an insulating matrix in this granular system.

3.8. References

[1] R. J. Cava, H. Takagi, R. M. Fleming, J. J. Krajewski, W. F. Peck, P. Bordet, M. Marezio, B. Batlogg, and L. W. Rupp, Physica C: Superconductivity **199**, 65 (1992).

[2] Y. Tokura, H. Takagi, and S. Uchida, Nature **337**, 345 (1989).

[3] *New Superconductors: From Granular to High* T_C (WORLD SCIENTIFIC, 2006), p. 244.

[4] N. Y. Ayoub, J. T. Markert, E. A. Early, C. L. Seaman, L. M. Paulius, and M. B. Maple, Physica C: Superconductivity **165**, 469 (1990).

[5] A. Gerber, T. Grenet, M. Cyrot, and J. Beille, Physical Review Letters **65**, 3201 (1990).

[6] J. R. Clem, Physica C: Superconductivity **153-155**, 50 (1988).

[7] P. W. Klamut, physica status solidi (a) **136**, 181 (1993).

[8] T. Hammad, International Journal of Modern Physics B, **21**,1051 (2012).

[9] R. Lortz, T. Tomita, Y. Wang, A. Junod, J. S. Schilling, T. Masui, and S. Tajima, Physica C: Superconductivity **434**, 194 (2006).

[10] A. Gerber, T. Grenet, M. Cyrot, and J. Beille, Physical Review B **43**, 12935 (1991).

[11] T. Grenet and M. Cyrot, Applied Superconductivity **1**, 925 (1993).

Chapter 4

Magneto-Transport and Magnetization studies on $Nd_{1.85}Ce_{0.15}CuO_4$ /Ag composites

In continuation of our studies on the magneto-transport and magnetization properties on the polycrystalline sample of the electron doped superconductor $Nd_{1.85}Ce_{0.15}CuO_4$ in the previous Chapter wherein we have highlighted the problem of granularity and its effect on physical properties, we now present our investigation on the influence of materials modification by silver addition on the above properties including critical current density in this Chapter.The effect of silver addition on ceramic superconductors has always been a topic of interest as in many cases it has resulted in an improvement of superconducting properties [1-5]. Studies on the introduction of silver into high-T_C superconductors (HTSC) like Bi–(Pb)–Sr–Ca–Cu–O and $YBa_2Cu_3O_7$ have revealed that Ag is found to improve their structural and superconducting properties [1,3,4]. Ag addition also leads to the enhancement of critical current density of almost all bulk high temperature superconductors including the rare earth cuprates, MgB_2 and rare earth iron pnictides, mainly due to an improvement in inter-granular coupling [6-8]. Moreover, Ag is also an established additive for improving mechanical properties of cuprate superconductors and contributes to grain growth [9]. It has been reported that the addition of silver reduces the normal state resistivity and enhances critical current density in $YBa_2Cu_3O_{7-\delta}$ ceramic superconductor [7]. However, the exact role of silver in improving some of the properties like the critical current density of superconductor/Ag composites still remains elusive and has been much debated [10]. Improved coupling between the grains (if silver resides at the grain boundaries), stronger flux pinning and even substitution of silver on the copper sites, which is unusual and quite interesting, can

be one of the reasons [11-14]. Motivated from the beneficial effects observed under Ag addition in several aforementioned HTSC, we have performed detailed structural and physical properties investigations on successfully synthesized superconducting NCCO/Ag composites. The effect of Ag addition (0-15 weight percent) into $Nd_{1.85}Ce_{0.15}CuO_4$ superconducting system on its crystal structure and local structural features has been investigated using Synchrotron X-Ray Diffraction (SXRD) and Raman spectroscopy. Low temperature magnetization studies have been carried out by employing Vibration Sample Magnetometer to study the effect of Ag addition on the superconducting and magnetic properties particularly the critical current density which has been estimated using Bean's critical state model. In addition, the temperature and electrical current dependent studies of electrical resistivity as well as Magneto resistance (MR) studies have been performed on the $Nd_{1.85}Ce_{0.15}CuO_4$+Ag composite system. Based on above measurements, a comparative study of the superconducting critical properties of the $Nd_{1.85}Ce_{0.15}CuO_4$+Ag composites with Ag=0, 5 and 15 wt.% have been carried out and the outcomes of these studies are presented here.

4.1. Synthesis of NCCO/Ag composites

The pure electron-doped cuprate $Nd_{1.85}Ce_{0.15}CuO_4$ and the $Nd_{1.85}Ce_{0.15}CuO_4$+Ag composite systems were prepared by the conventional solid state reaction method. For thesynthesis of $Nd_{1.85}Ce_{0.15}CuO_4$, high purity powders of Nd_2O_3, CeO_2 and CuO were used as the starting materials. Powders in the required stoichiometric ratio were well mixed and ground thoroughly in an agate mortar and then air annealed at 1273 K and this process was repeated for several grinding and heating cycles. In order to prepare the $Nd_{1.85}Ce_{0.15}CuO_4$+Ag composites, Ag powder was added to the samples in the solid state to the extent of 5 wt. % and 15 wt. % respectively and further air annealed at 1133 K.. This was followed by a final reduction stage by Ar annealing at the same temperature

(1133 K) for all the samples which is necessary to induce superconductivity. As Ag has a low melting point, the final sintering was carried out at 1133 K for the present series of $Nd_{1.85}Ce_{0.15}CuO_4$+Ag ceramics (designated as NCCO+Ag).

4.2. Characterization of NCCO/Ag composites

4.2.1. X- ray diffraction Measurements

The inital X-Ray Diffraction measurements were performed from lab source using STOE diffractometer with Si (911) zero back-ground plate. Subsequently, the Synchrotron X-Ray Diffraction measurements have been carried out on finely ground powders of $Nd_{1.85}Ce_{0.15}CuO_4$+Ag in the beam line BL-12 (ADXRD beam line) at INDUS-II Synchrotron source at RRCAT, Indore India. The XRD patterns were recorded on a MAR3450 image plate and the sample was mounted in Debye-Scherrer geometry. The 2D ring pattern recorded on the image plate was converted to the 2theta (2θ) versus intensity (I) plots, using the FIT2D program [15]. The wavelength and sample to detector distance were accurately calibrated by using XRD pattern of LaB_6 NIST standard. The Rietveld analysis of the XRD data (wavelength =0.665422 Å) was performed using GSAS-EXPGUI software [16]. An XRD study of the pellets has also been carried out to establish the orientation using a Laboratory Powder diffractometer (D500 STOE using Cu Kα radiation, operated with a power of 40 kV and 30 mA, in the Bragg-Brentano geometry).

In order to establish possible changes of crystallographic preferred orientation upon Ag addition to the system, X-ray diffraction (XRD) patterns of $Nd_{1.85}Ce_{0.15}CuO_4$+Ag (0 and 5 wt.%) pellets have been recorded. The indexed XRD patterns have been presented in Figure 4.1. It must be noted that very small fractions of impurity phases has been detected for both samples. The impurity phase in case of

$Nd_{1.85}Ce_{0.15}CuO_4$ + Ag 5 wt.% happens to be unreacted CuO. In the pristine sample an unidentified peak observed at 2θ = 27.6 which might be an impurity phase. The data have been analyzed with respect to intensity ratio variations. Figure 4.1 (inset) highlights the reduction in intensity of the (110) reflection upon Ag addition indicating a randomization of the small degree of preferred orientation initially present in the pristine $Nd_{1.85}Ce_{0.15}CuO_4$ sample.

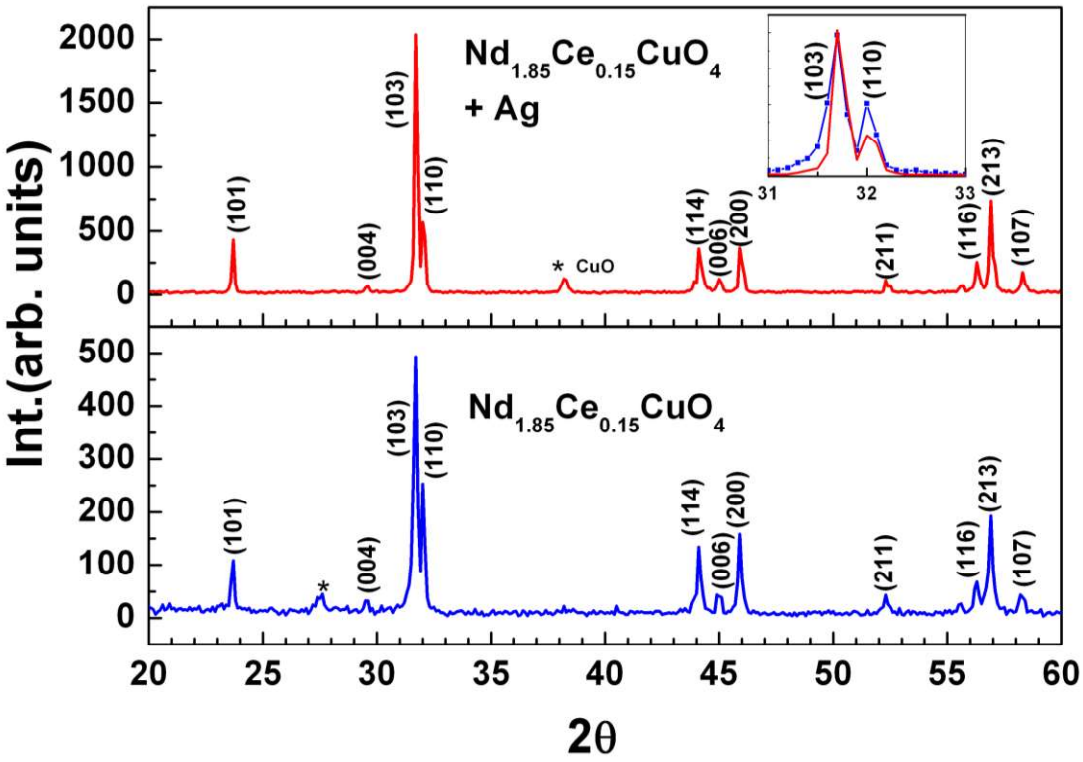

Fig. 4.1 XRD patterns of the $Nd_{1.85}Ce_{0.15}CuO_4$+Ag (0, 5, wt.%) pellets. Inset shows the intensity comparison of the (103) and (110) reflections for Ag 5wt.% (solid) versus Ag 0wt.% (dot)

In order to investigate the overall distribution of silver in the inter- and intra-granular regions and also to precisely determine the changes in lattice constants upon Ag addition, the Synchrotron XRD analysis and Rietveld refinement have been undertaken. The Rietveld refinement plots of the $Nd_{1.85}Ce_{0.15}CuO_4$+Ag system (Ag=0, 5 and15 wt. %) are presented in figures 4.2, 4.3 (a) & (b) respectively. The background function used is the Chebyschev polynomial of the first kind as given in the GSAS program. The

refinement has been carried out in the sequence: background, scale factor, lattice parameters, profile parameters, phase fractions and thermal vibration parameters.

Structural parameters of NCCO+Ag system is listed in Table4.1. The quantitative phase information is obtained assuming that the weight fraction W_p of the p^{th} phase in a mixture is given by $W_p = S_p Z_p M_p V_p / \sum_i S_i Z_i M_i V_i$; where S_p, M_p, Zp, V_p are the refined Rietveld scale factor, the mass of the formula unit, the number of formula units per unit cell and the unit cell volume, respectively of the phase p [17]. The summation in the denominator accounts for all crystalline phases in this case including $Nd_{1.85}Ce_{0.15}CuO_4$ and Ag.

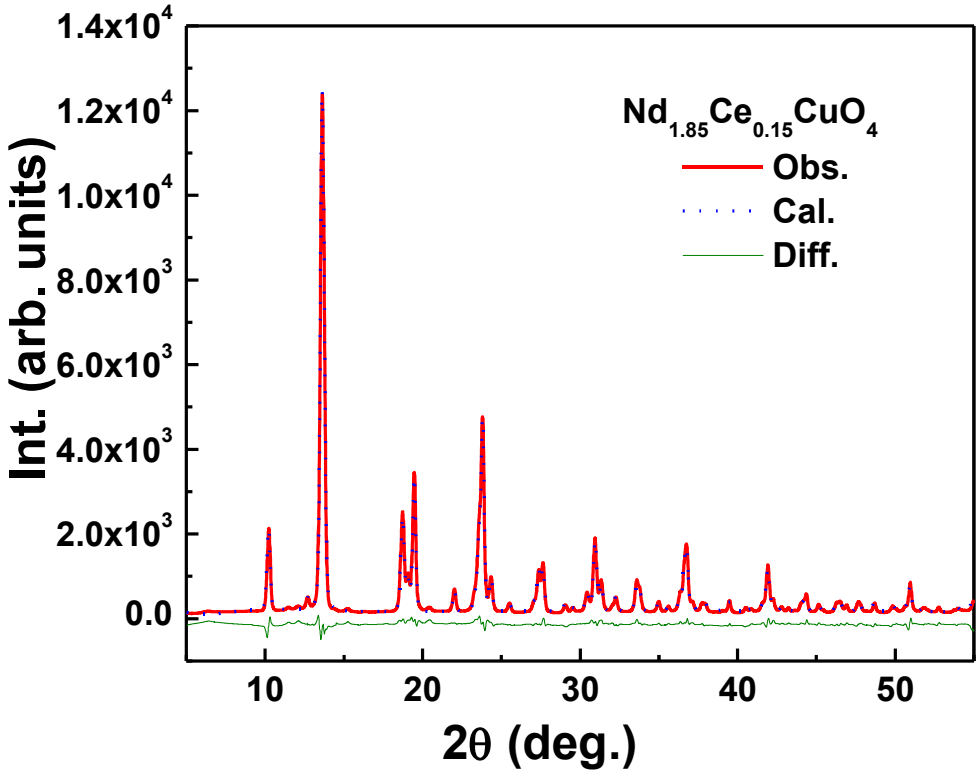

Fig. 4.2 Rietveld refined powder XRD plot of $Nd_{1.85}Ce_{0.15}CuO_4$

The results of Rietveld Refinement studies of $Nd_{1.85}Ce_{0.15}CuO_4$+Ag system (Table 4.1) indicate a small change in lattice parameter upon Ag addition (*c* lattice parameter decreases from 12.085 to 12.065 Å for the system $Nd_{1.85}Ce_{0.15}CuO_4$+Ag upon increasing Ag from 0 to 15 wt. %). This is associated with a very small decrease in the

concentration of free silver by around 1%. (Our estimated composition of the sample is $Nd_{1.85}Ce_{0.15}CuO_4$+14 Ag wt. % compared to the nominal composition for the sample $Nd_{1.85}Ce_{0.15}CuO_4$+15 Ag wt.%) showing evidence for possible incorporation of Ag in the lattice to the extent of roughly 1 wt. %. As it is well known that Ag takes the 1^+ and 3^+oxidation states and Ag^{3+} ion has an ionic radius 0.81 Å comparable to 0.68 for Cu^{2+}, it perhaps substitutes for Cu ion.

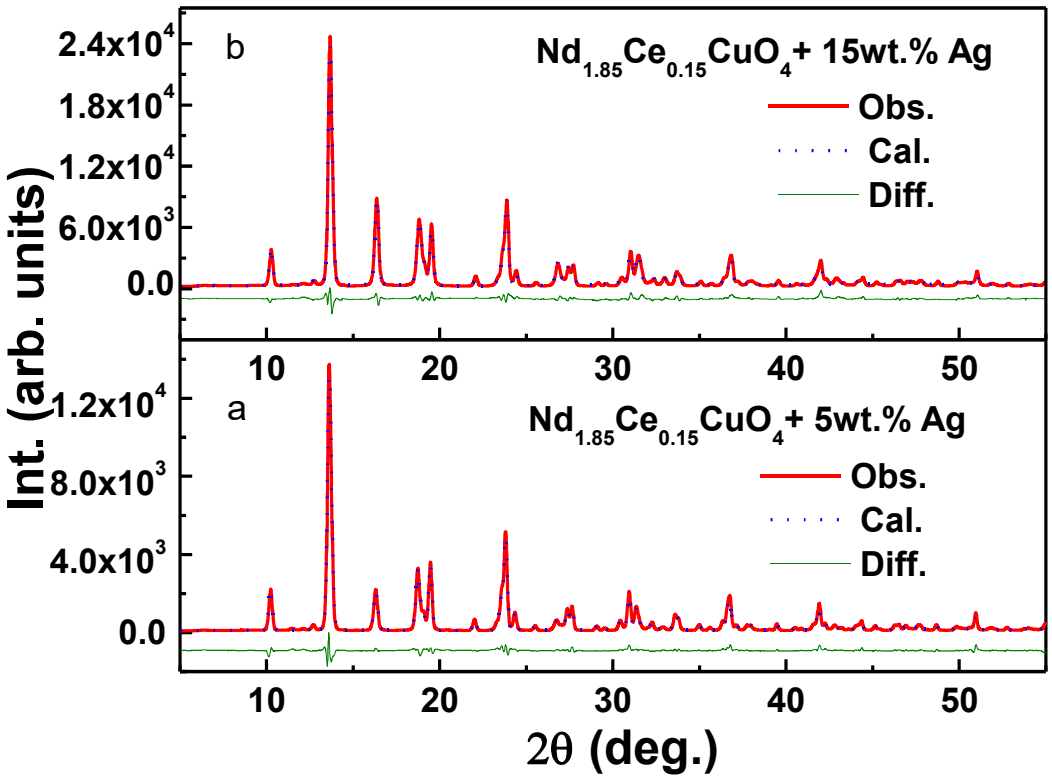

Fig. 4.3 Rietveld refined powder XRD plot of (a) $Nd_{1.85}Ce_{0.15}CuO_4$ + 5 wt.% Ag and (b) $Nd_{1.85}Ce_{0.15}CuO_4$ + 15 wt.% Ag

This may lead to additional electron doping similar to Ce^{4+} and consequent reduction of *c* lattice parameter, perhaps due to removal of apical oxygen defects upon electron doping (reduction of Cu^{2+}). A very light Ag doping for Cu, established for the $YBa_2Cu_3O_7$ superconducting system gives evidence for the possibility of a small but finite substitution of Ag for Cu in the cuprate superconductors [5].

4.2.2. SEM-EDS Characterization

The SEM images of NCCO + Ag (Ag=0, 5, 15 wt.%) have been shown in the Figure 4.4 (a), (b) and (d). The low sintering temperatures, being limited by the melting point of Ag, leads to sub-micron grain sizes, and due to the small sizes a certain amount of agglomeration is also present as seen in the SEM pictures. The average grain sizes of the samples as observed from SEM are roughly in the range of 650-900 nm for all the samples namely NCCO+Ag (Ag=0, 5, 15 wt.%). The presence of Ag in the Ag = 5 & 15 wt.% samples have been confirmed by elemental mapping for Ag (see Figures 4.4 (c) and (e)).

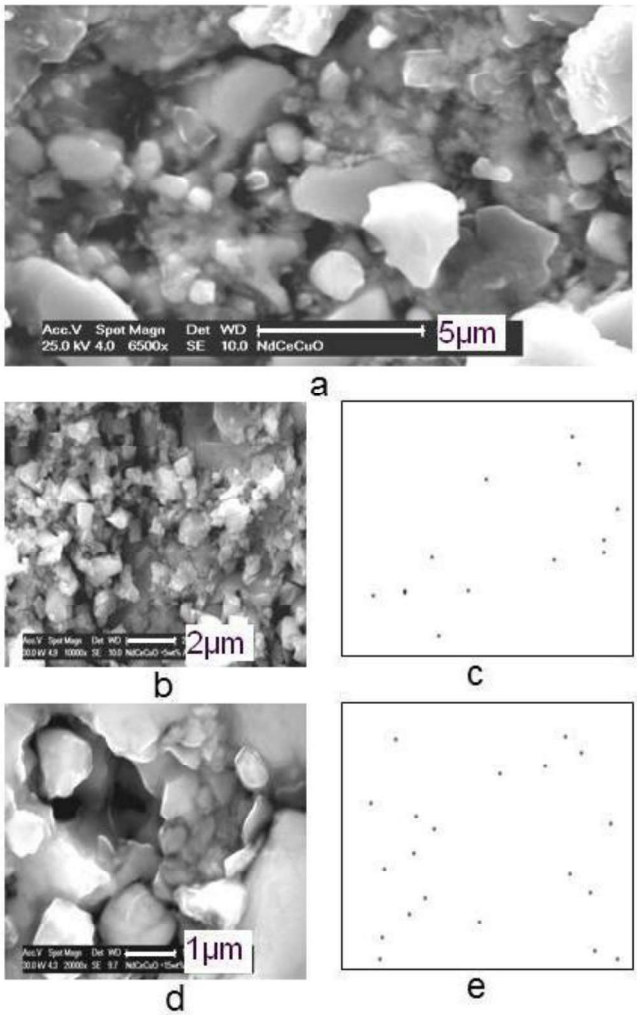

Fig. 4.4 (a) SEM Image of NCCO; (b) SEM image of NCCO+Ag 5 wt.% and (c) corresponding element map of Ag;(d) SEM image of NCCO+Ag 15 wt.% and (e) corresponding element map of Ag

The electron image and the corresponding elemental map for Ag indicate the presence of Ag distributed randomly and absence of its clustering. This, in conjunction with the XRD analysis indicating Ag as a second phase, led us to believe that Ag essentially may be located at the inter-grain spaces. Analysis of the crystallite size, namely, the coherent domain size as seen by X-ray has also been carried out by determining the X-ray line width. They indicate very small line broadening of 0.04-0.05^{o},which is presented for (101) reflection in Figure 4.5, leading to a crystallite size of ≈2000 Å as extracted using single peak analysis applying Scherer formula.

Table 4.1 Structural parameters refined from Synchrotron XRD data of NCCO + Ag system

Nominal Composition	**Lattice Parameter '*a*' Å(±0.0002) '*c*' Å(±0.0005)**		**Unit cell volume, Å^3**	**Silver Content Phase fraction, Sph Weight %**	
$Nd_{1.85}Ce_{0.15}CuO_4$	3.948	12.085	188.365		
$Nd_{1.85}Ce_{0.15}CuO_4$ +Ag 5 wt.%	3.947	12.082	188.22	0.2801	5.2%
$Nd_{1.85}Ce_{0.15}CuO_4$ +Ag 15 wt.%	3.940	12.065	187.29	0.7445	13.9%

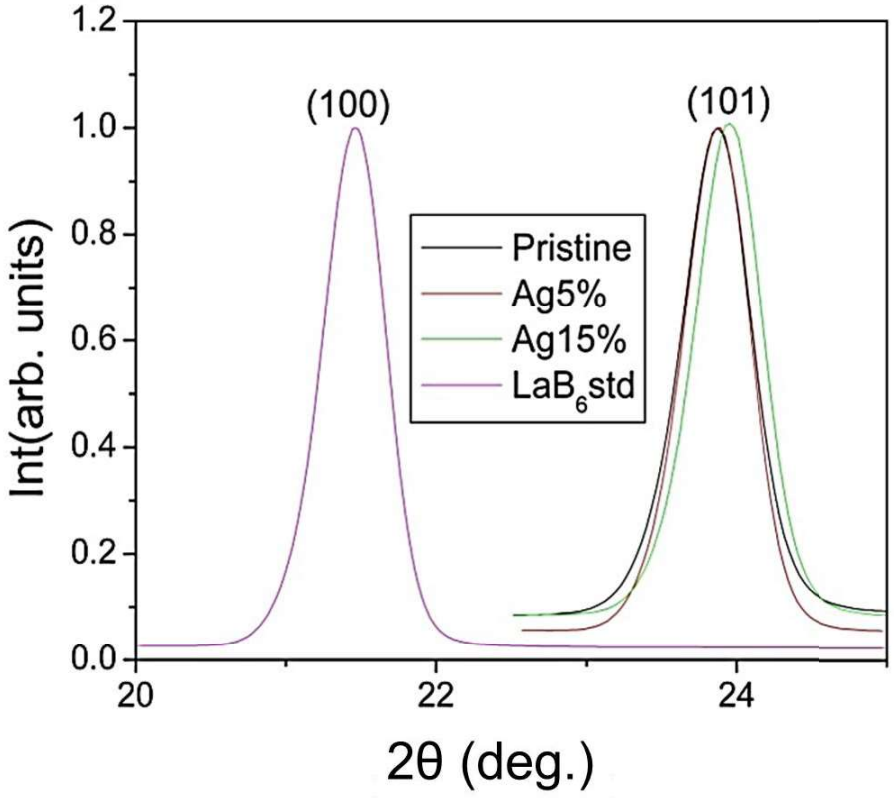

Fig. 4.5 Expanded view of the (101) reflections of the NCCO + Ag (0, 5, 15 wt. %) in comparison with the (100) reflection of standard LaB_6 taken under identical conditions

4.3. Raman Spectroscopy

Raman spectroscopic measurements have been carried out on pellets of $Nd_{1.85}Ce_{0.15}CuO_4$ and $Nd_{1.85}Ce_{0.15}CuO_4$+Agusing Renishaw in Via micro Raman spectrometer (Renishaw, UK) using 10mW power of the 514.5 nm Ar ion laser. Measurements were made in the backscattering geometry with Z axis of laboratory frame taken as direction of laser propagation and the sample surface as the XY plane. Polarized Raman measurements were carried out by inserting an analyzer and an additional half wave plate in scattered light path for parallel polarization (XX) and perpendicular polarization (XY) respectively. Data analysis was carried out using WIRE software of the Renishaw make in Via Raman spectrometer. Collected spectra were smoothed and corrected for background. Additional area normalization was done for un-polarized

spectra, while no further processing was done for polarized spectra. Un-polarized Raman spectra were fitted with Lorentzian line shapes for the observed main modes.

Raman spectroscopic studies have been carried out to probe the local structural changes, oxygen disorder and preferred-orientation effects associated with the addition of Ag to $Nd_{1.85}Ce_{0.15}CuO_4$. The room temperature un-polarized Z(X,XY)-Z and area normalized Raman spectra of $Nd_{1.85}Ce_{0.15}CuO_4$+xAg (x = 0, 5, 10 and 15 wt. %) system are presented in Figure 4.6. Intensity axis limits are kept equal for all spectra in order to compare relative intensity variations. The low energy Raman spectra below 700cm^{-1} exhibit five sharp phonon modes and a weak mode around 820 cm^{-1}, which may arise from two phonon scattering[18]. The sharp spectral feature at 223 cm^{-1} may be attributed in analogy with existing literature on the Raman response of $Nd_{1.85}Ce_{0.15}CuO_4$[19], to the crystal field excitations of the Nd^{3+} ion along Z direction (A_{1g}). The sharp feature at 326 cm^{-1} is a B_{1g} phonon associated with the out-of-phase *c* axis vibration of the oxygen atoms in the CuO_2 plane and the peak around 480 cm^{-1} is associated with the in-phase vibration of the oxygen atoms in the CuO_2 plane with E_g symmetry[20].

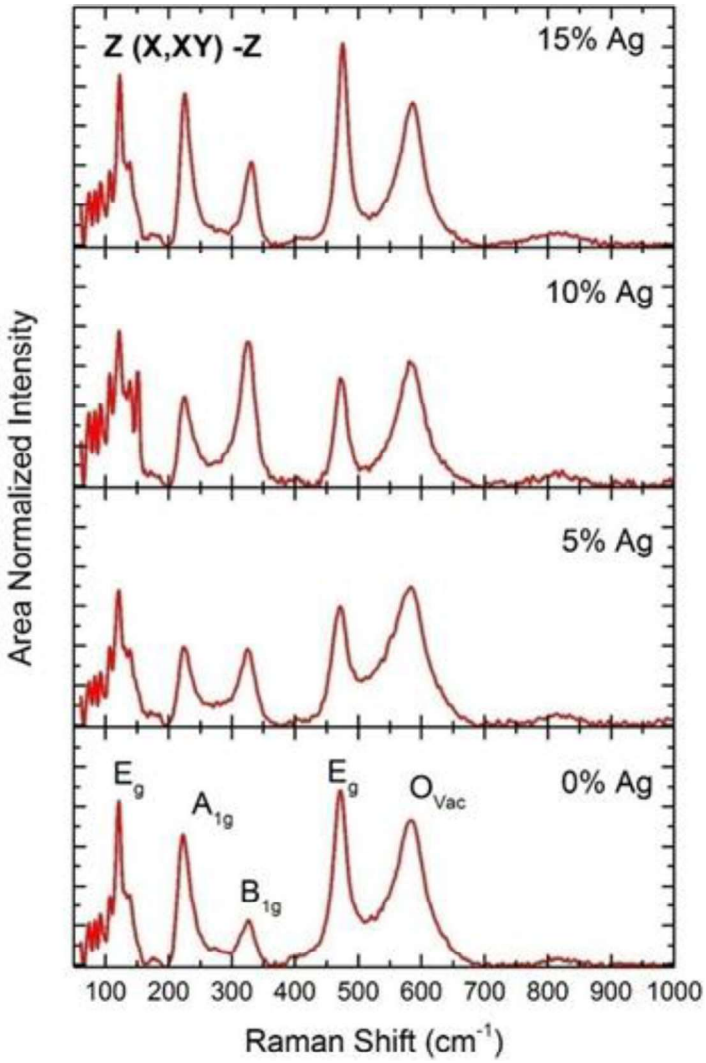

Fig.4.6 Raman spectra of the $Nd_{1.85}Ce_{0.15}CuO_4$+Ag (0, 5, 10 and 15 wt.%) pellets

The origin of the broad feature at 580 cm^{-1} may be a defect mode arising due to apical oxygen atoms in excess of O_4 and has been widely reported in literature [18-22]. In addition, a very broad satellite feature at 540 $cm^{-1}$is observed for the pristine (Ag content =0%) sample which is perhaps associated with a wider distribution of apical oxygen defect mode frequencies arising due to a broader distribution of the oxygen defects at interstitial sites. Apart from these major modes a sharp mode at ~120 cm^{-1} is observed in all samples. This mode is an E_g symmetry mode of $Nd_{1.85}Ce_{0.15}CuO_4$ analogous to the 480 $cm^{-1}E_g$Raman mode [22].The modes of the above set of unpolarised Raman spectra, for $Nd_{1.85}Ce_{0.15}CuO_4$ and $Nd_{1.85}Ce_{0.15}CuO_4$+Ag samples shown in Figure 4.6 were fitted with Lorentzian line shapes. Figure 4.7 shows the variation of mode frequencies with

increasing Ag addition. As seen from the figure, all modes show slight hardening with increasing Ag content. This is consistent with the unit cell volume reduction observed with increasing Ag addition, as shown in Table 4.1

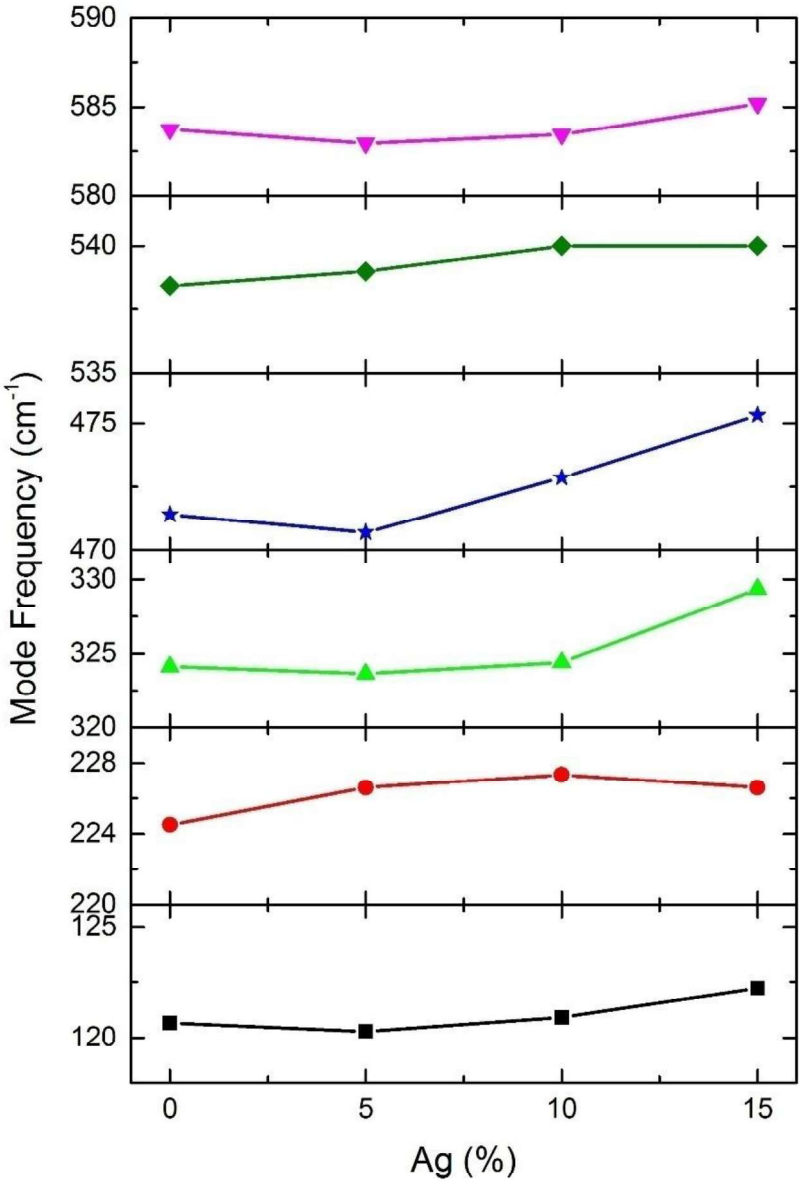

Fig. 4.7 Variation of mode frequencies with increasing Ag addition

Figure 4.8 shows variation of area under O-defect modes at 540 and 580 cm^{-1}. While the defect mode corresponding to 580 cm^{-1} shows a reduction, the 540 cm^{-1} mode is also reducing in intensity and nearly diminishes with increasing Ag content. This may be due to partial removal of some of the apical oxygen present in excess of O_4 by Ag defects which could lead to a shrinking of the *c* lattice constant as observed. The minor phonon

hardening is observed in Ag doped MgB_2 superconductor as well. A decrease is observed in phonon frequency with respect to the increase in lattice volume. This is described by the Gruneisen relation that expresses the dependence of phonon mode frequency with respect to change in volume of the unit cell.

$$\frac{d\omega}{\omega} = -\gamma \frac{dV}{V} \tag{4.1}$$

where, ω is the frequency and V is the related unit cell volume, $d\omega$ and dV are the variations in ω and V and γ is the Gruneisen parameter.

Influence of Ag addition on intensities of observed modes could not be analysed owing to the strong polarization effects, arising from orientation of a few grains sampled in the micron size laser spot. The incident laser of ~ 1μm spot diameter is linearly polarized and aligned in X direction of the laboratory frame. Considering the polycrystalline nature of the samples, Raman signal is expected to be arising from randomly oriented crystals. However, the small area probed by the laser spot can still introduce orientation induced polarization effects on the observed intensities of Raman active modes. This was indeed confirmed by measurements done at various spots with different grain sizes which showed varied intensities of observed modes for same sample.

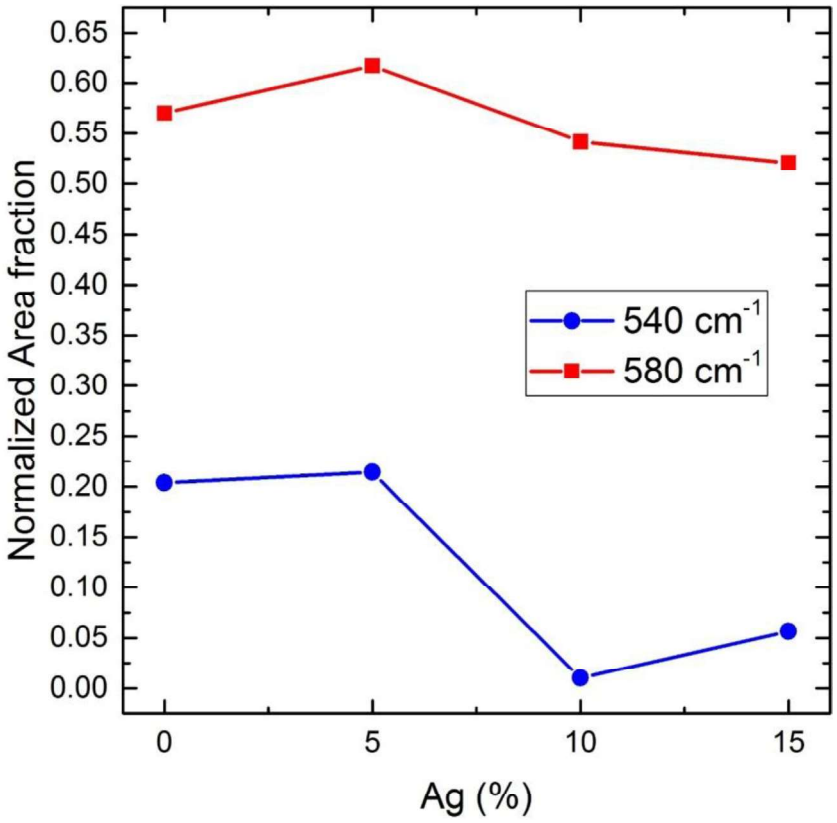

Fig. 4.8 Variation of normalized area under 540 and 580 cm-1 O-defect modes as a function of Ag content

The Polarized Raman Spectroscopic studies of the pristine $Nd_{1.85}Ce_{0.15}CuO_4$ as well as Ag doped samples were carried out. Figure 4.9 compares the Raman spectra of both parallel (XX) and perpendicular (XY) polarized scattering. Except B_{1g} mode at 325 cm^{-1}, all other modes show drastic reduction in intensity for perpendicular polarization, implying near symmetric nature of these modes.

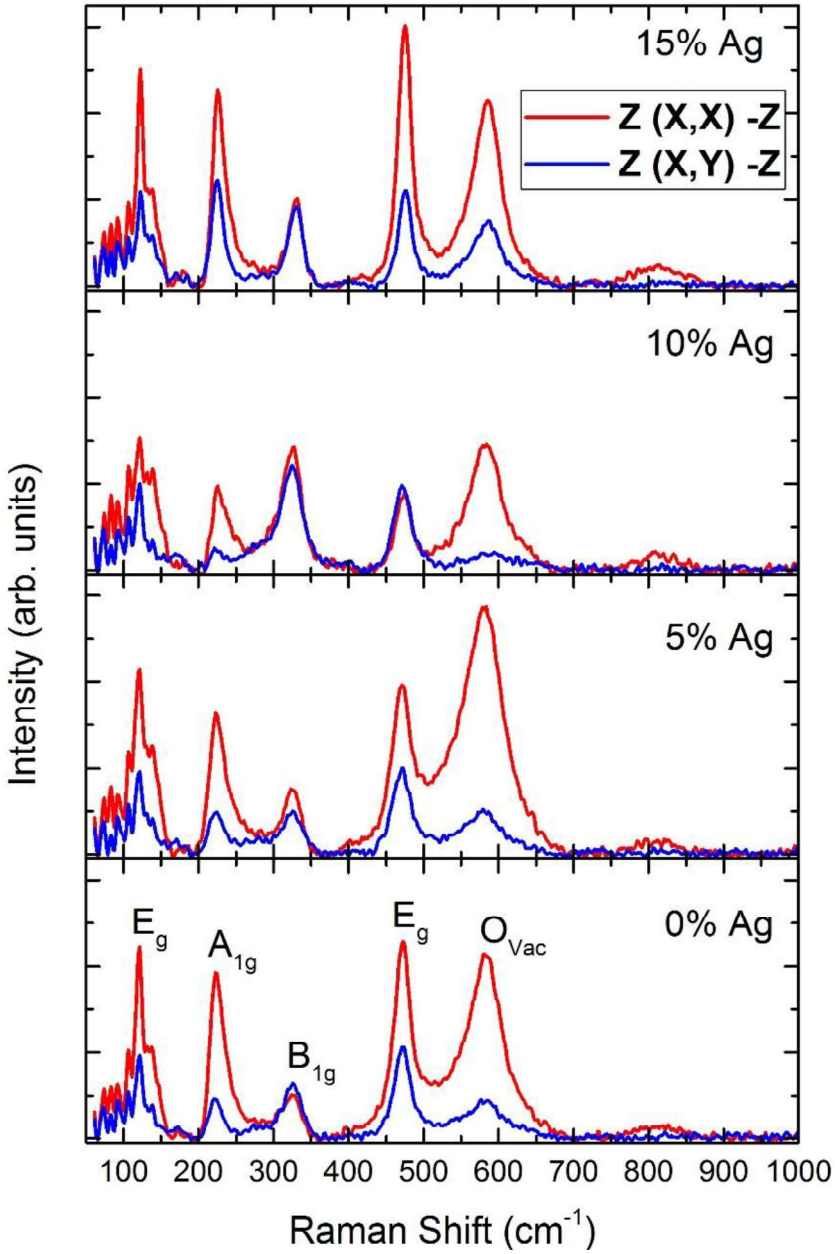

Fig. 4.9 Polarized Raman scattering spectra of both parallel (X,X), indicated by red lines and perpendicular (X,Y), indicated by blue lines

4.4. Magnetization

DC magnetization measurements were carried out on rectangular cuboid shaped samples (approximate dimensions: 1-2 mm x 0.8-1.2 mm x 0.6-0.8 mm), on a Cryogenics Ltd. MakeVibration Sample Magnetometer. For the magnetization measurements magnetic field is applied along the longest dimension to reduce the demagnetization factors.

The DC magnetization curves of the pristine system as well as Ag added system (5 wt.%, 15 wt.%) with respect to temperature have been shown in the Fig 4.10. In all the three cases, the superconducting transition temperature (T_C) is found to be around T_C ~23 K. It is to be noted that silver substitution has not resulted in a significant change in T_C. But interestingly, it is seen that Ag addition has contributed to increase in the diamagnetic shielding as the absolute value of $4\pi\chi$ has increased with the Ag addition (cf. Figure 4.10) .This increase in the diamagnetic shielding signal for the Ag added sample may be either due to the increase in superconducting volume fraction or due to the increase in current carrying capacity of the superconducting grains. As the increase in critical current density of the superconducting grains enhances the Meissner shielding currents, this would result in larger diamagnetic shielding signals. The absolute value of $4\pi\chi$ is significantly less than 1 for the present samples. As mentioned earlier, the field at which the magnetization has been measured is 100 Oe which is much higher than the reported value of the lower critical field (H_{C1}) of $Nd_{1.85}Ce_{0.15}CuO_4$ [23]. Hence the Meissner effect is expected to be incomplete. There is also a contribution due to the paramagnetic background from the paramagnetic rare earth (Nd^{3+}) ions in the superconducting $Nd_{1.85}Ce_{0.15}CuO_4$ lattice.

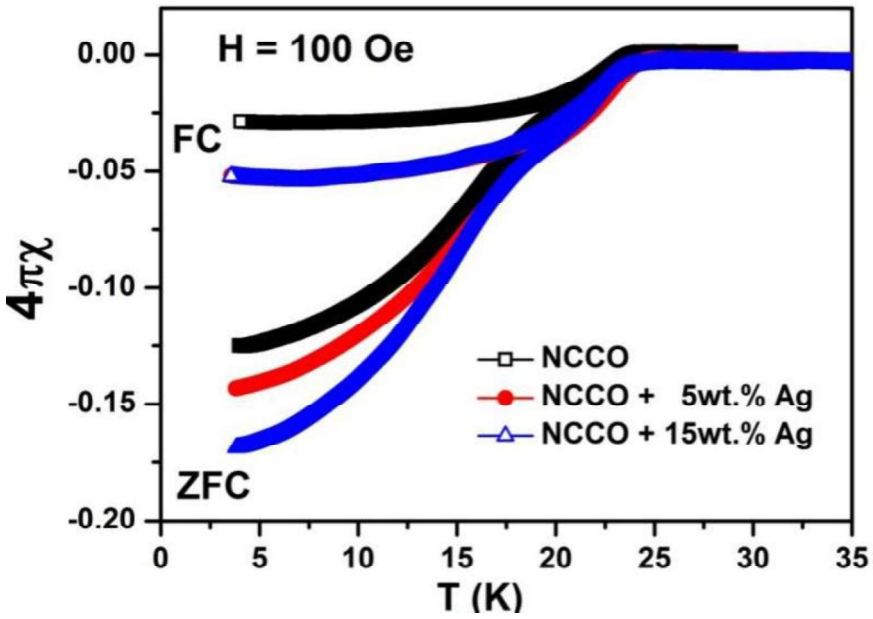

Fig. 4.10 Zero field cooled (ZFC) and Field cooled magnetization measurements as a function of Temperature of NCCO, NCCO+5 wt.% Ag and NCCO +15 wt.% Ag samples, under a field of 100 Oe

The ZFC curves measured at different fields for the Ag 5 wt. % sample have been shown in Figure4.11.

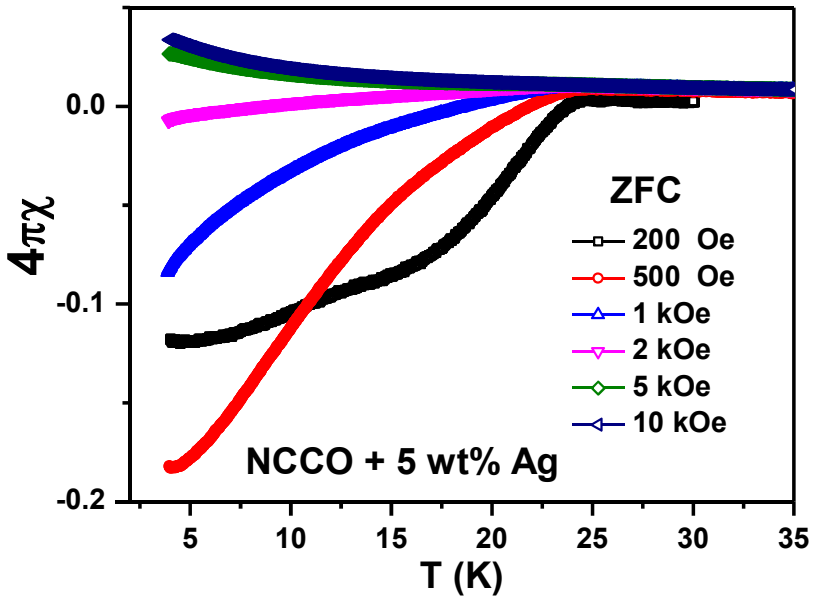

Fig. 4.11 Zero field cooled (ZFC) Magnetization measurements as a function of Temperature of NCCO + Ag 5 wt.% samples measured for different applied fields

This figure clearly shows the superconductivity in the background of strong paramagnetism. The ZFC curves measured at lower fields show sharp diamagnetic signal

at the superconducting transition temperature, T_C ~ 23 K. As the measuring field strength is increased, the strength of diamagnetic signal is significantly suppressed while the transition temperature reduced only slightly. For higher measuring fields (H > 2 kOe), the susceptibility is positive even below the superconducting transition temperature and the M-T shows typical paramagnetic behavior ($M \propto 1/T$) with a small kink at the superconducting transition temperature.

Figure 4.12 shows the zero field cooled (ZFC) M vs. T data for the samples, measured at 10 kOe. The paramagnetic nature of the samples at the field (10 kOe) is clearly evident in the figure. Left inset of the figure show the $1/\chi$ vs. T plot and the solid lines shows the Curie-Weiss fit to the high temperature part of the data. At higher temperatures (T > 50 K) the $1/\chi$ varies linearly with temperature for all the three samples.

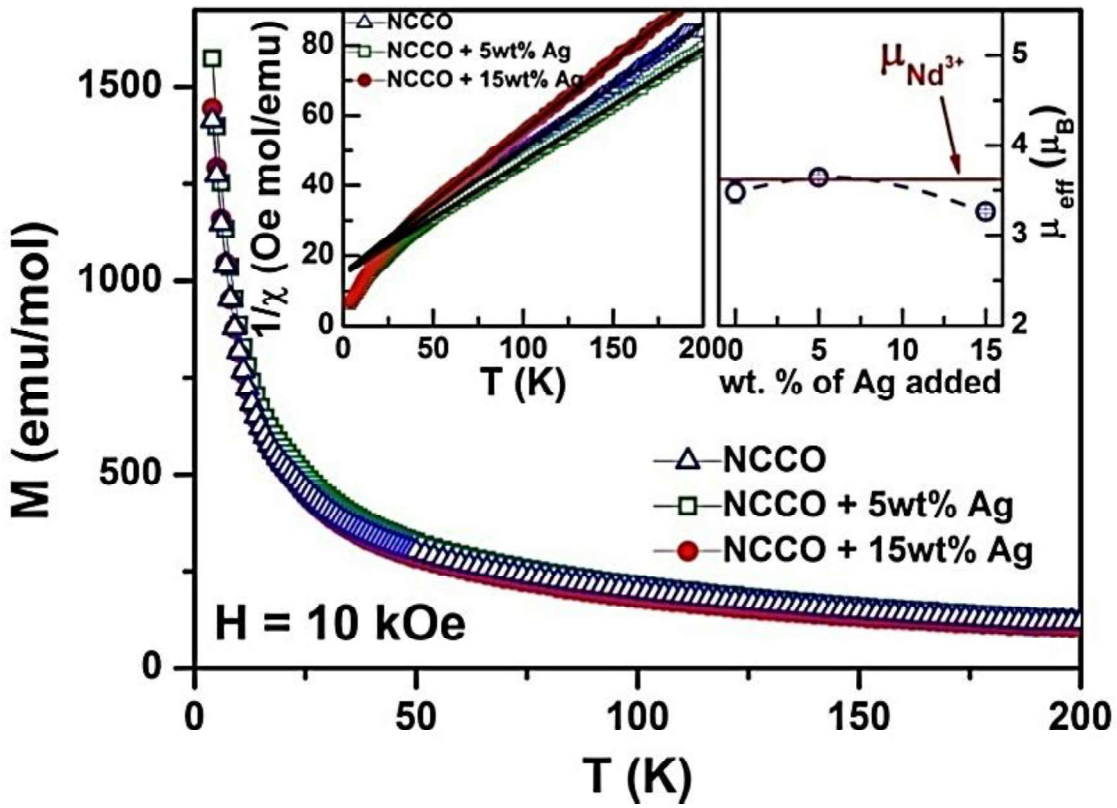

Fig. 4.12 Zero field cooled (ZFC) magnetization measurements as a function of Temperature for the Ag added NCCO samples measured at 10 kOe. Left inset: symbols show the $1/\chi$ vs. T plot and the solid lines shows the Curie-Weiss fit to the high temperature. Right insets shows the calculated effective magnetic moment.

From the Curie-Weiss fit to the high temperature part of the data the effective magnetic moment of the samples were estimated and is shown in the right inset of Fig. 4.12. The effective moment determined from the Curie-Weiss fit (blue symbols connected by dashed line) is close to the effective moment of Nd^{3+} ion.

4.5. Estimation of Critical current density (J_C)

For all the three systems investigated, critical current density (J_C) was calculated from the magnetic hysteresis loops. The M-H curves of all three systems have been plotted for comparison in Figure.4.13 (a). The M-H curves shows hysteretic behavior due to the superconductivity superimposed on to the linear paramagnetic moment. Inset of the Figure 4.13 (a) clearly shows the irreversible hysteretic type-II superconducting contribution near the zero field regions during the field increasing and decreasing cycles. The inset figure clearly shows the difference in M-H for the virgin and fully penetrated states. Figure4.13 (c) shows the M-H curves for the 5 wt.% Ag added sample measured at 4, 6 and 8 K.

Critical current densities in each case were calculated from the M-H curve as per the Bean's critical state model. Bean made use of a simple model to explain hysteresis in magnetization of a type II superconductor. He has considered a field independent critical current density. In this model the pinning force which is assumed to be uniform in the material is described in terms of critical current through the relation.

$$f_p = J_c \times \frac{\phi_0}{c} \qquad (4.2)$$

Considering a cylindrical sample and assuming that the applied field is greater than the critical field (H_{C1}), the flux density is the highest at the edges of the sample and lower in the inside of the sample. Because of the entry of vortices in the sample, large current is produced according to

$$\nabla \times \bar{B} = 4\pi \frac{\bar{J}}{c} \quad (4.3)$$

The flux density gradient is said to be in the critical state when the flux penetrates inward and the Lorentz force is not strong enough to overcome the pinning force. The circulating currents, which flow, have the value of J_C. The total flux inside the sample is less than that of the equilibrium case in the absence of pinning. Irreversible magnetization is difference of magnetization observed in these two cases. Bean's model can explain the hysteresis behavior of type II superconductors. The width of the magnetization of the M-H curve, δM is proportional to the critical current density of the sample. Hence the model is widely used in estimating the critical current density of superconducting materials from field dependent magnetization materials.

As only the high field data has been investigated in our VSM measurements the grains are essentially decoupled and the intra-granular critical current density has been calculated and is shown in Figure.4.13 (b) for pristine, 5wt. % and 15 wt.% Ag added samples for 4 K. The expression used for calculating the critical current (J_C) is $J_C = 20$ ΔM/d, where'd' is the average grain size of the sample and has been taken to be 800nm from the SEM study. It is observed that the intra-granular critical current density in the Ag added samples have shown significant change as compared to the pristine sample. At 4 K, the maximum J_C of the pristine sample is found to be 3.69x 10^6 A/cm^{2}whereas at the same temperature the value of J_C is observed to increase to 6.01x 10^6 A/cm^{2}for Ag 5 wt.% sample. For the Ag 15 wt.% sample, J_C has increased to 6.43 x 10^6 A/cm^2. J_C is seen to increase sharply at lower temperatures. Figure 4.13 (d) shows the variation of intra-granular critical current density for the 5wt.% Ag added sample for different temperatures 4, 6 and 8 K.

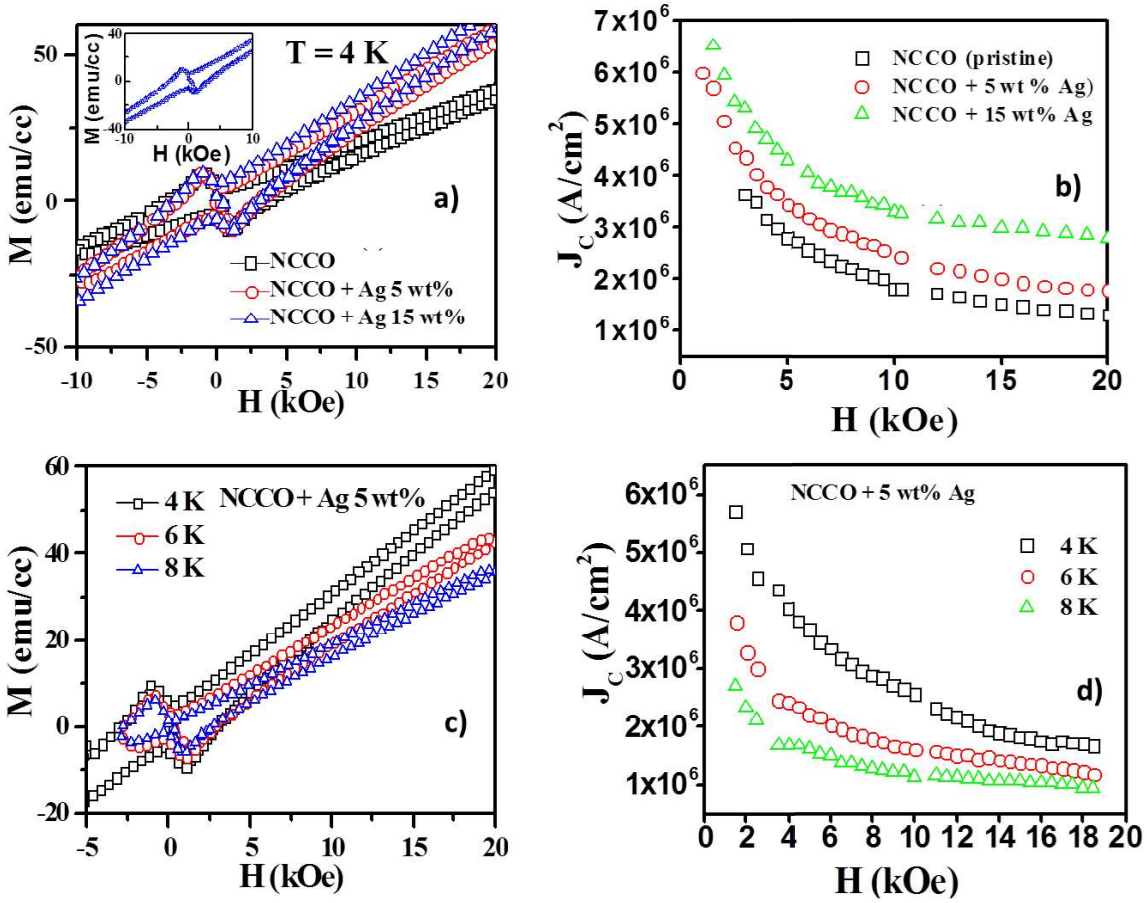

Fig. 4.13 Magnetic hysteresis loops (a) and critical current density vs. magnetic field plots (b) for the Ag added $Nd_{1.85}Ce_{0.15}CuO_4$ samples at 4 K. Inset of (a) shows the low-field zoomed M-H plot for the 15wt.% Ag added sample. Magnetic Hysteresis loop for NCCO (c) M-H plot of NCCO+Ag 5wt.% (d) Intra-granular J_c of NCCO+Ag 5wt.%.

In order to study the inter-granular transition and associated critical current behavior we have carried out bulk resistivity measurements as a function of electrical current. The data are presented for the pristine, 5wt. % and 15 wt. % Ag added samples in Figure4.14 (a), (b) and (c) respectively. It is seen that all samples attain zero resistance for the minimum value of applied current of 100μA. The superconducting transitions reveal a double step which has been reported in literature [24] and also discussed briefly in our studies on the pristine compound presented in Chapter 3. The first drop in resistance corresponds to the intra-granular transition and the second step observed corresponds to the inter-granular transition. Zero resistance is attained by Josephson junction coupling between the superconducting grains. When current applied is increased

the self-fields generated tend to destroy the Josephson junction coupling; this results in an increase in resistance [25]. From Figure4.14it is clear that the Ag added samples sustain higher values of current. In the case of pristine sample, the rough value of inter-granular critical current, that is, the current at which a finite increase in resistance is observed is of the order of 200-500μA whereas for the Ag added samples it is of the order of 5mA.While the pristine sample shows higher electrical resistivity and an insulating behavior for a current of 5 mA, the Ag added samples exhibit lower resistivity and do not show insulating behavior even for comparatively higher currents of 25mA. Literature studies in ceramic superconductors indicate that the inter-granular critical current density is found to dependent inversely on the normal state resistance of the grain boundaries [13]. This results in J_C being inversely proportional to the sample's resistivity in the normal state. Considering this fact coupled with our electrical resistivity data of Figure.4.14, it can be inferred that the Ag added samples exhibit higher inter-granular J_C compared to the pristine sample.

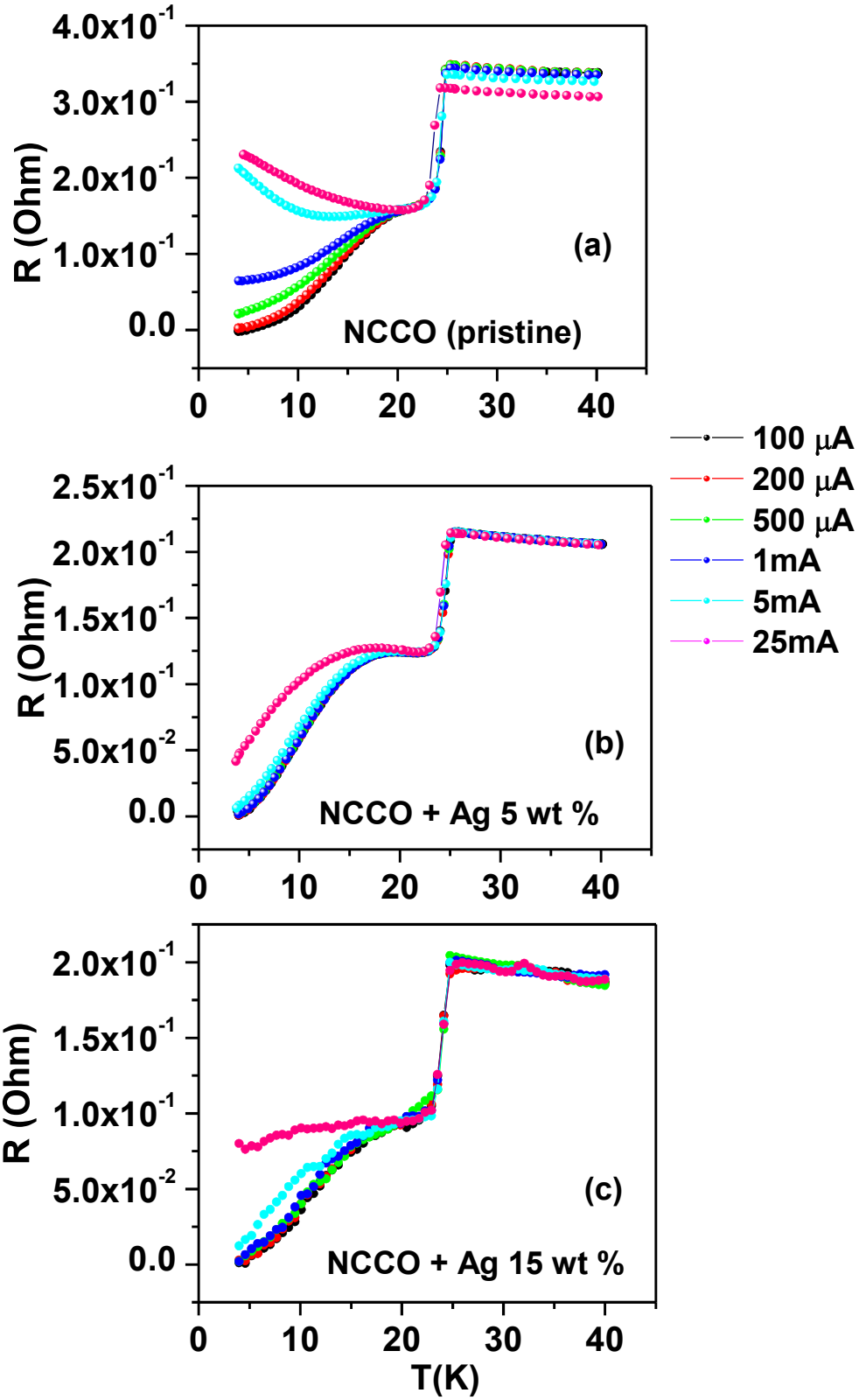

Fig. 4.14 Current dependence studies of (a) NCCO (pristine), (b) NCCO + Ag 5 wt%, (c) NCCO + Ag 15 wt%

Summarizing the study, in Figure 4.15, we show the variation of T_C,J_C(intra-granular), ρ and χ (DC), with respect to Ag addition. It is to be noted that the T_C has not shown any significant change with respect to Ag addition. The intra-grain J_C as mentioned has shown a significant increase. The inter-granular critical current inferred from resistivity measurements is also evidenced to increase with Ag addition. ρat 300 K for the pristine sample is 0.83 Ω cm and that of NCCO+5 wt % Ag is 0.25 Ω cm while NCCO+15 Ag wt.% shows the lowest value of resistivity at 0.05 Ω cm. The DC Susceptibility values also have shown an increase in magnitude from-0.125 emu/cc (NCCO pristine) to -0.170 emu/cc (NCCO+15 Ag wt.%).

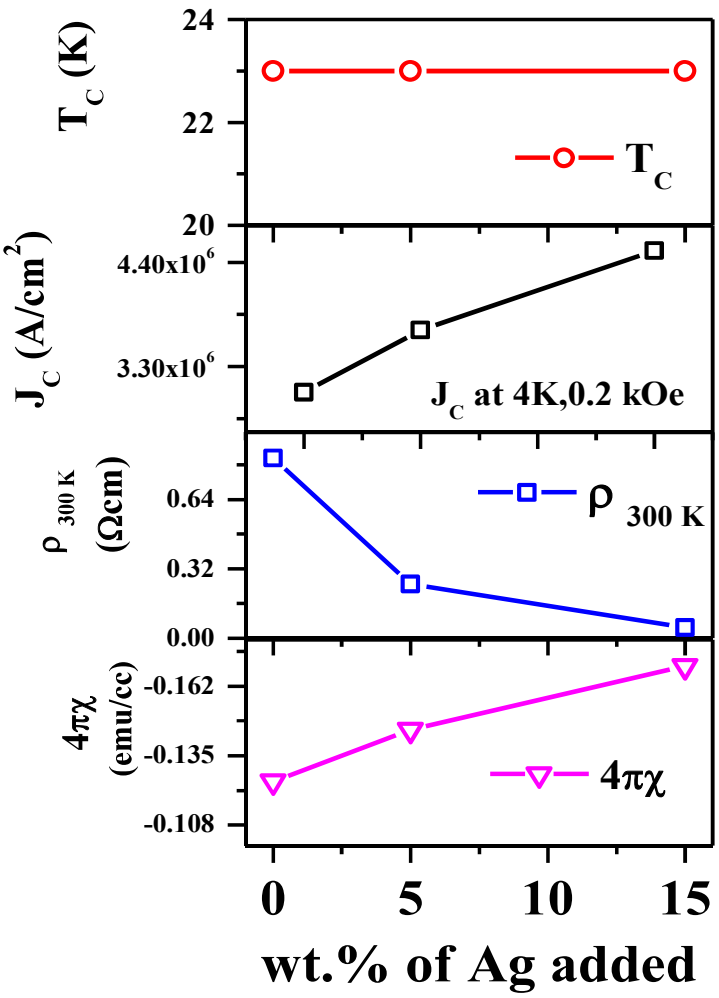

Fig. 4.15 Variation of Critical Temperature, Critical Current density (intra-granular) , Room temperature resistivity and Susceptibility with respect to weight % of silver.

The present observation of J_C enhancement correlates well with the enhancement reported in literature for the hole-doped YBCO/Ag superconducting composites[26]. Ag precipitates are unlikely to be pinning centers, as the precipitates are not of nanoscopic scale, and far exceed in size of the dimensions of the coherence length (15-30Å) [10]. Moreover ,a possible doping of Ag for Cu may also exist [27]. Ag doping can act as defects which can increase the critical current density by pinning the motion of the flux vortices. This enhancement in pinning by silver substitution may lead to an enhancement in intra-granular critical current density. Ag precipitates can influence the distribution of residual stress which in turn can lead to propagation of dislocation, which can act as effective pinning centers to enhance J_C [28,29].

4.6. Magneto resistance (MR) study of NCCO/Ag composites

The results of our magneto-transport studies on pristine NCCO highlighted in the previous chapter clearly indicates that unlike its hole doped counterparts, wherein weak links are also present, the granular features of electron doped superconductors are more sensitive to magnetic field. The electrical resistivity studies as a function of magnetic field carried out on NCCO/Ag composites, which are shown in Figure. 4.16 (a) - (c), indicate several interesting features analogous to the pristine sample: (i) It is observed that the zero resistance attained in zero magnetic field vanishes under application of even a small field of a few milli-Tesla (mT). The effect of magnetic field on weak links in n-type superconducting ceramics causes T_{C1} (the intra-grain transition), T_{C2} (inter-grain transition) to shift towards lower temperatures when the applied magnetic field is increased up to 3 T. (ii) It is observed that (see Figure. 4.16 (a)-(c)), a small field of B ~ 0.02 T inflicts a change in slope of ρ(T) leading to a drastic increase in its value which peaks around T_{JE} (Temperature at which Josephson junction coupling becomes prominent)~ 6.5K and decreases with further lowering of temperature. The height of this

peak is found to increase in the regime of comparatively lower fields of 0 to 0.08 T. T_{JE} appears to shift to lower temperature with increasing B up to 3T. (iii) In all the three cases (cf. Figure 4.16 (a), (b), (c)) at higher magnetic fields (B >3 T), the resistivity dip at T_{JE} is not observed. These non-monotonic resistive transitions (as explained in the previous chapter), which happens due to granular effects, persist even after the addition of Ag in the polycrystalline samples and the weak-link problem in this system is perhaps extremely complex and cannot be solved by alloying with Ag.

The resistive upper critical field of NCCO, NCCO+ Ag 5 wt.%, NCCO+Ag 15 wt.% and their temperature dependence has been investigated. Figure.4.16 (d), (e), (f) show the variation of upper critical field (H_{C2}) with respect to temperature. The upper critical field H_{C2} is determined as the field at which the resistivity in the transition region is 90% of the normal state resistivity. The variation of $H_{C2}$is seen to be linear near T_C for all three samples and found to be in close agreement with the Werthamer-Helfand-Hohenberg *(WHH)* model [30] which describe the behaviour of the upper critical field in conventional type-II superconductors. The highest value of slope, dH_{C2}/dT_C = -0.56, is found to be for the pristine sample (see Figure 4.16 (d)). Among the Ag added samples, NCCO + Ag 5 wt.% shows the highest value -0.36 (see Figure 4.16 (e)). The $H_{C2}(0)$ values calculated from the WHH formula $H_{C2}(0) = 0.69\, T_c \left({}^{dH_{C2}}/_{dT_C} \right)_{T_C}$ [30], are found to be 9.8 T , 6.3 T, 5.3 T for NCCO, NCCO+Ag5 wt.% and NCCO+Ag 15 wt.% respectively. The decrease in $H_{C2}(0)$ with Ag addition is consistent with the marginal decrease in T_C and may also possibly arise due to an increase in local site disorder.

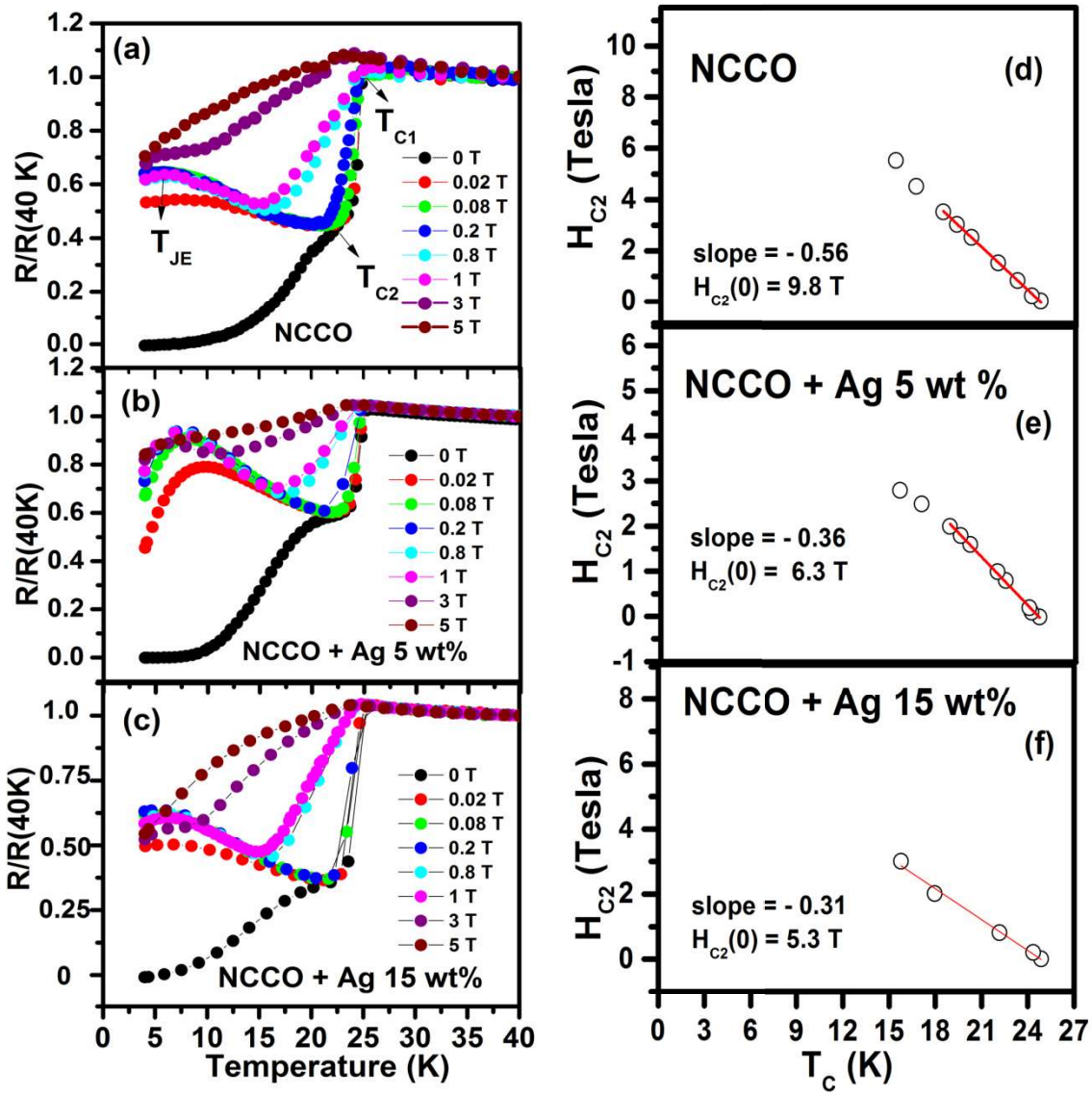

Fig. 4.16 (a), (b), (c) showing Temperature dependence of normalized resistance of NCCO, NCCO +Ag 5 wt.% , NCCO+Ag 15 wt.% taken in different magnetic fields as indicated and (d), (e), (f) showing Temperature dependence of HC2 of the same along with the line. Red lines represent the fit with WHH equations.

The isothermal Magnetoresistance plots of NCCO, NCCO+Ag 5 wt.% and NCCO+Ag 15 wt.% are shown in Figure. 4.17. From Figure 4.17 (b), (c), it is clearly observed that there is an increase of resistance (R) with an increase in magnetic field (B), bringing out three regimes: (i) large increase in R in low field regime (B<0.5), moderate increase of R for 0.5<B<2-3T and a marginal increase of R in the high field regime (B>3T) at 4 K and 10 K. In Figure 4.17 (a), it is seen that the pristine sample also

behaves in a similar manner with an exception at 4 K, where a slight decrease in resistance is observed as the field increases from 0.3 T to 2 T which is followed by a region of moderate variation up to 4 T and then an increase of resistance in the high field regime.In all the three cases (Fig. 4.17(a), (b), (c),) the resistance remains independent of field for temperatures $T>T_{C1}$~24K, as expected.

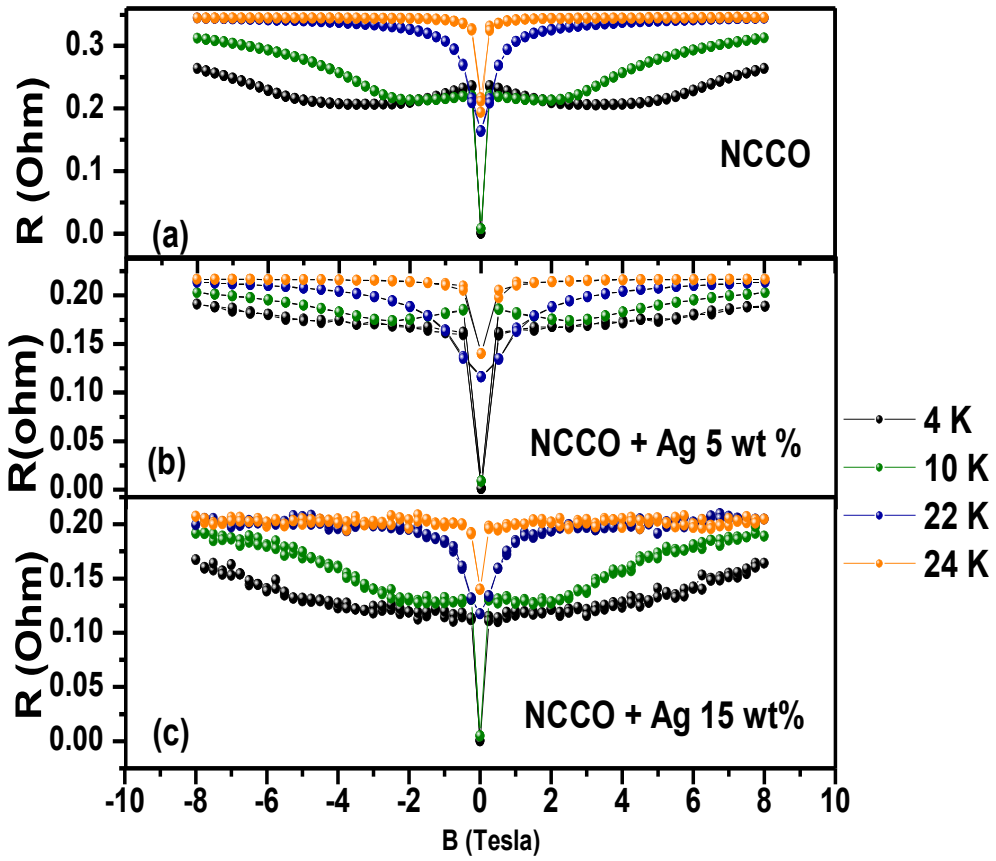

Fig. 4.17 (a), (b), (c) Isothermal Magneto-resistance plots of NCCO, NCCO + Ag 5 wt.% , NCCO + Ag 15 wt.% as a function of field respectively

The observed resistance versus field behavior at low temperature can be reconciled with the picture of granularity described in literature [24]. In the magneto-resistance studies, three general behaviors are observed

(i) Increase of resistance in low fields

(ii) A region of moderate variation/decrease in resistance at relatively higher fields

(iii) Increase in resistance, at very high fields

The initial increase of resistance under low fields can be attributed to the destruction of Josephson junction coupling. The subsequent decrease seen in resistance is due to the suppression of intragranular superconducting energy gap, which results due to the enhancement of quasiparticle tunneling. The increase in resistance, at very high fields may arise be due to the suppression of intragranular superconductivity. It is significant to note that the maximum increase of R in the low field is seen for the pristine sample, which systematically decreases with increase in Ag content. This may stem due to an improvement in inter-granular coupling upon addition of Ag.

4.7. Conclusion

The effects of the Ag addition on the electron doped cuprate, $Nd_{1.85}Ce_{0.15}CuO_4$ is investigated for the first time. The most important result is the significant increase in critical current density (J_C) upon silver addition. This scales well with the observed small but significant change in lattice parameter upon Ag addition which along with the quantitative Rietveld phase analysis gives evidence for possible incorporation of Ag in the lattice to the extent of ~ 1 wt.%. The rest of the silver is present as free silver, perhaps at the grain boundaries, as estimated quantitatively. The reduction in unit cell volume is consistent with the minor phonon hardening of all Raman modes upon Ag addition, observed in this study. Other interesting changes in structural features observed upon Ag addition include a diminishing of the apical oxygen defect mode as well as a randomization of preferred orientation. Our SEM studies indicate an average grain size of 800nm and no significant changes in grain size occur upon Ag addition. This is in contrast to the YBCO/Ag system, wherein both grain size and texturing increases upon Ag addition. However, despite the absence of grain size increase our low temperature electrical and magnetic property studies indicate that some of the superconducting properties including intra and inter-granular critical current densities (J_C) are significantly

enhanced upon Ag addition. The former has been studied by DC magnetization using VSM and the latter by current dependent electrical resistivity. The resistive superconducting transitions of NCCO/Ag composites show large granular effects which exhibit anomalous features in magneto-resistance behaviour. These anomalies have been qualitatively understood based on the interplay of Josephson junction coupling and quasi-particle tunneling; the combined effects of which dictate the evolution of the observed temperature and field dependent resistivity behaviour. The overall effects of granularity persist even upon the addition of Ag. The resistive upper critical field $H_{c2}(0)$of the NCCO, NCCO+ Ag 5 wt%, NCCO+ Ag 15 wt% systems has been estimated. The value of $H_{C2}(0)$ decreases with Ag addition from 9.8 T for NCCO to 6.3T and 4.9 T for NCCO + 5 wt. % and NCCO + 15 wt. % respectively. This may be due to an increase in local site disorder.

4.8. References

[1] D. Kumar, M. Sharon, P. R. Apte, R. Pinto, S. P. Pai, S. C. Purandare, C. P. D'Souza, L. C. Gupta, and R. Vijayaraghavan, Journal of Applied Physics **76**, 1349 (1994).

[2] S. K. Malik, C. V. Tomy, A. M. Umarji, D. T. Adroja, P. Ram, N. C. Soni, A. Mohan, and C. K. Gupta, Journal of Physics C: Solid State Physics **20**, L417 (1987).

[3] P. Rani, R. Jha, and V. P. S. Awana, Journal of Superconductivity and Novel Magnetism **26**, 2347 (2013).

[4] B. Srinivas and G. V. S. Rao, Bulletin of Materials Science **15**, 403 (1992).

[5] C. Zhang, University of British Columbia, 1991.

[6] D. X. Chen, Y. H. Shi, C. Navau, A. Sanchez, and D. A. Cardwell,

Superconductor Science and Technology **25**, 014010 (2012).

[7] D. Kumar, S. J. Pennycook, J. Narayan, H. Wang, and A. Tiwari, Superconductor Science and Technology **16**, 455 (2003).

[8] P. Rani, A. K. Hafiz, and V. P. S. Awana, Physica C: Superconductivity and its Applications **520**, 1 (2016).

[9] Y. H. Shi, A. R. Dennis, and D. A. Cardwell, Superconductor Science and Technology **28**, 035014 (2015).

[10] E. Mendoza, T. Puig, E. Varesi, A. E. Carrillo, J. Plain, and X. Obradors, Physica C: Superconductivity **334**, 7 (2000).

[11] P. d. Azambuja, P. Rodrigues Junior, A. R. Jurelo, F. C. Serbena, C. E. n. Foerster, R. n. M. Costa, G. B. d. Souza, C. M. c. Lepienski, and A. L. Chinelatto, Brazilian Journal of Physics **39**, 638 (2009).

[12] S. Hadi, A. B.-B. Ali, and S. Medhi, Superconductor Science and Technology **14**, 816 (2001).

[13] J. Jung, M. A. K. Mohamed, S. C. Cheng, and J. P. Franck, Physical Review B **42**, 6181 (1990).

[14] N. Yuichi, K. Kouji, I. Ryoji, and O. Akio, Superconductor Science and Technology **20**, 959 (2007).

[15] A. Hammersley, Journal of Applied Crystallography **49**, 646 (2016).

[16] B. H. Toby, Journal of Applied Crystallography **34**, 210 (2004).

[17] R. J. Hill and C. J. Howard, Journal of Applied Crystallography **20**, 467 (1987).

[18] S. Sugai and Y. Hidaka, Physical Review B **44**, 809 (1991).

[19] S. Jandl, M. Iliev, C. Thomsen, T. Ruf, M. Cardona, B. M. Wanklyn, and C. Chen, Solid State Communications **87**, 609 (1993).

[20] N. Munnikes, Technische Universität München, 2008.

[21] S. Hong, H. Jo, H. Cheong, and G. Park, Physica C: Superconductivity **418**, 28 (2005).

[22] Z. V. Popovic, A. Sacuto, and M. Balkanski, Solid State Communications **78**, 99 (1991).

[23] *Chemistry of High Temperature Superconductors* (WORLD SCIENTIFIC, 1991), p. 400.

[24] A. Gerber, T. Grenet, M. Cyrot, and J. Beille, Physical Review B **43**, 12935 (1991).

[25] P. W. Klamut, physica status solidi (a) **136**, 181 (1993).

[26] I. Dhingra, G. K. Padam, S. Singh, R. B. Tripathi, S. U. M. Rao, D. K. Suri, K. C. Nagpal, and B. K. Das, Journal of Applied Physics **70**, 1575 (1991).

[27] C. Zhang, A. Kulpa, and A. C. D. Chaklader, Physica C: Superconductivity **252**, 67 (1995).

[28] M. Junya, N. Yuichi, I. Teruo, and S. Yuh, Superconductor Science and Technology **12**, 563 (1999).

[29] B. Martínez, F. Sandiumenge, T. Puig, X. Obradors, L. Richard, and J. Rabier, Applied Physics Letters **74**, 73 (1998).

[30] N. R. Werthamer, E. Helfand, and P. C. Hohenberg, Physical Review **147**, 295 (1966)

Chapter 5

Magneto-Transport and Magnetization studies on $Nd_{1.85}Ce_{0.15}CuO_{4\pm\delta}$ thin films

From the point of view of understanding the mechanism of superconductivity in the cuprate materials, the study of magneto transport properties and magnetization of the electron doped superconductor $Nd_{1.85}Ce_{0.15}CuO_{4\pm\delta}$ thin films is crucial. The matter of interest here is the fact that the electrical properties of c-axis oriented epitaxial films of electron doped cuprates show substantive differences compared to that of hole doped cuprates [1]. The temperature dependence of normal state resistivity [2] and London penetration depth[3] are very well studied properties which clearly reveal such differences. For example, in $Nd_{1.85}Ce_{0.15}CuO_{4\pm\delta}$ single crystals and thin films, the normal state resistivity versus temperature curves have shown a T^2 dependence at low temperatures ($T<200K$)[4], which is very different from the linear temperature dependence of resistivity observed in the hole doped cuprate superconductors, $YBa_2Cu_3O_7$ and $La_{1.85}Sr_{0.15}CuO_4$[5,6].

Another even more interesting distinction is that the long range antiferromagnetic order in electron doped $Nd_{2-x}Ce_xCuO_4$can exist for larger values of x ($x \geq 0.12$) [7]and can even exhibit a co-existence with superconductivity[8]. Magneto-resistance studies on the under doped electron doped cuprates (non-superconducting) have already provided information regarding the coupling between the charges and background magnetism [9]. It is observed that the resistivity is sensitive to the interlayer magnetic order [9-11]. Hence, it would be interesting to study the magneto resistance of the $Nd_{1.85}Ce_{0.15}CuO_{4\pm\delta}$ both in its non-optimally annealed state (where we expect the

effects of antiferromagnetism also) and the superconducting state which is achieved by ex- situ reduction annealing.

In this chapter, the synthesis and characterization (by XRD and SEM) of $Nd_{1.85}Ce_{0.15}CuO_{4\pm\delta}$ thin films and the studies carried out on them by magneto transport and magnetization measurements have been presented. The films are synthesized by Pulsed Laser Deposition method using a KrF Excimer Laser. Magneto- transport properties have been studied in both the regimes, i.e., the film in its in-situ and ex-situ annealed states.

5.1. Synthesis and Characterization of thin films of electron doped super conductor $Nd_{1.85}Ce_{0.15}CuO_{4\pm\delta}$ (NCCO)

5.1.1 Synthesis

$Nd_{1.85}Ce_{0.15}CuO_{4\pm\delta}$thin films have been synthesized by the Pulsed laser Deposition method. During the optimization process three different substrates namely $LaAlO_3$, $SrTiO_3$ and MgO have been used. However, the subsequent studies have revealed that the change of substrates did not have any substantial effects on the physical properties of the films. Therefore, here we present all studies performed on the thin films deposited on the $SrTiO_3$ (STO) substrates. As per reports, films of the highest quality (including highest T_C) can be synthesized by performing deposition in N_2O atmosphere [12]. Nevertheless, superconducting films of lower T_C = 14-16 K have been synthesized using O_2 atmosphere also [13]. We have followed the latter method and carried out thin film depositions in the oxygen atmosphere by maintaining the oxygen pressure at 0.67 mbar. The laser fluence used is3.25 J/cm^2. The pulse energy is set at 260 mJ and the repetition rate being 5 Hz. The substrate was maintained at a temperature of 820°C during deposition. The as grown $Nd_{1.85}Ce_{0.15}CuO_{4\pm\delta}$ film, designated as NCCO has been subjected to an in-situ vacuum annealing at 740°C and has shown an onset superconductivity but without exhibiting zero resistivity. However, the full fledged

superconductivity with zero resistance has emerged in the film, designated as NCCO-S, after it was ex-situ annealed in Ar atmosphere. The thicknesses of the films measured using dektak profilometer were found to be nearly ≈ 300 nm. Further details regarding achievement of superconductivity shall be explained in the following sections.

5.1.2 X – Ray diffraction of NCCO films

X-ray diffraction measurements on NCCO and NCCO-S films have been carried out in the beam line BL-12 (ADXRD beam line) at INDUS-II Synchrotron source at RRCAT, Indore India. The patterns were recorded with a six circle diffractometer (Huber-5020) with NaI scintillation detector. The scanning was performed in θ-2θ mode and the associated plots are shown in Figure. 5.1.

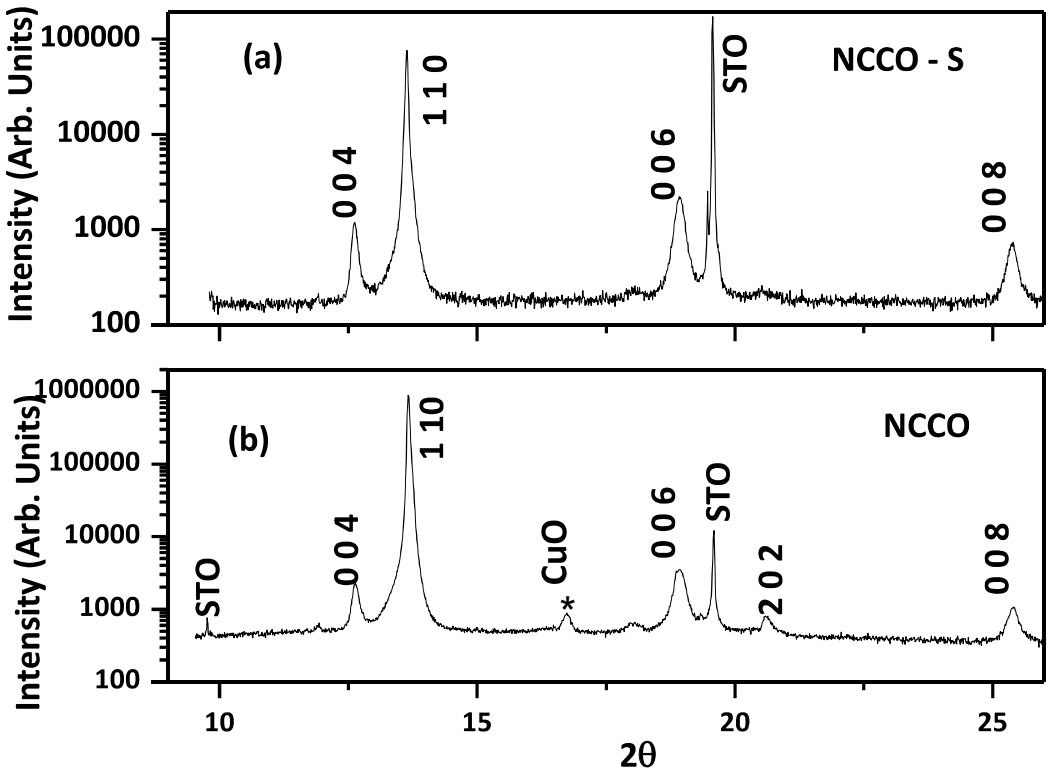

Fig. 5.1 X- ray diffraction scan of the films (a) NCCO-S, ex-situ annealed superconducting film (b) NCCO in-situ annealed film. Substrate reflections of SrTiO3 are denoted by STO

Apart from the substrate's reflections ($SrTiO_3$-STO) the major peaks corresponds to (00L) and (110) reflections[14]of the tetragonal T' structure observed in Nd_2CuO_4,

thereby indicating preferred orientation in the films. In the in-situ annealed film (NCCO) impurity peak which belongs to CuO and additional (2 0 2) reflection have been observed whereas the ex-situ annealed film is devoid of the same. The *a* and *c* axis lattice constants are determined to be 12.09 Å and 3.952 Å respectively which are in agreement with reported values of NCCO thin films [12].

5.1.3 Scanning electron microscopy (SEM)

The SEM images of NCCO-S film and NCCO bulk have been shown in Figure5.2. The films have shown better morphological characteristics compared to the bulk. In addition, the films exhibit better homogeneity as compared to the bulk sample. The compositional analyses of all the samples have been performed by Energy dispersive X- ray Analysis (EDAX). Typical EDAX spectrums of NCCO bulk and NCCO-S are presented in Figure 5.3 (a) and (b) respectively. The standard deviation of estimated values from compositional analysis of Ce was found to be 1.92 for the bulk and 0.13 for the film. The distribution of Cerium is seen to be more homogeneous in NCCO-S which can be attributed to the greater stoichiometric control in thin film growth. The Nd/Ce ratio at different regions in the NCCO-S film is found to be within the range of 11 to 12, which is closed to the optimum reported ratio of 12.3[15].

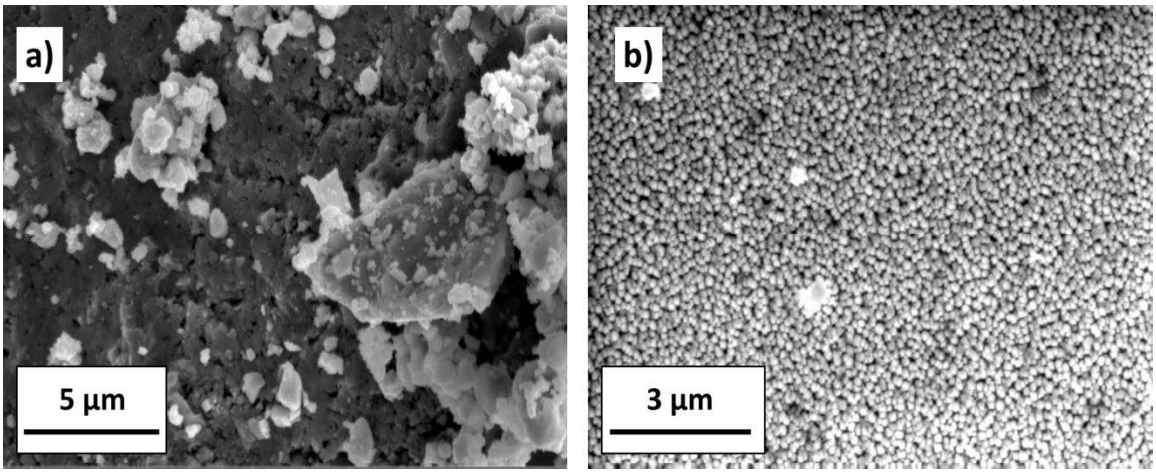

Fig. 5.2 SEM images of (a) NCCO bulk and (b) NCCO-S thin film

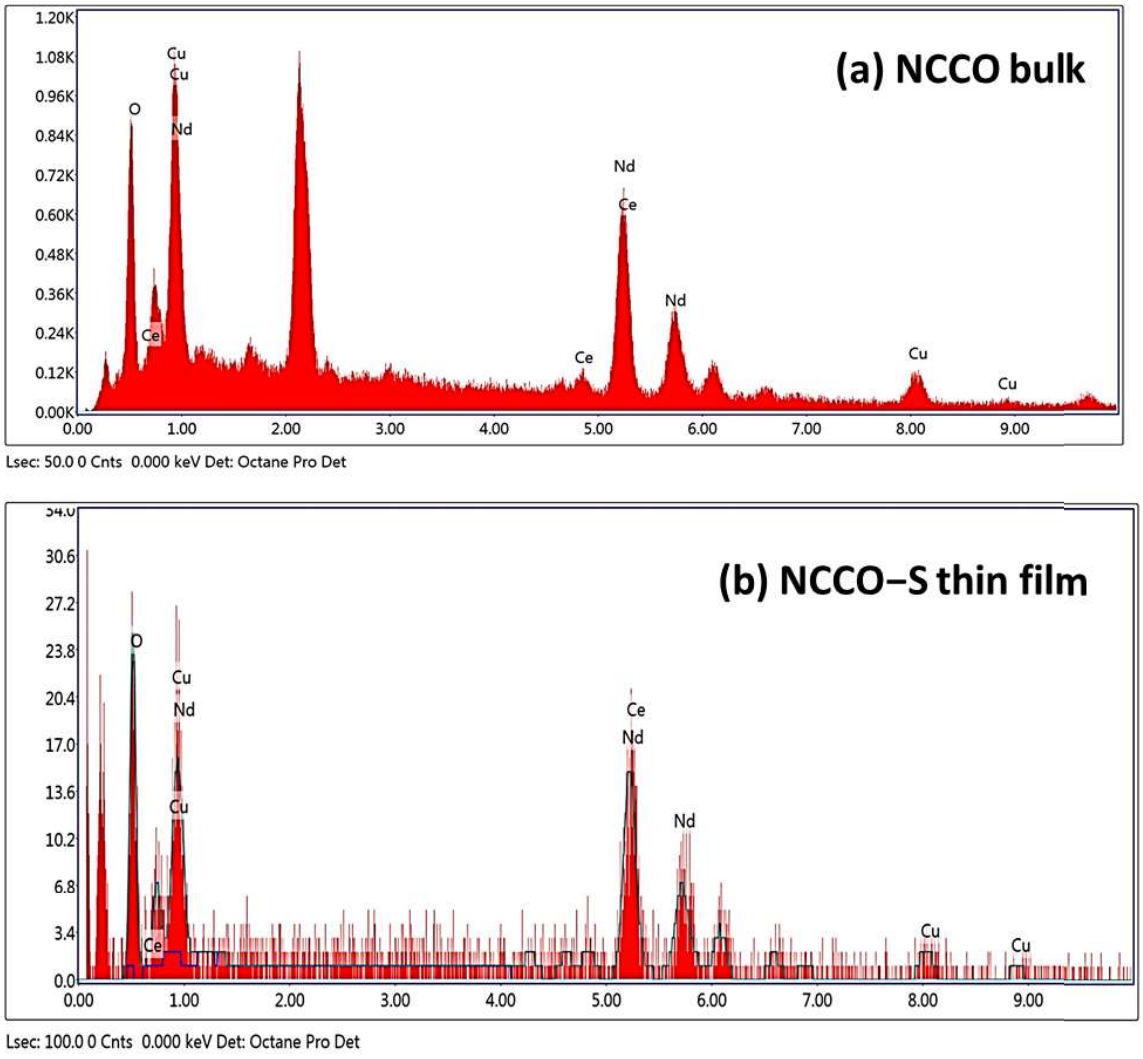

Fig. 5.3 Representative EDAX spectrums of (a) NCCO bulk (b) NCCO-S thin film

5.2 Magneto-Transport studies on NCCO

The temperature dependent resistance curves of the NCCO film (in-situ annealed at 740ºC) measured by applying magnetic field parallel (denoted as R_{in}) and perpendicular (denoted as R_{out}) to the plane of the sample are shown in Figure 5.4 (a) & (b) respectively. An interesting picture has emerged in this study which points to a co-existence of superconductivity and magnetism in this system. The salient features of temperature and field dependent behavior of R_{in} and R_{out} inferred from Figure 5.4 can be summarized as follows: At zero field, R_{in}& R_{out} decrease with temperature from 300K to 175K exhibiting metallic behavior, from 125 K to 175 K the resistance varies moderately

and almost levels off; and with further decrease in temperature the resistance increases showing semiconducting behavior. The metallic to semiconducting transition below 175K is attributed to the localization of the doped carriers [16]. Such a behavior has been reported in the as grown sample of NCCO which exhibits the effects of antiferromagnetism[17].

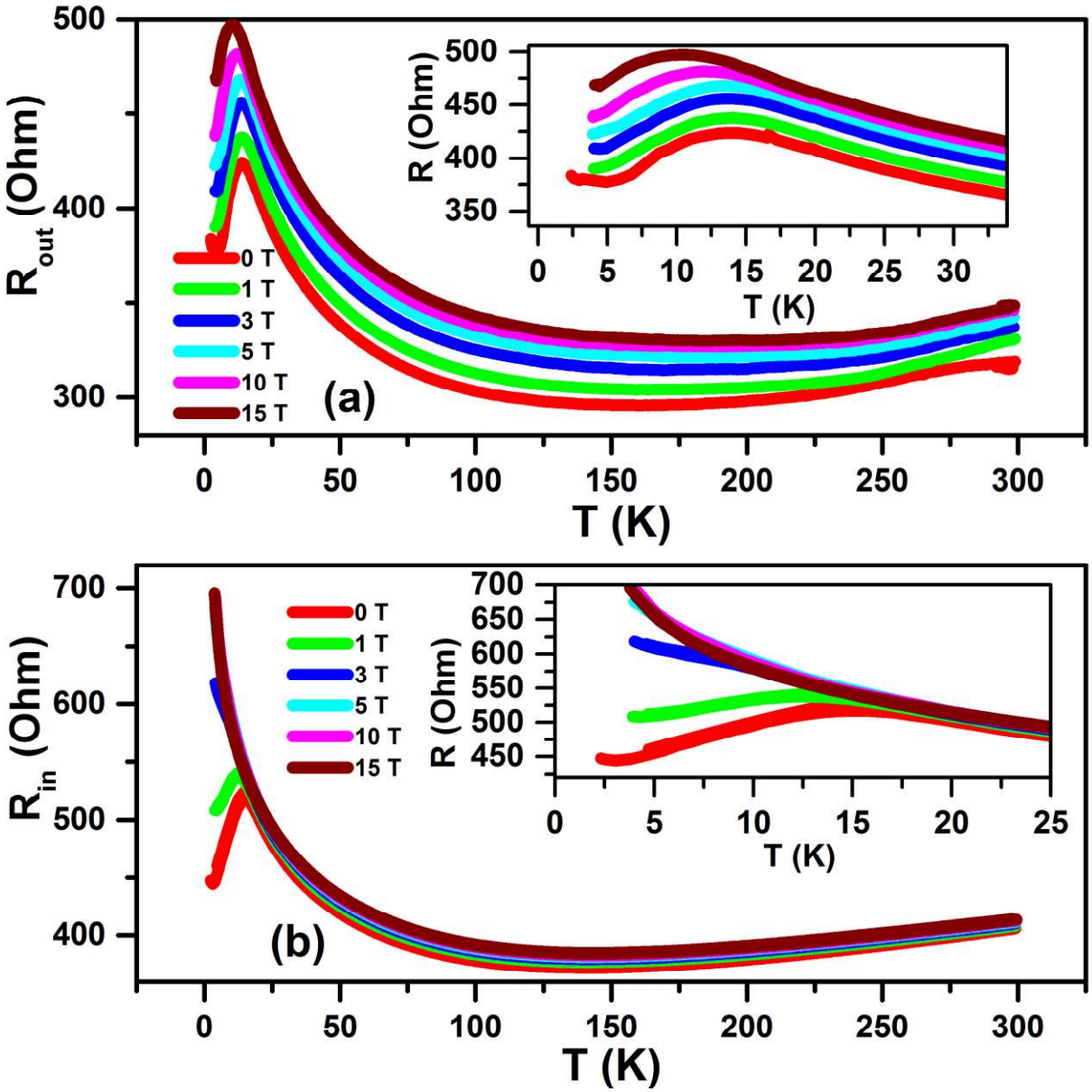

Fig. 5.4 Temperature dependent resistivity behavior of NCCO film (in-situ annealed) with magnetic field applied perpendicular to the plane of the film shown in (a) (R_{out}) and parallel to the plane of the film shown in (b) (R_{in}). Insets in (a) & (b) depict the expanded view of graphs at low temperatures to reveal the effect of magnetic field on $R_{out}(T)$ & $R_{in}(T)$.

The subsequent lowering of temperature shows a sudden dip in the resistance around 13.6 K which may arise due to the onset of filamentary superconductivity (see Figure5.4). Under application of magnetic field, the superconductor like dip shifts progressively to lower temperatures; and the overall resistance (R_{in} (T) & R_{out} (T)) increase with increasing the field (see Figure 5.4 & insets therein). Such a behavior is expected to occur in non-optimally reduced samples [18] in which the co-existence of antiferromagnetism with superconductivity can be realized. It should be mentioned that, the normal state resistance value of R_{in} is found to be ~415 Ω which is fairly higher than that of R_{out} (~314 Ω) at 300 K. This is in contrast to reported coefficient of resistance anisotropy R_{out}/R_{in} as high as 120 for superconducting thin films of NCCO [19]. Moreover, the resistance dip which happens at the same temperature of 13.6 K persists only up to a field of 1 T in R_{in}. For higher fields the resistance increases exponentially at low temperatures and reaches a maximum of 700Ωs for a field of 15 T at 4 K.

In order to obtain more insight regarding this behavior, we measured resistance as a function of field for the NCCO film at several fixed temperatures. The isothermal magneto resistance (MR) measured at 4K, 7K and 10K have been shown in Figures 5.5(a)-(c) respectively. In the case of R_{in}, it has been observed that the in-plane resistance initially increases rapidly with field then exhibits a marginal variation at higher fields. On the other hand, the application of magnetic field does not have such an impact on R_{out}. Even at comparatively higher fields of ~ 7 T, the MR values of R_{out} changes merely by 2%. The saturation behavior of R_{in} is probably due to the advent of some filamentary superconductivity.

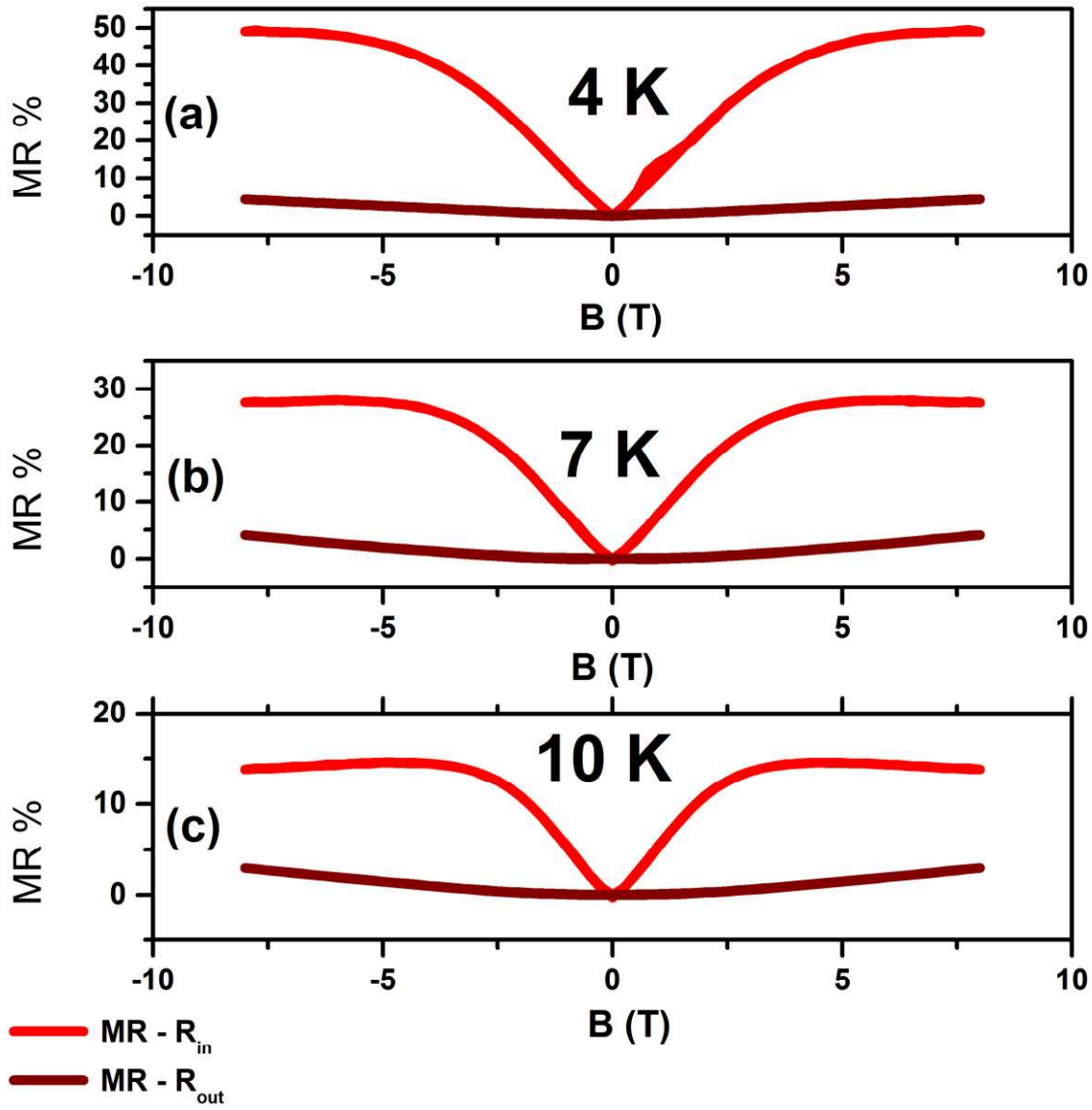

Fig. 5.5 Isothermal magneto resistance behavior of Rin and Rout at (a) 4K (b) 7 K (c) 10 K

Figure 5.6 represents the MR behavior of the NCCO-S film at 20K which is in the non-superconducting regime. Now, if the film was wholly superconducting one does not expect any change in MR once the temperature is above the transition temperature (T_C). In contrast, although the magnitude of MR is comparatively very low, it shows a step like behavior for R_{in}. In this case, the resistance increases up to a field of 1.7 T and then decreases at higher fields. R_{out} in comparison, does not show this step-like behavior,

rather it just increases narrowly with respect to increase in field and has a tendency of saturation at higher fields.

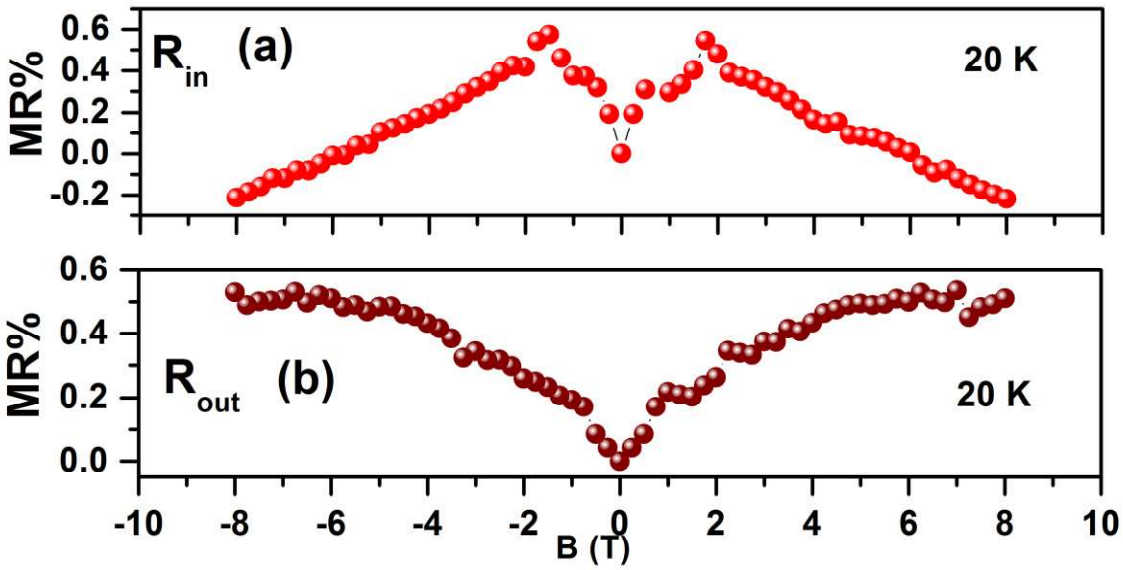

Fig. 5.6 Isothermal magneto resistance behavior of Rin (a) and Rout (b) at 20 K

The observed behavior can be understood as follows: As mentioned earlier the as grown samples are non-superconducting and antiferromagnetic. The reduction annealing procedure suppresses the antiferromagentic phase and leads to the appearance of superconductivity. Hence a non-optimally annealed sample can still possess some antiferromagnetic nature. The co-existence of antiferromagnetism and superconductivity in $Nd_{2-x}Ce_xCuO_4$ single crystals has been reported before [20]. In the antiferromagnetic regime the interaction between the charge carriers and the Cu^{2+} spins holds more prominence and hence dictates the transport behavior [21]. In the parent compounds of hole doped cuprates the Cu^{2+} spins order in the collinear structure, that is all the spins are parallel or antiparallel [22] whereas in the parent compounds of electron doped cuprates Cu^{2+} spins order in non collinear structure [23]. The effect of magnetic field on electron doped cuprates (when antiferromagnetism is prominent) is such that its application along the CuO_2 planes will result in a transition from the non-collinear state to the collinear state and thereby significantly influencing the magneto transport property. The step like

increase in MR of R_{in} at 20 K is attributed to this transition from non-collinear to collinear spin alignment in adjacent CuO_2 planes, with the increase in magnetic field [7]. This behavior persists only up to a certain value of field (1.7 T in our case), after that the MR behavior is different as it is in the collinear structure [11]. However, neutron scattering measurements have clearly proved that this transition is not observed when magnetic field is aligned in the c axis ($R_{out,}$ in our case). This behavior is expected and is consistent with literature reports [7,11,4]. It is important to mention that this magneto resistance behavior arises from spin and is devoid of any orbital terms [11]. Hence, we have performed the similar measurements by fixing the direction of magnetic field (in plane) and changing the direction of the applied current. It can be seen in Figure. 5.7 that the resistance behavior has not shown any changes with respect to change of direction in current. The fall of resistance is again observed up to field of 1 T in both the cases.

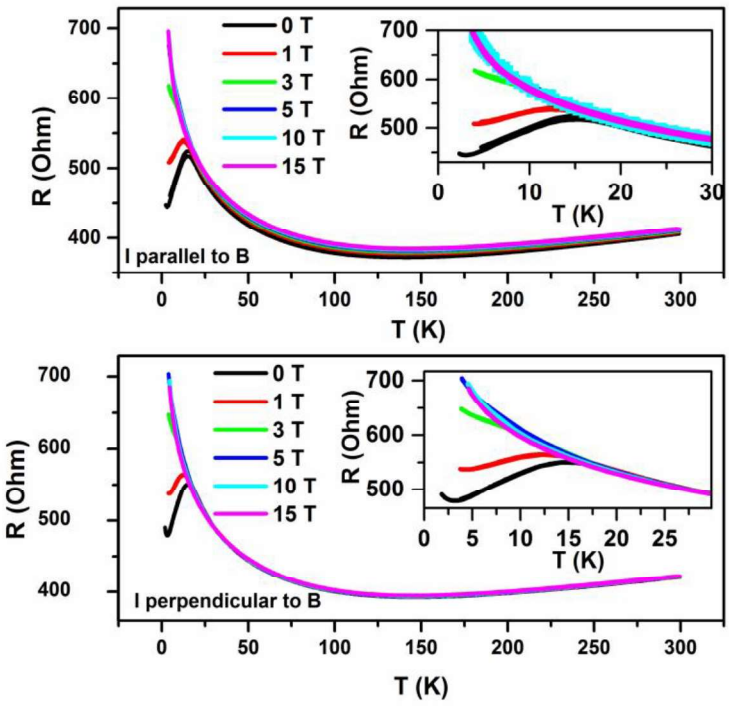

Fig. 5.7 Resistance versus Temperature as a function of field for NCCO non superconducting film with application of current in parallel as well as perpendicular direction with respect to magnetic fields.

5.3 Emergence of Superconductivity in $Nd_{1.85}Ce_{0.15}CuO_4$ thin film (NCCO- S)

In order to obtain superconductivity, the film was subjected to an ex situ annealing in Ar atmosphere at different temperatures starting from 600°C to 900°C. The time of annealing was fixed to be for 5 hours in all the annealing procedures. The samples were reduced using the protect annealing method [25]. "Protect annealing" method is a reduction annealing method where we can protect the surface from over reduction in a stronger reducing condition. To protect the surface of the films during Ar annealing, the films are covered with polycrystalline powders having the same composition. Hence the samples can be annealed in lower oxygen pressure for a longer time. In Figure 5.8, the temperature dependent resistivity behavior of NCCO film submitted to a series of Ar annealing schedules is shown.

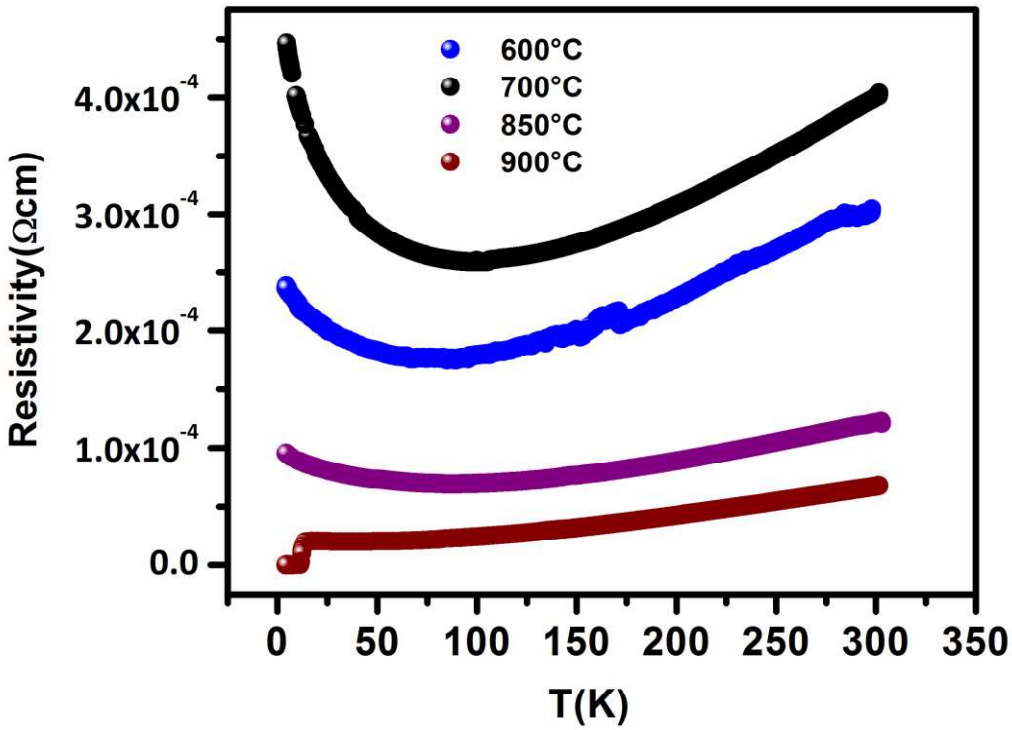

Fig. 5.8 Emergence of superconductivity in NCCO-S film when submitted to ex-situ annealing in Ar atmosphere, the transition is observed at 14 K and the annealing has been performed at Ar atmosphere for 5 hours at different temperatures.

Although the metallic to semiconductor transition behavior with the lowering of temperature persisted for the initial schedules of annealings at comparatively lower temperatures, it must be noted that the normal state resistance value has shown a consistent decrease with respect to the increase in annealing temperature. The emergence of superconductivity with a transition temperature of 14 K was observed after an annealing procedure at 900°C (See Figure 5.8). Superconducting films with T_C = 14 - 16 K have been synthesized using O_2 atmosphere as per recent reports as well[13].

The hole doped cuprates show linear temperature dependent behavior of resistivity. However, the resistivity of electron doped cuprates show T^2 dependence [2,26]. In present studies on thin film, both the in plane (R_{in}) and out of plane resistivity (R_{out}) behaviors show the same non-linearity with respect to temperature. This is also in contrast with the hole doped cuprates [27,28]. For temperatures below 200 K, the resistivity is fitted to the equation 5.1(see Figure 5.9)

$$\rho = \rho_0 + AT^2 \qquad (5.1)$$

where, ρ_0 is the residual resistivity and A is the electron electron scattering amplitude. The electron-electron interaction is considered to be the possible reason for this non linearity to arise in resistivity behavior with respect to temperature. This behavior persists over a narrow range of temperature. At higher temperatures, the data does not fit properly to equation 5.1. However, a better agreement is obtained when we fit it with T^2(ln T) where lnT is the correction term which has been attributed to 2 D electron- electron scattering [2].

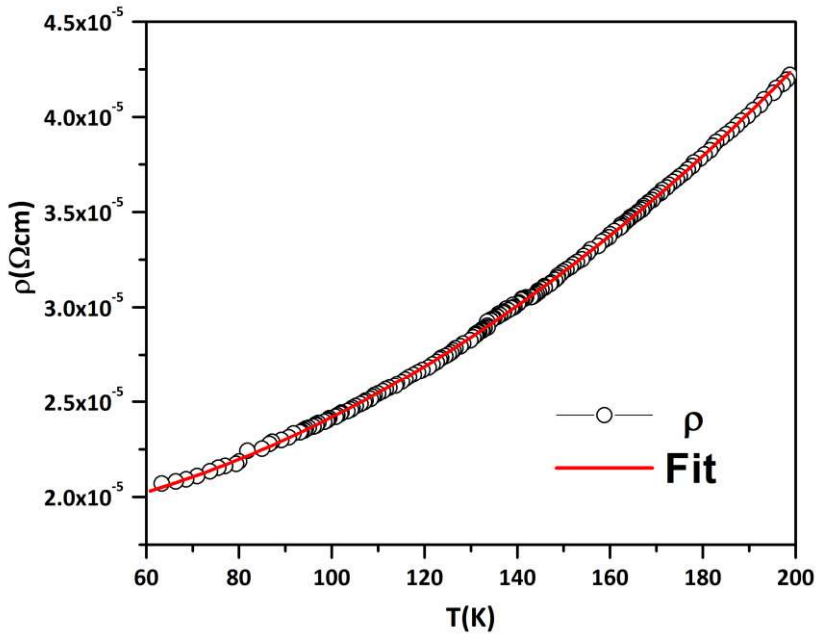

Fig. 5.9 Resistivity versus Temperature plot of NCCO-S thin film. The red line is a fitting curve from equation (5.1).

The values of ρ_0 and A deduced from the fit, are found to be $\rho_0 \sim 18$ μΩcm and A ~ 10^{-4} μΩ cm K^{-2} which are in accordance with literature reports [2]. As mentioned earlier, there exists a deviation from the T^2 behavior of resistivity at higher temperatures for T > 200 K. This is not surprising as one can imagine that the low dimensional nature of the NCCO film is responsible for the enhancement of electron-electron scattering. Theoretically the relaxation rate of quasi particle two dimensional free electron system is given by [29,30]

$$1/\tau_{ee} = \left(\frac{T}{T_f}\right)^2 \ln\left(\frac{T_f}{T}\right) \qquad (5.2)$$

Hence the equation used for fitting in the region of temperatures greater than 200 K is

$$\rho(T) = \rho_0(T) = \rho_0 + K\left(\frac{T}{T_f}\right)^2 \ln\left(\frac{T_f}{T}\right) \qquad (5.3)$$

where K is a constant and T_f is the Fermi Temperature. The logarithmic correction to T^2 behavior is a characteristic of a two dimensional fermionic system. The Fermi Temperature T_f is obtained from the fit (seeFigure5.10) is found to be ~ 2043 K. Such a

low value of Fermi Temperature has been reported for cuprate superconductors and this happens due to the low charge carrier concentrations [31,32].

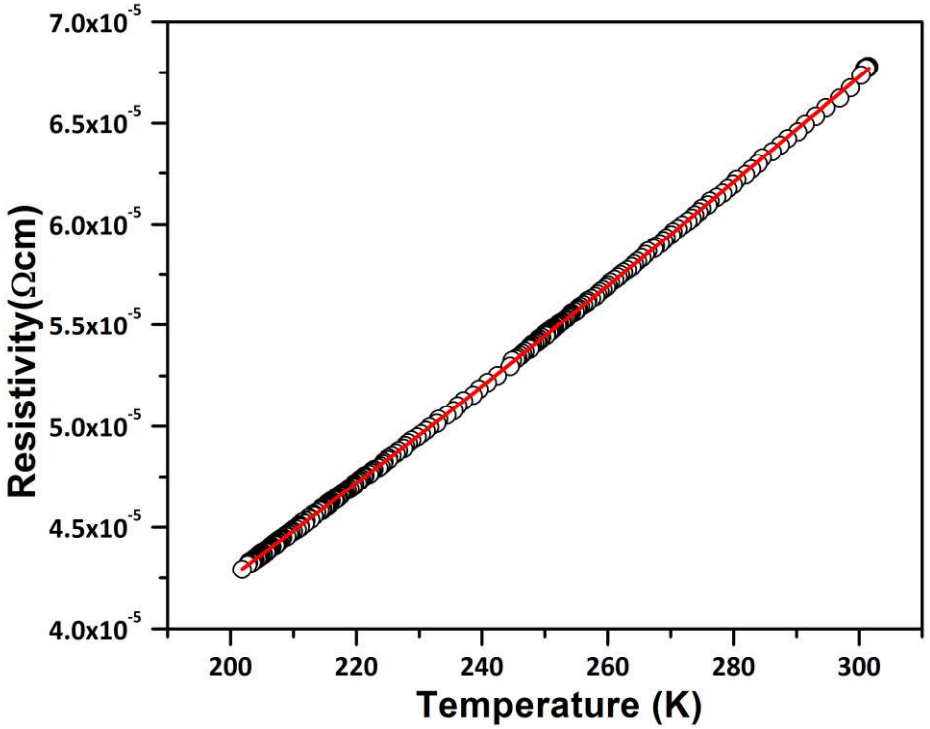

Fig. 5.10 Resistivity versus Temperature plot of NCCO-S thin film above 200 K. The red line is the fitting curve from equation (5.3)

Figure 5.11 reveals the resistance (with magnetic field applied parallel (R_{in}) and perpendicular (R_{out}) of plane) versus temperature behavior of superconducting $Nd_{2-x}Ce_xCuO_4$ (x=0.1) thin film with T_C = 14 K. In case of R_{out} (field applied parallel to *c* axis), the T_C shifts to lower temperatures with respect to an increase in applied field and we observe some broadening in the same as well. However, this broadening is not up to the extent of broadening observed in the hole-doped counterparts like YBCO. For fields above 1 T, the drop of resistance to zero value vanishes. But for R_{in}, the zero resistance drop is maintained even for comparatively higher fields like 8 T and the transitions do not show larger shifts, thereby indicating the sizeable anisotropy of superconducting properties of $Nd_{1.85}Ce_{0.15}CuO_4$ thin films.

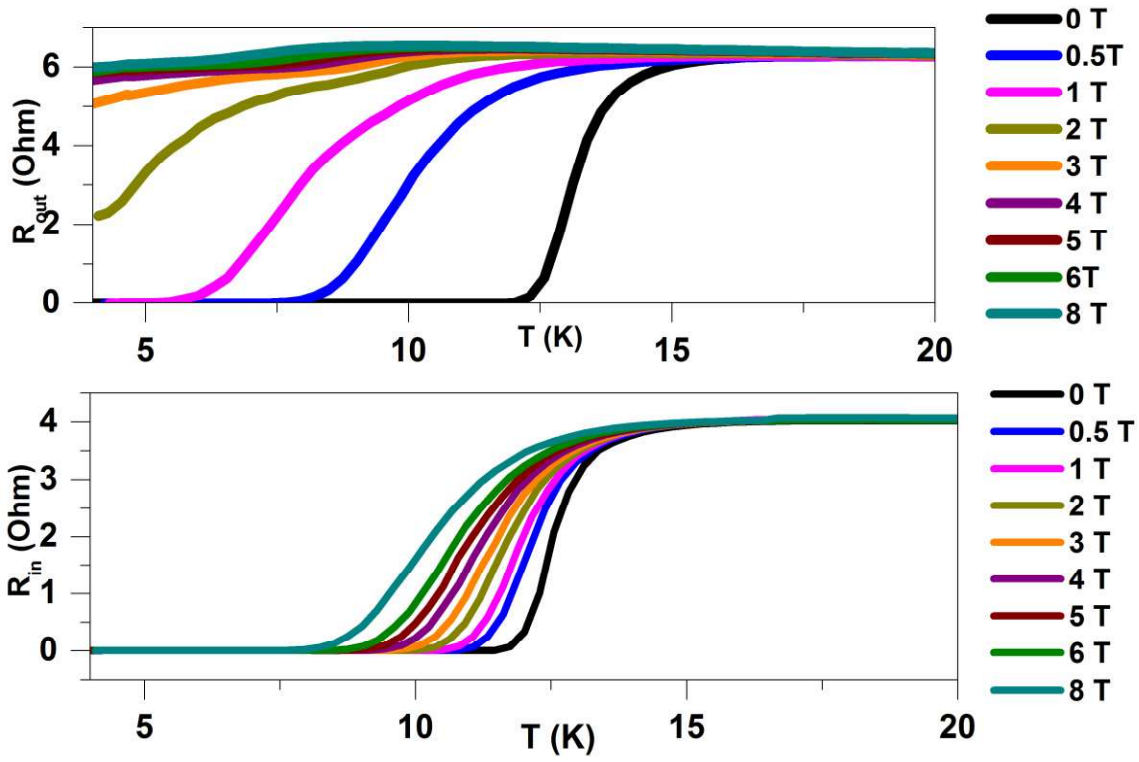

Fig. 5.11 Resistivity versus Temperature plot as a function of field of NCCO-S thin film

We obtained the critical field versus critical temperature plot from analyzing the resistance versus temperature curves in different applied fields. $H_{C2}(0)$ values were estimated both in plane as well as out of plane, from Werthamer-Helfand-Hohenberg formula.

$$H_{c2}(0) = -0.693 \left(\frac{dH_{c2}}{dT}\right)_{Tc} T_c \qquad (5.4)$$

The values deduced via the linear extrapolation of the lines on the field axis at T = 0 K, were found to be 27.82 T for R_{in} and 2.2 T R_{out} (Figure.5.12). The corresponding coherence lengths for R_{in} and R_{out} were estimated using the formula $\xi_{in} = \left(\frac{\phi_0}{2\pi H_{c2}^{R_{out}}}\right)^{1/2}$ and $\xi_{out} = \left(\frac{\phi_0}{2\pi H_{c2}^{R_{in}}}\right)^{1/2}$ respectively. The calculated values, $\xi_{ab} \approx 386$ Å and $\xi_c \approx 34$ Å are in near agreement with literature reports. Charikova et al. [33]reported

the highest coherence length of 273 Å for $Nd_{2-x}Ce_xCuO_4$ at x = 0.2 and the lowest comes $\xi \approx 80$ Å for the composition $Nd_{1.85}Ce_{0.15}CuO_4$.

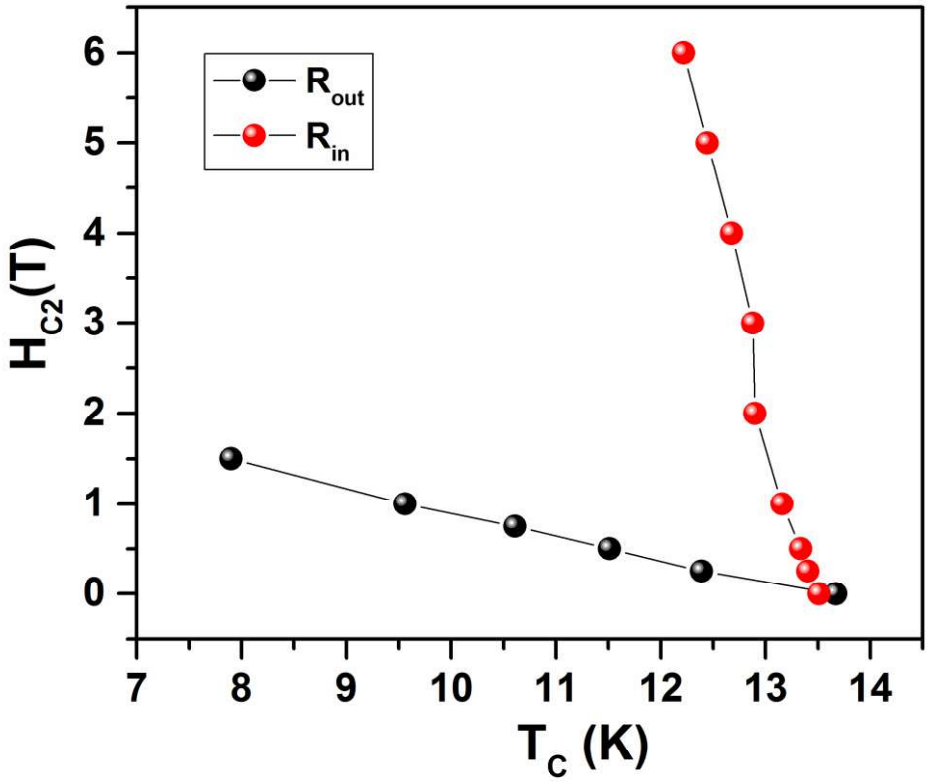

Fig. 5.12 Upper critical field versus Critical Temperature for field applied in parallel (Rin) and perpendicular directions to the a−b plane of NCCO-S thin film.

The anisotropy factor $\gamma = H_{c2}^{\|ab}/H_{c2}^{\|c} \approx 12$, is higher than that of hole doped superconductor YBCO [34-36] whereas lower than the values shown by $La_{2-x}Sr_xCuO_4$and $Bi_2Sr_2CaCu_2O_8$[36]. Fairly recent reports of $Nd_{1.85}Ce_{0.15}CuO_4$ epitaxial films, have shown higher value of $\gamma \approx 30$ [37]. Crystalline quality and distribution of oxygen influence the anisotropy and hence the anisotropic factor.

Figure 5.13 shows the Arrhenius behavior of resistance with respect to different values of magnetic field. The linear behavior below the 20 % of the normal resistance shows that the resistance is due to a thermally activated process. The equation that holds in this region of interest is

$$R = R_0 \exp\left(-U/K_B T\right) \qquad (5.5)$$

where, K_B is the Boltzmann constant and U is the activation energy. As per Tinkham [38], $U = U_0\,(1-t^2)(1-t^4)^{1/2}$where $t = {}^{T}/_{T_c}$ and $U_0 \approx H^{-\alpha}$, the exponent is influenced by magnetic field. We have used equation (5) to fit the linear regions of the Arrhenius plots and thereby we have deduced the values of U_0 for different applied fields.

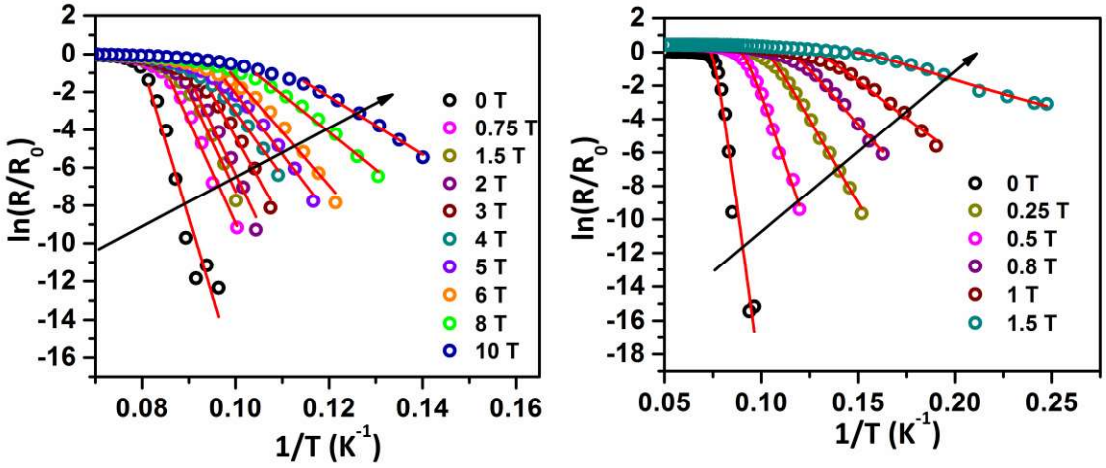

Fig. 5.13 Arrhenius plots of the resistance R(T) for the different values of applied magnetic fields. Red lines are the fitting curves as per equation (5.5)

The behavior of pinning activation energy with respect to application of inverse of applied magnetic fields is shown in the Figure5.14. The fitting has been done based on the power law equation U_0 = K. $H^{-\alpha}$ and K, α are used as the fitting parameters. We do not observe constant behavior of pinning potential energy for R_{in} as reported by Guarinoet. al [37] at lower fields (B ~ 1T). Hence from the present result it cannot be argued that it is a single vortex pinning regime. The value of α is found to be 0.2 in high fields (2 T < B < 10T) regime and 0.8 for in the low fields (0.15 < B <2 T) regime.However, for R_{out}, α value is found to be 1.2. The cross-over of α from 0.2 to 0.8 happens at a field of 2 T. This can be a cross-over of the pinning mechanism of dimensions[39]. The $Bi_2Sr_2Ca_1Cu_2O_x$ thin films which are highly anisotropic go through vortex lattice deformation resulting in double kinks in superconducting planes which in turn result in two dimensional pancake vortices with α = 0.5 whereas the pinning

behavior of less anisotropic YBCO films are explained by shearing of vortex lattice devoid of any kinks in the superconducting planes (this comes from three dimensional anisotropic vortices). The corresponding value of α is found to be 1 as per literature reports [40].The estimated values of α indeed points to a cross over from a quasi two dimensional behavior to a three dimensional behavior which occurs due to the presence of a collective pinning regime constituting of two different pinning centres with varying dimensions [39].

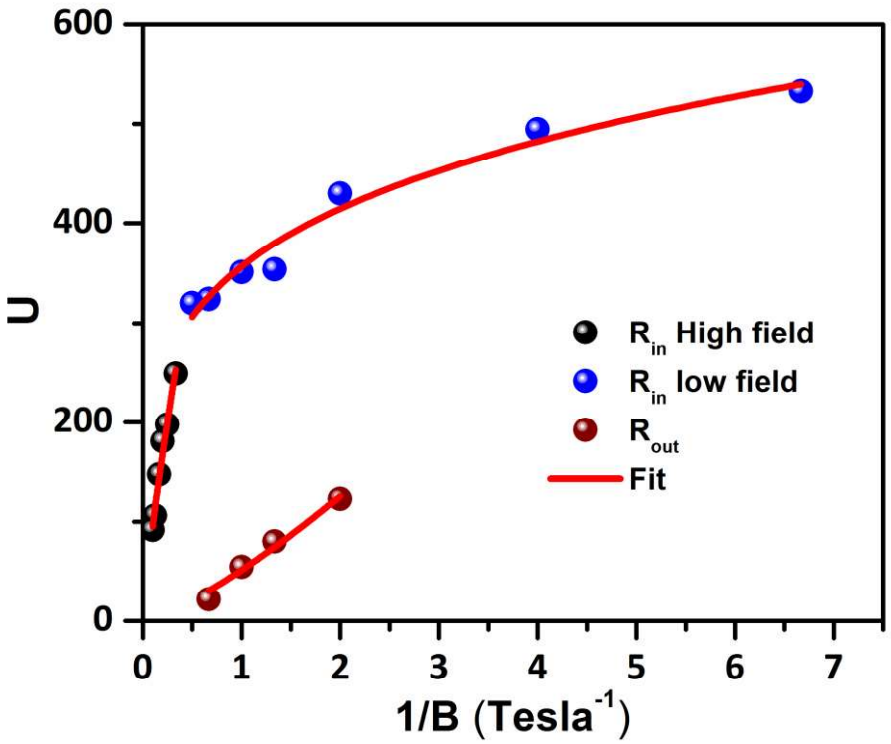

Fig. 5.14 Pinning activation Energy with respect to inverse of magnetic fields applied in perpendicular (R_{out}) and parallel (R_{in})to the plane of the film). The red lines are fitting curves of power law dependence.

Figure5.15 reveals the anisotropy of magneto resistance behavior of the superconducting film. It has been observed that for R_{out} the resistance goes through a steep increase at lower fields and has a tendency to saturate at comparatively lower value of fields like 4 T at 4 K. This field of saturation of resistance is shifted to lower values as the temperature is increased. For instance at 13 K, the saturation starts at 0.3 T. In

contrast R_{in} remains in its superconducting state even for very high fields such as 15 T for a temperature of 4 K.

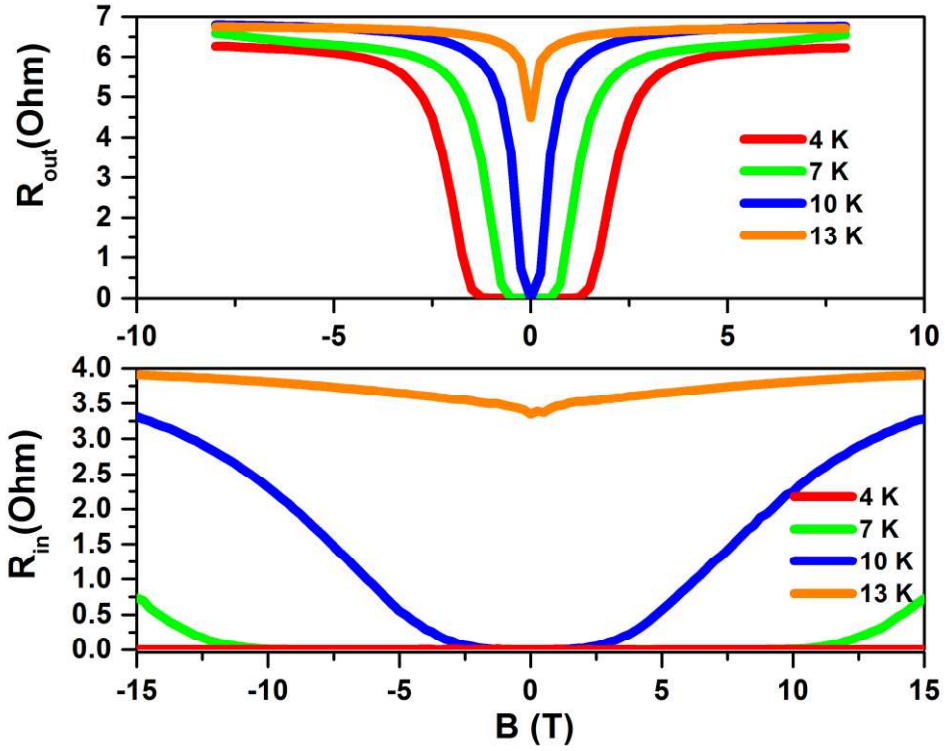

Fig. 5.15 Magneto resistance behavior of the superconducting film when field applied parallelly (R_{in}) and perpendicularly (R_{out}) to the plane of the film

5.2 Magnetic Hysteresis and Estimation of J_C of NCCO-S

Figure 5.16 shows the M-H curves of the film measured at different temperatures namely 2 K, 4 K and 6 K. The critical current density was estimated from the M – H curve using the Bean's critical state model. The intra-granular J_C is calculated from the expression $J_C = 20\ \Delta M/d$, where 'd' is the average grain size and calculated to be 0.1 μm from the SEM images. The maximum J_C value of ~ $1.93 \times 10^5 A/cm^2$ is obtained at a temperature of 2 K for a field of 0.01 T. For the same field at 6 K the J_C has its value lowered by one order, the value being 6.4×10^4 A/cm^2. The observed values are in agreement with literature [40].

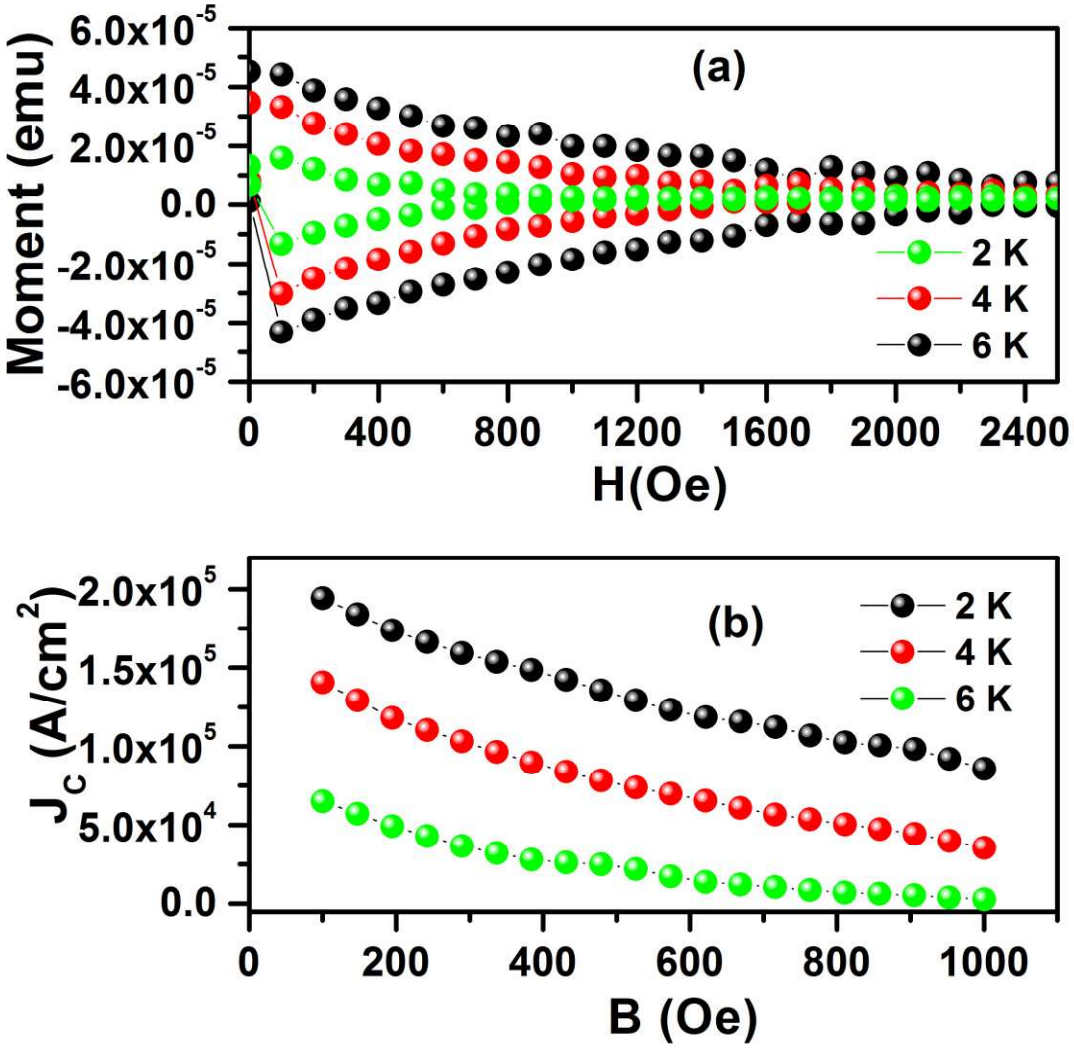

Fig. 5.16 (a) Magnetic hysteresis of NCCO-S film (b) Estimated J_C of the film at different temperatures

5.4 Conclusion

The thin film of $Nd_{1.85}Ce_{0.15}CuO_4$ has been synthesized using Pulsed Laser Deposition Method. A detailed magneto transport study has been performed on the in-situ annealed film. The in plane magneto - resistance (R_{in} ; B ‖ to the plane of the film) at 20 K revealed interesting step like transitions which happen due to alignment of Cu^{2+}spins from non-collinear to collinear arrangement under the application of field. This points to the co-existence of superconductivity and antiferromagnetism in the film, as the non reduced films of these compounds are antiferromagnetic. Superconductivity was obtained (T_C~14 K) in the film by ex-situ annealing in Ar atmosphere at 900°C for 5 hours. The

resistivity versus temperature curves of the film shows a T^2 dependence (attributed to electron – electron scattering) unlike the linearity exhibited by hole-doped cuprates. A sizeable anisotropy was observed in the electrical resistivity of thin films. R_{in} and R_{out} were measured with respect to temperature as a function of field and after analysis the anisotropy factor was found to be ≈ 12.

5.5. References

[1] H. Haensel, A. Beck, F. Gollnik, R. Gross, R. P. Huebener, and K. Knorr, Physica C: Superconductivity **244**, 389 (1995).

[2] C. C. Tsuei, A. Gupta, and G. Koren, Physica C: Superconductivity **161**, 415 (1989).

[3] C. W. Schneider, Z. H. Barber, J. E. Evetts, S. N. Mao, X. X. Xi, and T. Venkatesan, Physica C: Superconductivity **233**, 77 (1994).

[4] Y. Hidaka and M. Suzuki, Nature **338**, 635 (1989).

[5] M. Gurvitch, A. T. Fiory, L. S. Schneemeyer, R. T. Cava, G. P. Espinosa, and J. V. Waszczak, Physica C: Superconductivity **153-155**, 1369 (1988).

[6] S. I. Park, C. C. Tsuei, and K. N. Tu, Physical Review B **37**, 2305 (1988).

[7] X. H. Chen, C. H. Wang, G. Y. Wang, X. G. Luo, J. L. Luo, G. T. Liu, and N. L. Wang, Physical Review B **72**, 064517 (2005).

[8] K. Yamada, K. Kurahashi, Y. Endoh, R. J. Birgeneau, and G. Shirane, Journal of Physics and Chemistry of Solids **60**, 1025 (1999).

[9] T. Thio *et al.*, Physical Review B **38**, 905 (1988).

[10] Y. Ando, A. N. Lavrov, and S. Komiya, Phys. Rev. Lett. **90**, 247003 (2003).

[11] A. N. Lavrov, H. J. Kang, Y. Kurita, T. Suzuki, S. Komiya, J. W. Lynn, S. H. Lee, P. Dai, and Y. Ando, Phys. Rev. Lett. **92**, 227003 (2004).

[12] S. N. Mao, X. X. Xi, Q. Li, T. Venkatesan, D. P. Beesabathina, L. Salamanca-Riba, and X. D. Wu, Journal of Applied Physics **75**, 2119 (1994).

[13] A. Gupta, G. Koren, C. C. Tsuei, A. Segmüller, and T. R. McGuire, Applied Physics Letters **55**, 1795 (1989).

[14] M. Hoek, F. Coneri, D. P. Leusink, P. D. Eerkes, X. R. Wang, and H. Hilgenkamp, Supercon. Sci. Technol. **27**, 044017 (2014).

[15] A. I. Ponomarev, T. B. Charikova, A. N. Ignatenkov, A. O. Tashlykov, and A. A. Ivanov, Low Temperature Physics **30**, 885 (2004).

[16] J. S. Horwitz, D. B. Chrisey, M. S. Osofsky, K. S. Grabowski, and T. A. Vanderah, Journal of Applied Physics **70**, 1045 (1991).

[17] M. Suzuki, Physical Review B **39**, 2312 (1989).

[18] M. Ikeda, T. Yoshida, A. Fujimori, M. Kubota, K. Ono, Y. Kaga, T. Sasagawa, and H. Takagi, Journal of Physics: Conference Series **108**, 012016 (2008).

[19] T. B. Charikova, N. G. Shelushinina, G. I. Harus, D. S. Petukhov, O. E. Petukhova, and A. A. Ivanov, Physica C: Superconductivity and its Applications **525-526**, 78 (2016).

[20] A. I. Ponomarev, T. B. Charikova, G. I. Kharus, N. G. Shelushinina, A. O. Tashlykov, A. V. Tkach, and A. A. Ivanov, The Physics of Metals and Metallography **104**, 67 (2007).

[21] T. Uefuji, T. Kubo, K. Yamada, M. Fujita, K. Kurahashi, I. Watanabe, and K. Nagamine, Physica C: Superconductivity **357-360**, 208 (2001).

[22] T. Wu, C. H. Wang, G. Wu, D. F. Fang, J. L. Luo, G. T. Liu, and X. H. Chen, Journal of Physics: Condensed Matter **20**, 275226 (2008).

[23] D. Vaknin, S. K. Sinha, D. E. Moncton, D. C. Johnston, J. M. Newsam, C. R. Safinya, and H. E. King, Phys. Rev. Lett. **58**, 2802 (1987).

[24] S. Skanthakumar, J. W. Lynn, J. L. Peng, and Z. Y. Li, Physical Review B **47**, 6173 (1993).

[25] M. Matsuura, P. Dai, H. J. Kang, J. W. Lynn, D. N. Argyriou, K. Prokes, Y. Onose, and Y. Tokura, Physical Review B **68**, 144503 (2003).

[26] M. Horio *et al.*, Nature Communications **7**, 10567 (2016).

[27] N. Tralshawala, J. F. Zasadzinski, L. Coffey, and Q. Huang, Physical Review B **44**, 12102 (1991).

[28] V. Dinesh, K. K. Choudhary, and R. K. Singh, Supercon. Sci. Technol. **15**, 1119 (2002).

[29] K. Levin, J. H. Kim, J. P. Lu, and Q. Si, Physica C: Superconductivity **175**, 449 (1991).

[30] C. Hodges, H. Smith, and J. W. Wilkins, Physical Review B **4**, 302 (1971).

[31] G. F. Giuliani and J. J. Quinn, Physical Review B **26**, 4421 (1982).

[32] H. Takagi, S. Uchida, and Y. Tokura, Phys. Rev. Lett. **62**, 1197 (1989).

[33] S. W. Tozer, A. W. Kleinsasser, T. Penney, D. Kaiser, and F. Holtzberg, Phys. Rev. Lett. **59**, 1768 (1987).

[34] T. B. Charikova, G. I. Harus, N. G. Shelushinina, O. E. Sochinskaya, and A. A. Ivanov, Low Temperature Physics **37**, 293 (2011).

[35] K. Nagasao, T. Masui, and S. Tajima, Physica C: Superconductivity **468**, 1188 (2008).

[36] U. Welp, W. K. Kwok, G. W. Crabtree, K. G. Vandervoort, and J. Z. Liu, Phys. Rev. Lett. **62**, 1908 (1989).

[37] C. Panagopoulos, T. Xiang, W. Anukool, J. R. Cooper, Y. S. Wang, and C. W. Chu, Physical Review B **67**, 220502 (2003).

[38] A. Guarino, A. Leo, G. Grimaldi, N. Martucciello, C. Dean, M. N. Kunchur, S.

Pace, and A. Nigro, Supercon. Sci. Technol. **27**, 124011 (2014).

[39] M. Tinkham, *Introduction to Superconductivity: Second Edition* (Dover Publications, 2004).

[40] C. C. Chin and T. Morishita, Physica C: Superconductivity **207**, 37 (1993).

[41] C. Cirillo, A. Guarino, A. Nigro, and C. Attanasio, Physical Review B **79**, 144524 (2009).

Chapter 6

Summary and Future Outlook

6.1. Summary

The work presented in this thesis has focused on magneto-transport and magnetization studies on the electron doped superconductor $Nd_{1.85}Ce_{0.15}CuO_4$ (NCCO). The studies have been performed on three different aspects of NCCO. The initial studies were performed on bulk superconducting NCCO to understand the intricacies of its normal and superconducting state properties. This is followed by material modification of NCCO by Ag addition and investigation on the effect of Ag incorporation on the superconducting properties of NCCO/Ag composite system. In addition to this, with an eye on improving the sample quality and exploration of the superconducting and antiferromagnetic regimes, the studies have been carried out on NCCO thin films as well. The bulk samples were synthesized by solid state reaction and the thin films were synthesized by Pulsed Laser Deposition. The summary of the major results of this thesis is presented below:

- In Chapter 3, the magneto-transport properties of the polycrystalline electron doped superconductor NCCO have been studied. The resistivity measurements showed double superconducting transitions attributed to intra and inter-grain contributions, a behaviour which has been observed for weakly coupled granular superconducting systems. The sensitivity of NCCO superconductor to reduction annealing (which induces superconductivity in electron doped cuprates) has been studied. It has been observed that the durations and temperatures, for which the annealing has been performed, influence the resistance behavior in a profound manner. The effect of two different annealing conditions (standard annealing and

prolonged annealing) on the temperature dependent electrical resistivity behavior of NCCO has also been examined. The observed non monotonic resistivity behavior has been qualitatively explained in terms of the competition of opposing effects of temperature and magnetic field on Superconductor-Insulator-Superconductor (S-I-S) Junctions, energy gap and quasi particle tunneling. These interpretations which satisfactorily explain the observed resistivity behavior is based on the picture that the weakly coupled granular superconducting sample is in the form of isolated superconducting grains embedded in an insulating matrix.

- The effect of Ag addition on the superconducting properties of NCCO has been investigated in Chapter 4. Significant increase in critical current density was observed in the Ag added samples. This correlates well with Rietveld analysis of NCCO/Ag composites which shows a small but significant change in lattice parameter in NCCO upon Ag addition, which points to a possible substitution of a small fraction of Ag (~ 1 wt%) in the lattice (at the Cu sites). The rest of the Ag is present as free silver probably at the grain boundaries. The reduction in unit volume of NCCO observed upon Ag addition is consistent with the minor phonon hardening of all Raman modes observed in NCCO/Ag composites. The randomization of preferred orientation and the diminishing of the apical oxygen defect mode observed in the Ag added samples are the other interesting changes in structural features observed, after Ag addition. The current dependence studies indicate that the Ag added samples sustain higher values of intergranular critical current and hence showing marginal improvement of the granular properties. Nonetheless, the granular effects persist in NCCO/Ag composites and consequently non monotonic resistivity transitions are observed in their temperature dependent resistance behavior with respect to application of magnetic

field. The resistive upper critical field value decreases upon Ag addition and this might be due to an increase in local site disorder.

- In Chapter 5, detailed magneto-transport studies have been performed on the thin films of $Nd_{1.85}Ce_{0.15}CuO_4$ in the in-situ annealed state (say NCCO) and the ex-situ annealed state (NCCO-S). In both the cases, resistance has been measured with respect to temperature in the presence of various magnetic fields, applied parallely (resistance in this case is referred as R_{in}) and perpendicularly (R_{out}) to the plane of the film. R_{in} and R_{out} have been measured with respect to magnetic field for fixed temperatures as well (Isothermal Magneto resistance (MR)). Although an advent of superconductivity is observed for the NCCO film at T ~ 14 K, the most important result is observed in the in plane magneto resistance (R_{in}) of NCCO, at 20 K. The step like transitions observed in the MR at this temperature arise due to the alignment of Cu^{2+} spins from the non collinear to collinear arrangement under the application of magnetic field. This type of transition is observed in the antiferromagnetic state of NCCO. This is relatable because the unannealed state of NCCO is antiferromagnetic. This led us to point out that there is a coexistence of superconductivity and antiferromagnetism in the in-situ annealed sample. Superconductivity was achieved in the ex-situ annealed film (NCCO- S) at T_C~14 K. The resistivity versus temperature behavior of the films shows T^2 dependence which is typical for electron doped superconductors and is attributed to electron – electron scattering. R_{in} and R_{out} were measured with respect to temperature for NCCO-S also. Upper critical field of NCCO-S have been calculated for both R_{in} and R_{out}. The ratio of these critical fields $H_{C2}^{R_{in}} / H_{c2}^{R_{out}}$ was found to be ~ 12, which

reveals that sizeable anisotropy exists in the system. From magnetization measurements, the critical density of the film was estimated.

6.1 Future Outlook

1. Effect of Ag addition in superconducting NCCO thin films

In addition to the reports of how the critical current density improves upon Ag addition in cuprate superconductors like $YBa_2Cu_3O_7$, MgB_2 etc.,[1,2], the Ag added composites in the thin film form have shown better superconducting properties attributed to better inter-grain connectivity, stoichiometric control and homogeneity of the constituents [3-5]. The enhancement of critical current density with Ag addition in $Nd_{1.85}Ce_{0.15}CuO_4$ (NCCO) is a major result of this work. It will be very interesting to see the effect of Ag addition on $Nd_{1.85}Ce_{0.15}CuO_4$ thin film form. The studies in this thesis work have already shown that the thin films of NCCO possess better homogeneity in Ce concentration and the effects due to granularity are largely suppressed. Hence, further improvement of the superconducting properties is expected if NCCO/Ag composites can be synthesized in thin film form.

2. Bilayers of $Nd_{2-x}Ce_xCuO_4$and Nd_2CuO_4

Heterostructures made from films of cuprate superconductors have shown significant enhancement in critical temperatures (T_C) [6,7]. The critical temperature of bilayers of $La_{2-x}Sr_xCuO_4$ showed 50% of enhancement compared to the single compound film when an overdoped layer (x = 0.35) was coated above an under-doped layer (x = 0.12). The T_C of the heterostructure was 32 K [8]. Moreover, bi-layers and nano-layers of electron doped compounds have been utilized for device applications and exploration of basic physics [9,10]. Hence it will be worthwhile to synthesize the bilayers

of overdoped and underdoped $Nd_{2-x}CexCuO_4$and investigate superconductivity in the heterostructures.

3. Superconductivity in Nd_2CuO4 thin films

The electronic phase diagram of cuprate superconductors still remains a mystery. The parent compounds of the cuprates are Antiferromagnetic insulators and superconductivity supposedly develops by doping holes or electrons to the copper oxide layers. The parent compound of NCCO is Nd_2CuO_4 which is an antiferromagnetic insulator. The popular belief is that when a tetravalent Ce is doped in the trivalent Nd site it ends up donating electrons to the CuO_2 layers and after submission to reduction annealing, superconductivity emerges. However, there are reports of superconductivity in Nd_2CuO_4 thin films itself, yielding comparatively higher $T_C \sim 30$ K, grown by metal organic decomposition [11]. It has been suggested that complete removal of apical oxygen through the reduction process is the key to superconductivity. This leads to the idea that reduction annealing is the most crucial step in electron doped superconductors rather than electron doping. The phenomenon of superconductivity in $Nd_2CuO_4$was recently reconfirmed by Naito et al.[12]. Even then, detailed investigation must be performed to investigate the superconductivity in these materials to answer important questions related to the mechanism of superconductivity in electron doped cuprate superconductors.

6.2 References

[1] B. A. Malik, M. A. Malik, and K. Asokan, Chinese Journal of Physics **55**, 170 (2017).

[2] C. Shekhar, R. Giri, R. S. Tiwari, O. N. Srivastava, and S. K. Malik, Journal of Applied Physics **101**, 043906 (2007).

[3] G. Z. Li, M. A. Susner, S. D. Bohnenstiehl, M. D. Sumption, and E. W. Collings, Applied Surface Science **357**, 452 (2015).

[4] M. Lorenz, H. Hochmuth, D. Matusch, M. Kusunoki, V. L. Svetchnikov, V. Riede, I. Stanca, G. Kastner, and D. Hesse, IEEE Transactions on Applied Superconductivity **11**, 3209 (2001).

[5] X. Tang, Y. Zhao, W. Wu, N. H. Andersen, and J. C. Grivel, Journal of the European Ceramic Society **35**, 1761 (2015).

[6] A. Gozar, G. Logvenov, L. F. Kourkoutis, A. T. Bollinger, L. A. Giannuzzi, D. A. Muller, and I. Bozovic, Nature **455**, 782 (2008).

[7] Z. Z. Li, H. Rifi, A. Vaurès, S. Megtert, and H. Raffy, Physical Review Letters **72**, 4033 (1994).

[8] O. Yuli, I. Asulin, O. Millo, D. Orgad, L. Iomin, and G. Koren, Physical Review Letters **101**, 057005 (2008).

[9] A. Di Bernardo *et al.*, Nature Communications **8**, 14024 (2017).

[10] M. Hoek, F. Coneri, N. Poccia, X. Renshaw Wang, X. Ke, G. Van Tendeloo, and H. Hilgenkamp, APL Materials **3**, 086101 (2015).

[11] O. Matsumoto, A. Tsukada, H. Yamamoto, T. Manabe, and M. Naito, Physica C: Superconductivity and its Applications **470**, 1029 (2010).

[12] M. Naito, Y. Krockenberger, A. Ikeda, and H. Yamamoto, Physica C: Superconductivity and its Applications **523**, 28 (2016).